Acoustic Emission Analysis of Snow

Diploma Thesis

Submitted to the

Faculty of Electrical and Information Engineering

of

Graz University of Technology

by

Klemens Mayer

Assessor

Univ. Prof. Dipl.-Ing. Dr. Otto Koudelka

Graz University of Technology

Institute of Communication Networks and Satellite Communications

Advisors

Dipl.-Ing. Maria Fellner, MBA

JOANNEUM RESEARCH Forschungsgesellschaft mBH

DIGITAL - Institute for Information and Communication Technologies

Dipl.-Ing. Michael J. Moser

Graz University of Technology

Institute of Electrical Measurement and Measurement Signal Processing

Dr. Ingrid Reiweger

Dr. Jürg Schweizer

WSL Institute for Snow and Avalanche Research SLF, Davos

2011

STATUTORY DECLARATION

I declare that I have authored this thesis independently, that I have not used other than the declared sources / resources and that I have explicitly marked all material which has been quoted either literally or by content from the used sources.

....

Abstract

Continuous monitoring of failure processes inside a snowpack could be a missing link to fully understand natural dry-snow slab release. Existing continuous monitoring systems already deployed have the drawback that they are rather detection than warning devices. It is believed that greater insight into fracture processes at the micro and meso scale could be gained by analyzing acoustic emissions (AE). For this purpose, basic laboratory research was carried out with a commercial acoustic emission recording system and a special shear apparatus for loading snow samples. Besides classical parameters like amplitude or signal duration emphasis was placed on the frequency spectra. Accordingly, wide band sensors most sensitive from 100 kHz to 1 MHz were used to record various frequency bands. Despite this fact, most signals had their main energy in a region around 30 kHz. Smaller accumulations could be detected in regions around 100, 200 and 500 kHz. Apart from that, possible precursor signals could be detected prior to catastrophic failure, characterized by long durations and high energy. Finally, three dimensional location of failure events in layered snow samples showed that acoustic emission activity is concentrated in the weak layer. The results look promising, but further laboratory research is needed to draw reliable conclusions. Systematical parameter variation and a further improved sensor coupling in terms of consistency should be aimed. For field deployment, challenges are the snow's strong damping and complex wave propagation properties, varying considerably in space and time.

Zusammenfassung

Kontinuierliches Überwachen von Bruchvorgängen innerhalb der Schneedecke könnte helfen die Vorgänge vor und bei trockenen Schneebrettlawinen vollständig zu verstehen. Derzeitig verwendete kontinuierliche Überwachungssysteme sind nur in der Lage bereits stattgefundene Lawinenabgänge zu detektieren. Die Methode der Schallemissionasanalyse (SEA) könnte besseren Einblick in die nichtsichtbaren mikroskopischen Bruchvorgänge ermöglichen. Hierzu wurden Experimente im Kältelabor mit professionellem SEA-System und einem Scherapparat für Schneeproben durchgeführt. Sowohl die klassischen zeitbezogenen Parameter als auch Parameter im Frequenzbereich wurden analysiert. Die meisten Signale hatten ihre Hauptenergie in einem Band um 30 kHz. Auch in Bereichen rund um 100, 200 und 500 kHz konnten Spitzen in der Signalenergie beobachtet werden. Detektierte Warnsignale vor katastrophalen Brüchen waren tendenziell von langer Dauer und hoher Energie. Dreidimensionale Lokalisationsexperimente zeigten, dass die Schallemissionskonzentration in geschichteten Schneeproben in der Schwachschicht lag. Die Resultate sind vielversprechend, um verlässliche Schlüsse zu ziehen sind jedoch weitere Experimente notwendig. Einzelne Parameter müssen systematisch variiert werden, außerdem sollte für noch konstantere Ankopplungsbedingungen der Sensoren gesorgt werden. Für Feldexperimente dürften sich die hohe Dämpfung und die komplexen Wellenasubreitungseigenschaften von Schnee als größte Herausforderungen erweisen.

Acknowledgments

It is a pleasure to thank those who made this thesis possible. My first thanks go to my supervisors Maria Fellner, Michael Moser, Ingrid Reiweger and Jürg Schweizer. In numerous discussions - personally, via conference calls and email - they guided me through the various technical and scientific disciplines combined in this thesis.

Thanks to Jürg Schweizer and Ingrid Reiweger for giving me the chance to be part in the wonderful research team at SLF Davos. I also want to thank Stephan, Christoph, Fabiano, Lukas and Ben for all the help in the laboratory and everyone else at SLF for making it such a great time.

My thanks go to the members of the Space Technology and Acoustics group at JOANNEUM Research and especially to Maria Fellner for supporting this research topic from the first minute on. I also want to thank Prof. Dr. Otto Koudelka for assessing this thesis.

Last but not least thanks to my parents, brothers and sisters, my son Jan, Andrea and Alena for their great support.

Contents

List of Figures

List of Tables

Chapter 1

Introduction

Avalanches are a considerable natural hazard in mountain regions, and therefore an adequate avalanche warning service is from great importance to save lives and reduce economical losses (e.g. Munter 2009). There are various classifications of avalanches (e.g. McClung and Schaerer 1993; Schweizer et al. 2003), mainly depending on snow conditions and fracture mechanics. In this research, emphasis is placed on the fracture mechanical processes leading to natural dry-snow slab avalanches. These avalanches occur in dry snow (contrary to wet-snow) and involve the release of a cohesive slab (contrary to loose snow) by shear failure in a weak layer below. The term "natural" refers to the fact that no artificial triggering (e.g. skiers, explosives) is required prior to avalanche release. Hence, natural avalanches occur due to natural effects like gradual uniform loading (precipitation) or meteorological changes (Schweizer et al. 2003). Any dry-snow slab avalanche release follows three main process steps: Starting with an initial failure (1) a crack inside the snowpack is introduced which, at favorable conditions may propagate (2) and may reach a size big enough to cause a snow slab to glide off (3). As depicted in fig 1.1, these three steps can be related to three scales, micro, meso, and macro scale (Schweizer et al. 2003).

The initial process leading to natural avalanches, i.e. the crack initiation without any external triggering, is still not fully understood. It is believed that snow-failure processes at the micro scale (10^{-4} m), also called "bond breaks" occur in extremely weak zones. If they reach a significant size reaching the meso scale, they may be able to be self propagating. Schweizer (1999) reviewed many of the existing models based on this weak spot theory, but no verification of these models could be done yet due to the weak spot's transient nature and spatial variability. Thus, two basic questions are aimed to be solved.

1. What are the exact processes inside the snowpack (spatially and temporally) leading to natural dry-snow slab avalanches?

2. Is it possible to monitor and distinguish precursor events prior to avalanche release in order to improves avalanche warning systems?

Continuous monitoring of the non-visible processes inside the snowpack is needed to answer

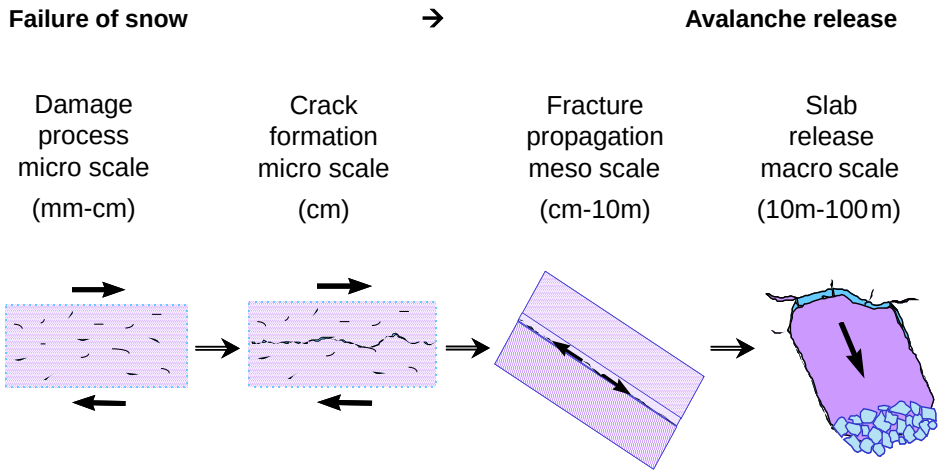

Figure 1.1: Conceptual model of dry snow slab avalanche release (Schweizer et al. 2003).

these questions. For visible processes, i.e. avalanches (which reach the macro scale, compare Figure 1.1), this monitoring is possible by detection devices such as seismometers, radar, light beam an trip wires (McClung and Schaerer 1993) which partly are in practical use. Obviously, only already released avalanches are reported and no further information about the avalanche is provided. On the other hand, snow mechanical tests like the classical Rutschblock test (RB) or more recent methods like for example the Propagation Saw Test (PST) provide more informations about the snowpack before a possible avalanche release (Schweizer and Jamieson 2010). Unfortunately, great human dedication is needed, and the demand for continuous monitoring is not at all satisfied. A physical phenomenon known as "acoustic emissions" might fulfill the requirements of continuous snowpack monitoring at every scale (e.g. McClung and Schaerer 1993; Sommerfeld 1982; Reiweger et al. 2010; van Herwijnen and Schweizer 2011).

Figure 1.2 depicts the phenomenon of acoustic emissions in snow. Every failure event inside a snowpack produces elastic waves, so-called acoustic emission waves. Their frequency and amplitude characteristics depend strongly on the size of failure. While small events produce high-frequency waves (small wavelength) with low amplitudes, amplitude and wavelength increase with increasing failure size (St.Lawrence 1980). This fact is important for choosing the right instrumentation. Low-frequency signals are recorded with geophones, high-frequency signals with acoustic emission transducers. The terminology in this field of research tends to be slightly ambiguous. The term acoustic emission in engineering and material science is basically used for ultrasonic emission, i.e. signal frequencies higher than 20 kHz. Still, it is common practice and according to the standards to use the term acoustic emission also for low-frequency signals in the audible (20 Hz to 20 kHz) and even sub audible region (infra sound). Some authors use the term seismic signals instead of acoustic emission signals for these low frequency regions (e.g. van Herwijnen and Schweizer 2011). When generally speaking about acoustic emission, this distinction is not

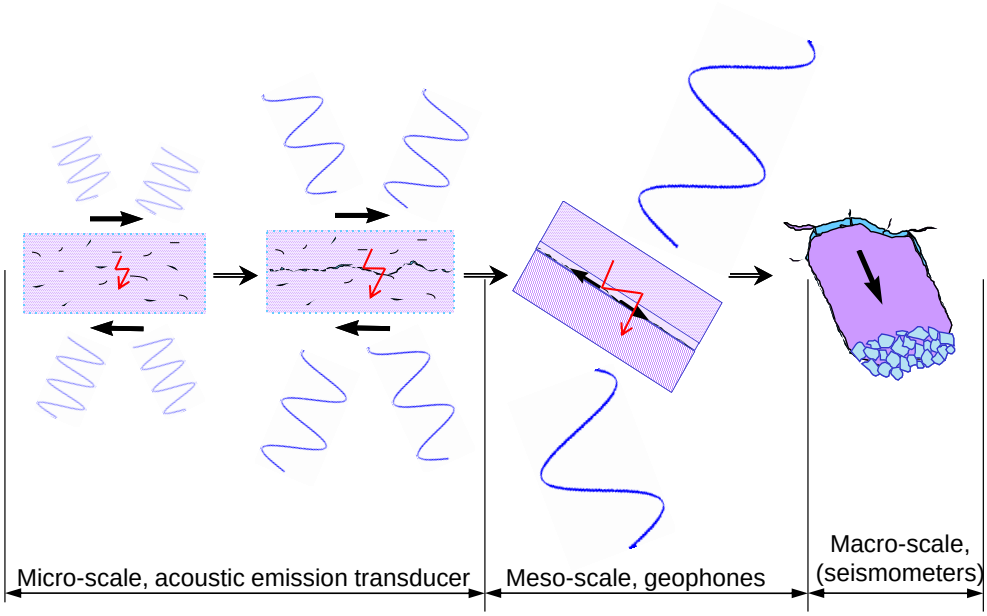

Figure 1.2: Acoustic emissions of snow and instrumentation depending on the size of failure (adapted from (Schweizer et al. 2003)). Small failures produce low amplitude emissions with high frequency. The larger the failure, the higher the amplitude and the lower the frequency.

necessarily needed. But when it comes to instrumentation and recording as stated above, it is very useful. Accordingly, throughout this work the term "acoustic emission" refers to the utilization of passive elastic waves inside a material in general. As soon as distinction is important, acoustic emission will refer to ultrasonic waves and the term seismic will refer to signals with frequencies below 200 Hz (origin at meso- and macro scale).

The idea of using acoustic emission techniques in snow to assess snowpack stability actually had its pioneers in the 1970s. In laboratory experiments, St.Lawrence et al. (1973) reported acoustic emissions recorded with geophones in the audio spectrum (20-7000 Hz) from snow samples under uniaxial compression. Acoustic emissions were associated with rates of deformation corresponding to brittle fracture of the snow sample. The existence of the Kaiser effect in snow, which signifies that in loading cycles there is no AE activity before reaching the previous loading level, was reported from Bradley and St.Lawrence (1975). Emphasis was placed on the frequency region between 50 and 100 kHz. An acoustic emission response model as function of stress and strain was developed by St.Lawrence (1980). Besides laboratory research, also field research was carried out in order to utilize AE activity to better understand natural slab release. Using three geophones recording AE signals in the range between 1-30 Hz, Sommerfeld (1977) observed that periods before and during avalanches were associated with high noise, while periods of known

stability were associated with low noise. St.Lawrence and Williams (1976) conducted similar field experiments with geophones, also detecting seismic signals which could not be related to extrageneous noise or visible avalanche activity. High correlation was found between instabilities detected by seismic monitoring of the study slope and the onset of widespread instability throughout the mountain range.

Problems in determining fracture properties arise from their strong dependence on the type of snow and strain or stress history (St.Lawrence and Bradley 1977; Mellor 1975). This history defines the current condition of the snowpack. Besides the current condition, the actual rate of loading and deformation is a highly crucial factor determining the possibility of catastrophic failure (e.g. McClung and Schaerer 1993; Schweizer 1999). Loading at small rates gives the snow time to heal itself, i.e. bond breaks are compensated by resintering processes at the same time, which results in plastic behavior (McClung 1986). St.Lawrence and Bradley (1977) also attribute lack of acoustic emission activity to this phenomenon. At a certain loading rate, the number of damage processes exceed the number of healing processes and a residual stress arises and stays in the snowpack (Camponovo and Schweizer 2001; Schweizer et al. 2003). Its exact location, magnitude and persistence cannot be reconstructed exactly, which in fact closes the circle to the unknown snowpack history. Considering these delicate points it seems not too surprising that avalanches have also been released without any precursory acoustic emission activity. And, even worse, sometimes quiescent periods were observed to be an indicator for snow-slope instability (Bowles and St.Lawrence 1977). More information from inside the snowpack is needed in order to explain these ambiguities. In all the reported field experiments emphasis was placed on the signals in the seismic range, i.e. signals having their origin at the meso and macro scale. Further insight into fracture processes might be gained by simultaneously analyzing the ultrasonic acoustic emission signals originating at the micro scale.

Detecting and recording ultrasonic acoustic emissions in snow is more challenging compared to seismic signals mainly because of their low amplitudes. With its wide range of characteristics, snow is not an easy material to treat in terms of wave propagation. Snow shows high and frequency-depended damping, and how elastic waves (structure born sound) exactly travel inside a snowpack is difficult to determine (Sommerfeld 1982). In addition, as far as a natural snowpack is concerned, it always consists of various layers with different properties, i.e. snow is not a homogeneous medium (e.g. Schweizer et al. 2003; Reiweger et al. 2010). For the high-frequency elastic waves this means that there are boundaries all over the place which cause reflection, diffraction and artefacts in the signals. In order to work around these problems, the present work is based on research regarding ultrasonic emissions from snow in the cold laboratory. Laboratory work ensures constant conditions, both as far as the environment as well as the snow samples are concerned. Obviously, basic considerations on wave propagation and issues regarding instrumentation can be done easier in a well controlled environment. It is assumed that only if these basic considerations are verified, a reliable system can be deployed in the field (Reiweger et al. 2010). The aim of this

work thus was to gain insight into the following questions:

- Which AE parameters are capable of describing and distinguishing different breaking processes inside the snowpack?
- How are process parameters, classical parameters, and frequency parameters related to each other in time and frequency domain?
- Is it possible to discriminate different types of signals and assign failure mechanisms?
- Are there distinct precursor signals prior to catastrophic failure?
- Is it possible to locate failure events inside a snow sample?

The thesis is structured as follows: To begin with, chapter 2 will provide with the most important basics on acoustic emission testing. Chapter 3 will bring up necessary basics of snow characteristics and mechanical properties. Additionally, AE related to snow will be covered and important related fields like wave propagation in snow considered. The experimental setup for this present study will be described in chapter 4. After that, chapter 5 presents the results of the various measurements, which will be discussed in chapter 6. Finally this thesis concludes in chapter 7, where important findings are summarized and a possible picture is drawn how this promising research topic could be continued.

Chapter 2

Acoustic emission technique

This Chapter will give a theoretical and practical introduction into the field of acoustic emission (AE) techniques in general. Two main strategies in AE signal analyzing, the parameter-based and the signal-based approach, are discussed. First, the "classical" acoustic emission parameters are described and their importance is highlighted. Then emphasis is placed on so called signal-based AE techniques, where not only signal parameters are extracted but the entire waveforms are stored and analyzed in real time. After introducing the principles of event localization, the measurement chain and wave propagation are discussed as central practical AE concerns. Acoustic Emission related to snow and snow acoustics will be discussed in Chapter 3.

2.1 Basics

Acoustic emission testing is a non-destructive testing method and widely used in both engineering and geotechnical applications, either to evaluate material properties or to monitor exposed structures in laboratory or field tests. AE waves are defined as transient elastic waves generated by the release of energy within a material or by a process (DIN EN 1330-9 2000). More precisely, localized strain energy is released suddenly, which causes sudden displacements sending structure-borne sound waves into the structure. Strain obviously is a result of stress, depending on the material's Young's modulus (Hooke's law). The signal's amplitudes are usually very low and cover mostly frequency regions in the ultrasonic region. The acoustic emission phenomenon, also known as microseismic activity, is in fact commonly observed in most solids including metals, ceramics, rocks, concrete, glass wood, plastics and also ice (Reginald Hardy Jr. 2003). Extensive research was especially done for concrete (e.g. Grosse 1996; Finck 2005) or rock (e.g. Shiotani et al. 2001; Manthei 2001). In terms of wave propagation and sensor technology, AE-techniques are quite similar to ultrasonic (US) testing methods. As Figure 2.1 shows, the main difference is the source. While US methods work with known input signals sent into the structure by US-transmitters, the AE waves are produced directly inside the specimen due to mechanical loading.

Acoustic emission signals occur in various shapes, depending on the material and source mechanisms. Two main groups of signals can be distinguished: Burst signals and continuous

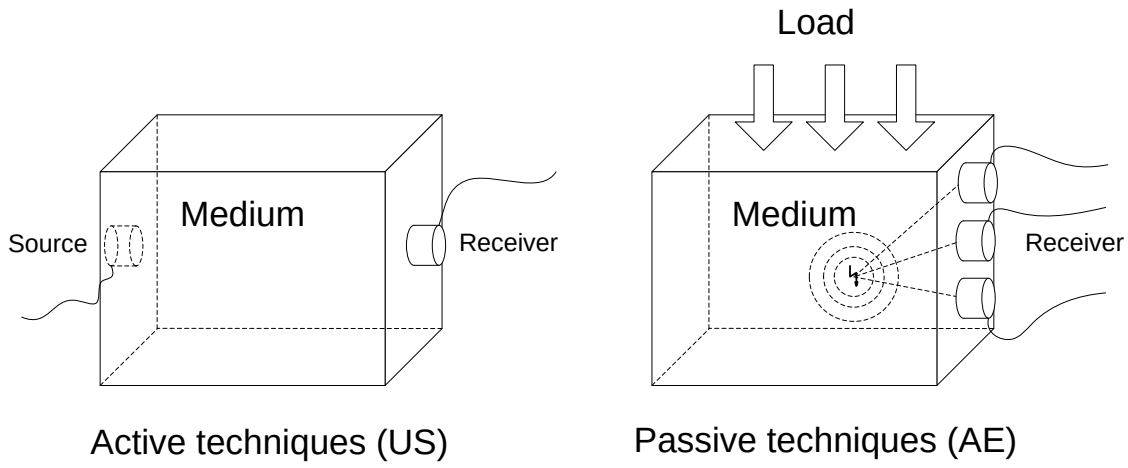

Figure 2.1: Comparison of non-destructive principles using active or passive techniques (Grosse 1996).

emission of acoustic waves. Compared to classical (audible) acoustic signals in air, there are two main points to consider when dealing with AE-signals:

- The frequency range may cover the audible region (20 Hz to 2 kHz) but is usually much higher (around some hundred kHz) and can reach even in the MHz region
- Air-borne sound waves can only propagate as longitudinal waves because air cannot support shear stress. Conversely, AE-signals are generated inside solid materials and thus are so-called structure-borne sound waves. They propagate as longitudinal P-waves (pressure or primary waves), transverse S-waves (shear or secondary waves), and other interfacial waves such as surface waves, reflected waves, diffracted waves, and guided waves (Grosse and Ohtsu 2008).

There are many applications of AE testing, covering a wide range of tested materials. Basically, almost every material which supports propagation of elastic waves can be investigated. Limiting factors are often high attenuation of AE waves (which is a problem with snow of low density) and anisotropic character of materials. This is for example true for composites and a challenging factor because the AE waves are partially reflected and diffracted on borders inside the specimen.

2.2 Parametric AE analysis versus signal-based AE-analysis

In contrast to previous research on acoustic emissions of snow, this project is the first which employs signal-based AE-analysis of snow. Parametric AE technique is often called "classical" AE testing, since it was the only possible kind of AE analysis for decades. Significant parameters are extracted from the AE signals resulting in low data storage. Conversely, performing signal-based AE-analysis means that the waveforms are stored and can be analyzed by the various

methods in digital signal processing, including powerful analysis in the frequency domain. In most cases it is convenient to use both techniques, since frequency domain parameters can be easily misinterpreted because of the frequency dependent measurement chain. Therefore, descriptions of both techniques are provided in the following sections.

2.2.1 Parametric AE

Typical AE signals are high frequency waveforms, covering a range from 20 kHz up to 1 MHz, depending on the material properties. Sampling and storing AE-signals thus results in big amount of data, which was an unsolvable problem in the early stages of AE testing. The solution was to find characteristic parameters in the signal, which can be extracted by analogue circuits and be stored easily. Figure 2.2 shows a typical AE signals with its characteristic parameters. These parameters still are the most concise way to specify AE signals. It is therefore important to use the terminology, which is defined in various standards, for example (e.g. DIN EN 1330-9 2000), correctly.

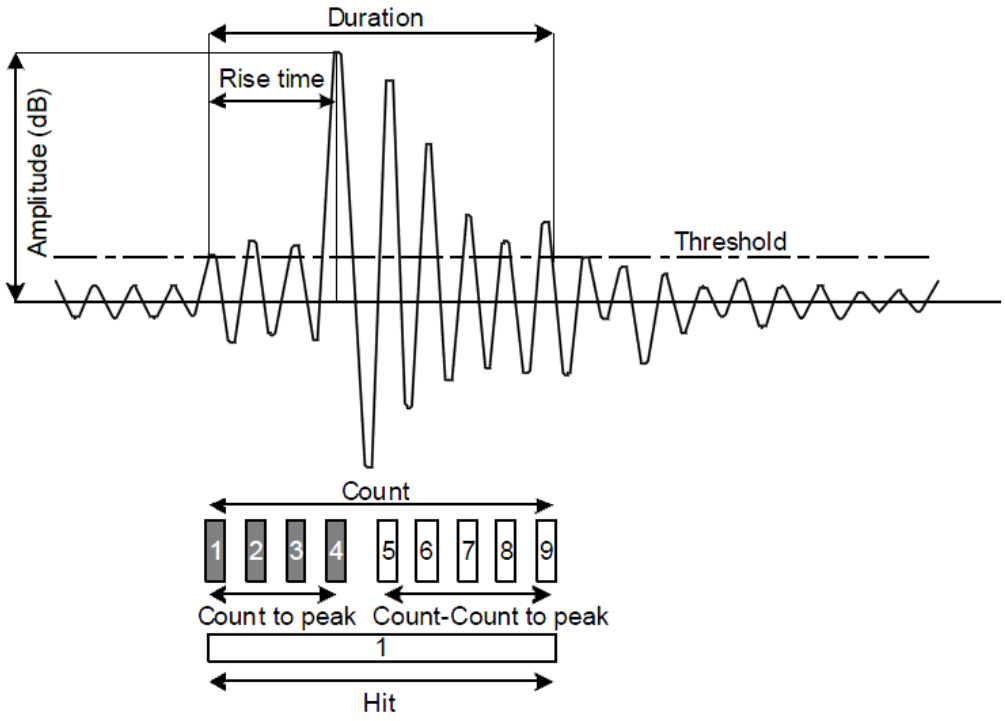

Figure 2.2: AE signal parameters (Grosse and Ohtsu 2008).

The main set of parameters consists of:

Hit A hit is an actual detected and measured AE-signal. It starts with the crossing of a predefined threshold and ends after the last crossing of the threshold.

Count or ringdown count Every hit consists of one or more counts. Every threshold crossing

within a hit is referred to as a count. The number of counts is affected by the following parameters (Miller and McIntire 1987):

1. The sensor frequency
2. The damping characteristics of the sensor
3. The damping characteristics of the structure
4. The threshold level

AE signals can either have a broad frequency distribution (noisy character) or a dominant main frequency. Theoretically, regarding only the main frequency of a signal, it can be represented as

$$V = V_0 e^{-Bt} sin(\omega t) \tag{2.1}$$

where V_0 is the initial signal amplitude, B the decay constant (greater than 0), t the time and ω the angular frequency. Using the threshold voltage V_t, the number of counts N can be given as

$$N = \frac{\omega}{2\pi B} ln \frac{V_0}{V_\mathrm{t}} \tag{2.2}$$

Duration The duration of one hit, i.e the time from the first threshold crossing to the last.

Amplitude The highest amplitude (peak amplitude) within one AE signal (hit).

Rise time The time from the first threshold crossing to the highest peak.

Energy Signal energy of a transient AE signal. With V being the voltage output of the AE sensor and R the electrical resistance of the measurement unit, the energy U is defined as

$$U = \frac{1}{R} \int_0^\infty V^2(t) dt \tag{2.3}$$

Apart from that, there are a number of parameters which are basically derived mathematically from the main parameters described above. The most important of these additional parameters are:

Count to peak The number of threshold crossings (counts) until the signals reaches its maximum.

Average frequency Average frequency of the entire AE signal (hit), derived by counts/duration.

Initiation frequency Average frequency of the signal from the first threshold crossing until the time where the maximum amplitude (peak amplitude) occurs. It is thus derived by counts to peak /rise time.

Reverberation frequency Average frequency of the signal from the time of the maximum amplitude (peak amplitude) until the last threshold crossing (counts - counts to peak)/(duration - rise time).

2.2.2 Signal-based AE

Signal-based (quantitative) AE technique is a term for all AE approaches based on storing and analyzing complete AE waveforms. This fact allows for various powerful data analysis methods, especially in the frequency domain. Loss of information through the reduction to single parameters is avoided. Of course effort is needed in the sector of data management. Considering possible signal frequencies of 2 MHz and higher, sample rates of more than 10 M Samples may be needed. The fact that AE signals have very low amplitudes also requires a high-resolution analog-to-digital converter. So there are various pros and cons of both AE approaches, parameter-based and signal-based. Not surprisingly, both approaches are currently applied, with success for different applications (Grosse and Ohtsu 2008). Systems which include both techniques can be used in order to combine the advantages, which was the chosen approach for this research. Only viewing and analyzing AE signals in the frequency range might be misleading, especially for not well-known materials like snow, which in addition is difficult to treat because of its continuous metamorphosis (Joachim Sell, Physical Acoustics Corporation, personal correspondence). Recording AE signals requires important considerations on the various elements in the measurement chain and the wave propagation characteristics inside the specimen.

2.3 Source localization

Source localization of acoustic emission events is an inversive problem and works similar to earthquake localization algorithms (Grosse and Ohtsu 2008). Its basis is a time-distance relationship implied by the velocity of the sound wave. A minimum number of sensors according to the localization mode is needed. For three-dimensional localization, an acoustic wave originated from the same source has to be monitored at four different sensor locations. With these sensor coordinates and the wave velocity, the location of the event can be calculated by solving the set of equations:

$$t_i = t_0 + \frac{1}{v}\sqrt{(x_i - x)^2 + (y_i - y)^2 + (z_i - z)^2} \tag{2.4}$$

(x_i, y_i, z_i) are the sensor coordinates, (x, y, z) the desired location vector of the event hypo center and t_0 the origin time. An important requirement is to have exact knowledge about the wave speed in the sample. Moreover, since different waves (longitudinal P-waves, transversal S-waves etc. see Chapter 2.5) travel with different velocities it is of vital importance to discriminate what kind of wave had been detected. In scales large enough (earthquakes), P- and S-waves can be easily distinguished because of the P-waves higher wave speed. In smaller scales, like often the case in acoustic emission testing, the difference in the arrival time of P- and S-wave is very small and the S-wave can be hidden in the so called coda of the P-wave. This fact implies a limiting factor for accurate localization results. Furthermore, great influence on the localization accuracy is given by the type of automatic onset detection. Finally, equation 2.4 implies that the specimen has homogeneous and isotropic properties because the direct ray path is used for the calculation of the source location. If a layered or even a heterogeneous and anisotropic material is tested, the

effects of the material on wave propagation and the ray path should be taken into consideration for an accurate localization.

2.4 The measurement chain

2.4.1 AE sensors

Following the path of an AE signal, the first element passed is the AE-sensor and the coupling between specimen and sensor. The big majority of AE sensors available work with piezoelectric elements for transduction. These elements are located inside a casing, with damping material on top and a wear plate on the side which is in contact with the specimen. A schematic diagram of a typical AE sensor is depicted in Figure 2.3. Since the low level AE signals are strongly attenuated in air, the couplant layer has to contain as little air as possible. In the special case of this research handling with snow specimen, the couplant layer consists of ice, created through slight melting and refreezing of water on the snow surface. (See Chapter 4.5).

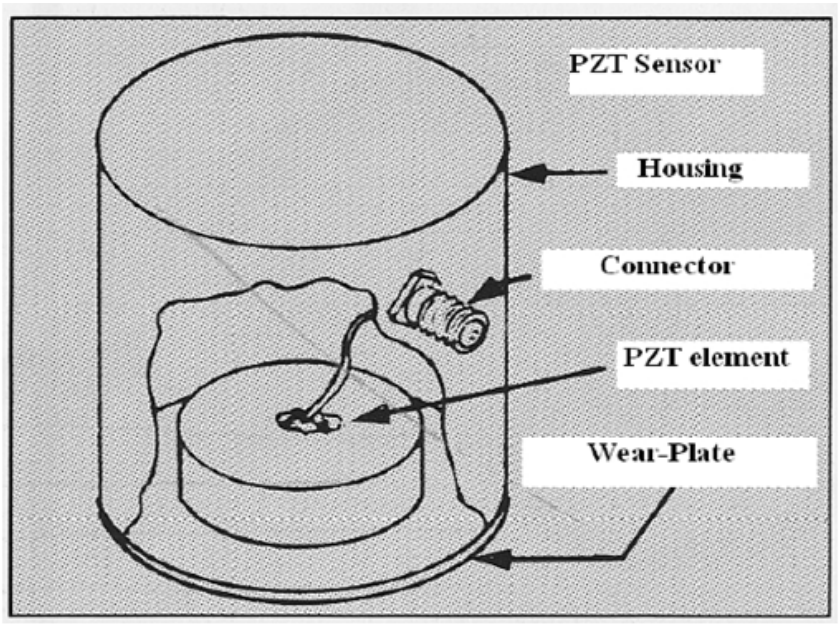

Figure 2.3: Piezoelectric acoustic emission transducer, schematic (Grosse and Ohtsu 2008).

For many applications it is important to know that an AE sensor's sensitivity depends on the direction of the AE signal relative to the sensor. Most sensors are designed to respond best to the component normal to the surface of the sensor. Unfortunately, there are no sensitivity pattern available for the sensors at purchase, and deriving the patterns in own measurements needs high effort (Grosse and Ohtsu 2008).

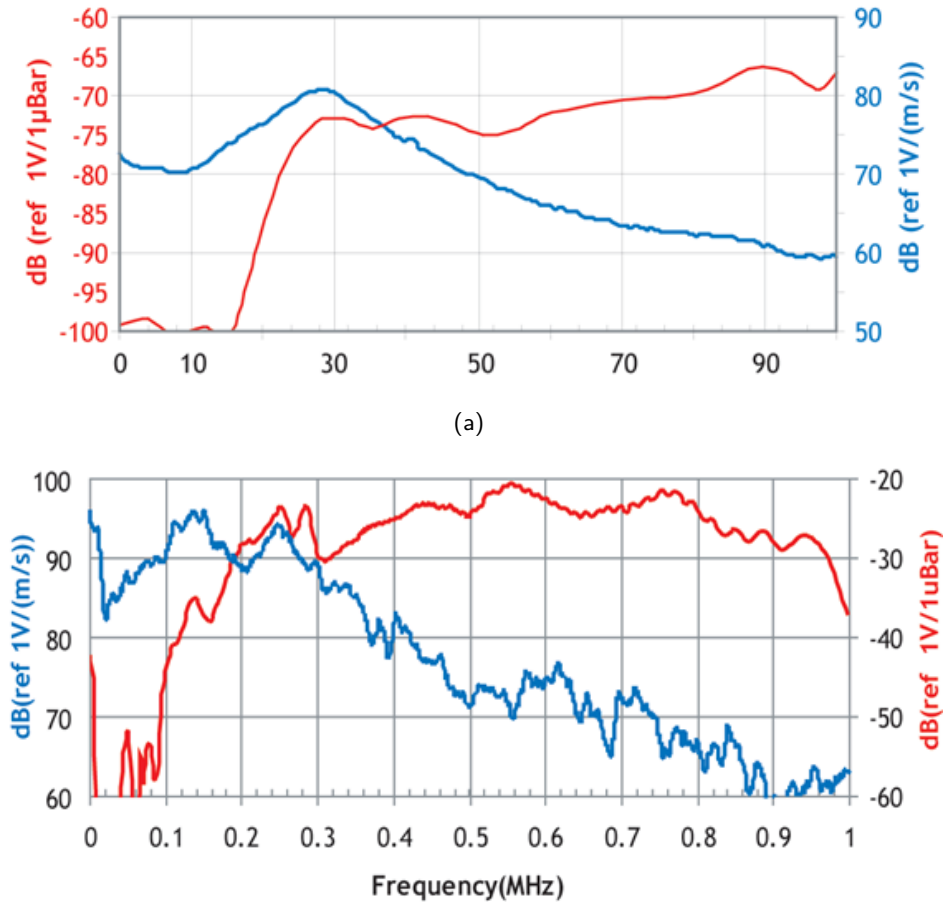

Figure 2.4: Resonant sensor versus wide band sensor (Physical Acoustics Corporation). (a) typical resonant sensor with a narrow band of sensitivity. (b) frequency characteristics of a typical wide band sensor. The red and blue lines indicate different calibration techniques (see Figure 2.5).

Types of Sensors

In terms of frequency range and transfer function, two main types of AE sensors can be distinguished:

- resonant AE sensors
- wide band AE sensors

Figure 2.4(a) and (b) show frequency characteristics of the two different sensor types. Resonant AE sensors have a narrow frequency characteristic with a significant peak at the resonant frequency of the piezoelectric element. The sensitivity at this frequency is relatively high, while other frequency bands are damped strongly. Commonly used resonant sensors have their resonance frequency between 20 kHz and 150 kHz. On the other hand, wide band sensors consist of

several piezoelectric elements, which results in a wide frequency characteristic with various small peaks. They are usually available with a more or less flat frequency response between 100 kHz and 1 MHz. This wide frequency range brings two drawbacks.

1. The overall sensitivity, also at one of the several small resonance frequencies, is considerably lower than the sensitivity of a resonant sensor.

2. The frequency response is far from being completely flat. Level differences in the recorded signal for different frequencies of more than 10 dB can occur and have to be taken into account when analyzing the frequency content of the signal.

Therefore, if the expected frequency range of the AE signal is known and no frequency domain investigations are done, resonant sensors with their resonance frequencies according to the main AE signal energy are the best choice. This is the case for many applications, for example monitoring of pressure vessels or fatigue testing of elements in civil engineering. However, if the material is unknown and knowledge about its AE source mechanisms during load are to be gained by frequency analysis, it is important to use wide band sensors.

Sensor calibration

With every purchased AE sensor there comes a calibration curve which displays the sensor's sensitivity versus frequency. Even sensors of the same type show differences in this curve. The reason for this are the complicated relationships between physical dimensions and masses of the several piezoelectric elements. There are two main procedures used for sensor calibration (Keprt and Benes 2008):

White Noise Continuous Sweep method This method (ASTM E976-84, Standard Guide for Determining the Reproducibility of AE Sensor Response) which is also known as face-to-face or reciprocity calibration is the commonly used procedure. A wide band ultrasonic emitter is coupled to the sensor (face-to-face) and stimulated with a continuous sine wave, which frequency is swept over the range of interest. The Face-to-face Technique is based on voltage output per unit of pressure input (ref 1V/μbar) and is recommended for continuous AE monitoring applications.

Transient Surface Wave Calibration Also known as step force calibration method (ASTM E1106 Standard Test Method for Primary Calibration of Acoustic Emission Sensors), this method uses a transient event (breaking of a glass capillary or a pencil lead) as excitation. These sources simulate quite well AE signals of transient character and broad frequency distribution. The metal test block should be big enough to not record any reflections from boundaries. The electrical output signal then is proportional to the speed of the surface wave where the sensor is located, thus ref 1V/(m/s)). For applications producing mainly transient AE signals, this calibration curve should be considered.

The sensor manufacturer Physical Acoustics Corporation (PAC)shows both calibration curves, it is therefore important to know the difference and, if possible, the expected character of the

AE signals in the specific application. Figure 2.5 illustrates the difference for the PAC WSα wide band sensor.

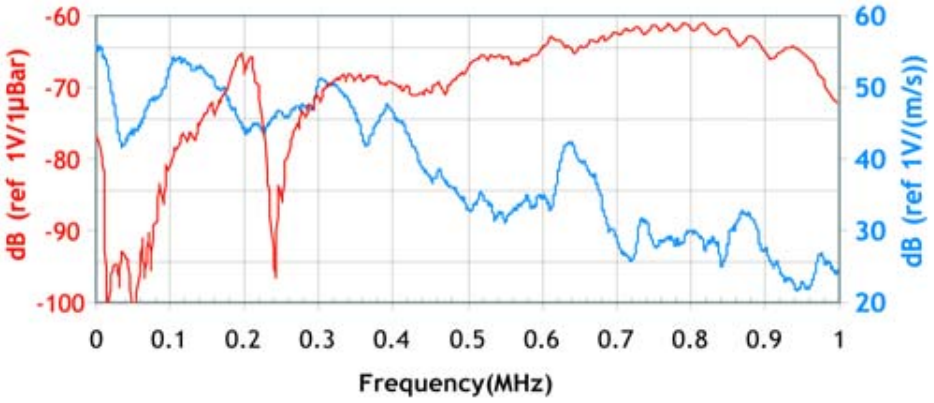

Figure 2.5: Calibration curve of the sensor WSα, Physical Acoustics Corporation. Blue line: Transient Surface Wave Calibration. Red line: White Noise Continuous Sweep method.

2.4.2 Data acquisition

Piezoelectric AE sensors transform displacement signals into low level electric voltage signals. These signals have to be amplified in order to reduce noise after the analog-to-digital converting. This is done in an analog preamplifier unit with gains usually ranging between 20 and 60 dB. A second analog processing step is a band pass filtering. This is important to avoid aliasing affects by sampling signals containing frequencies higher than half the sampling frequency. Apart from that, only the frequency range interesting for the particular application is recorded. After this analog section in the measurement chain, the signal is sampled by an analog-to-digital converter. Main requirements are good resolution, high sampling frequency and quick storing of the waveforms.

2.5 Wave propagation

Compared to usual waves in acoustics, AE waves are of special nature. AE waves are so called structure born sound waves, i.e. they propagate in solid media. Whereas inviscid fluids and gases can support only dilatational (longitudinal) acoustic waves, another form of vibrational wave, the distortional (transverse) wave, can exist in unbounded elastic solids because they can support shear stress (e.g. Fahy 2001). When AE waves reach structure boundaries, also surface waves (Rayleigh waves, love waves) occur. At boundaries inside a structure, e.g. in layered media, interfacial waves arise. This section will first describe the two wave modes in infinite media, then cover surface waves and finally conclude with considerations on important wave propagation effects.

2.5.1 Waves in infinite media

The equations of motion for displacements in a linear, elastic, homogeneous and isotropic body, known as the Navier's equations of elasticity are given as (e.g. Rose 1999):

$$(\lambda+\mu)u_{j,ij}+\mu u_{j,ij}+\rho f_i=\rho\ddot{u}_i \quad (i,j=1,2,3) \tag{2.5}$$

where

u_i = the Cartesian components of the particle displacement vector;
λ, μ = material parameters (Lamb's constants) representing elastic properties of the medium;
ρ = density of the medium; and
ρf_i = the applied force.

In scalar Cartesian notation, this represents three equations:

$$(\lambda+\mu)\frac{\partial}{\partial x_1}(\frac{\partial u_1}{\partial x_1}+\frac{\partial u_1}{\partial x_2}+\frac{\partial u_1}{\partial x_3})+\mu\nabla^2 u_1+\rho f_x=\rho\frac{\partial^2 u_1}{\partial t^2} \tag{2.6}$$

$$(\lambda+\mu)\frac{\partial}{\partial x_2}(\frac{\partial u_1}{\partial x_1}+\frac{\partial u_1}{\partial x_2}+\frac{\partial u_1}{\partial x_3})+\mu\nabla^2 u_2+\rho f_y=\rho\frac{\partial^2 u_2}{\partial t^2} \tag{2.7}$$

$$(\lambda+\mu)\frac{\partial}{\partial x_3}(\frac{\partial u_1}{\partial x_1}+\frac{\partial u_1}{\partial x_2}+\frac{\partial u_1}{\partial x_3})+\mu\nabla^2 u_3+\rho f_z=\rho\frac{\partial^2 u_3}{\partial t^2} \tag{2.8}$$

where

$$\nabla^2=(\frac{\partial^2}{\partial x_1^2}+\frac{\partial^2}{\partial x_2^2}+\frac{\partial^2}{\partial x_3^2}) \tag{2.9}$$

The vector displacement $\bar{u}$ can be expressed via Helmholtz decomposition as the gradient of a scalar and the curl of the zero divergence vector:

$$\bar{u}=\nabla\Phi+\nabla\bar{H}. \quad \nabla\bullet\bar{H}=0 \tag{2.10}$$

where Φ and $\bar{H}$ are scalar and vector potentials, respectively. This decomposition and some derivations (Rose 1999) lead to the equations:

$$\nabla^2\Phi=\frac{1}{c_L^2}\frac{\partial^2\Phi}{\partial t^2} \tag{2.11}$$

and

$$\nabla^2\bar{H}=\frac{1}{c_T^2}\frac{\partial^2\bar{H}}{\partial t^2} \tag{2.12}$$

with c_L and c_T being the velocities for the longitudinal and transverse waves respectively:

$$c_L=\sqrt{\frac{\lambda+2\mu}{\rho}} \tag{2.13}$$

$$c_T = \sqrt{\frac{\mu}{\rho}} \tag{2.14}$$

Equations (2.11) and (2.12) are independent of each other, which means that longitudinal waves and shear waves propagate without interaction in unbounded media. For practical reasons, it is convenient to exchange the Lamb's constants with the more familiar elastic constants E (Young's modulus) and ν (Poisson's ratio). Figure 2.6 and Figure 2.7 show the schematic particle motion for longitudinal and transverse waves. Longitudinal and transverse wave velocities are derived as:

$$c_L = \sqrt{\frac{E(1-\nu)}{\rho(1-\nu-\nu^2)}} \tag{2.15}$$

$$c_T = \sqrt{\frac{E}{2\rho(1+\nu)}} \tag{2.16}$$

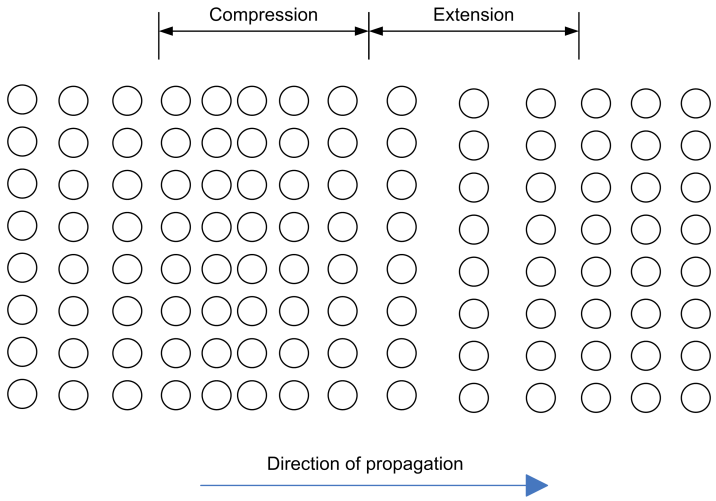

Figure 2.6: Particle motion for dilatational or longitudinal waves (Miller and McIntire 1987).

2.5.2 Waves in semi-infinite media

Whereas in infinite media only P- and S- waves propagate, several types of waves form at boundaries inside a medium or at the surface. These so-called surface waves are analogous to waves on the surface of water (Meyers 1994). Apart from that, when elastic waves encounter a boundary between two media, energy is reflected and transmitted from and across the boundary (Graff 1991). If the boundary is a free surface, a pure reflection process will occur. Generally, an incident wave is converted into two waves on reflection, a behavior which is called mode conversion. Longitudinal waves are affected as well as transversal waves, however differently in detail. In the following, the most important considerations on mode conversion are stated for longitudinal wave incident.

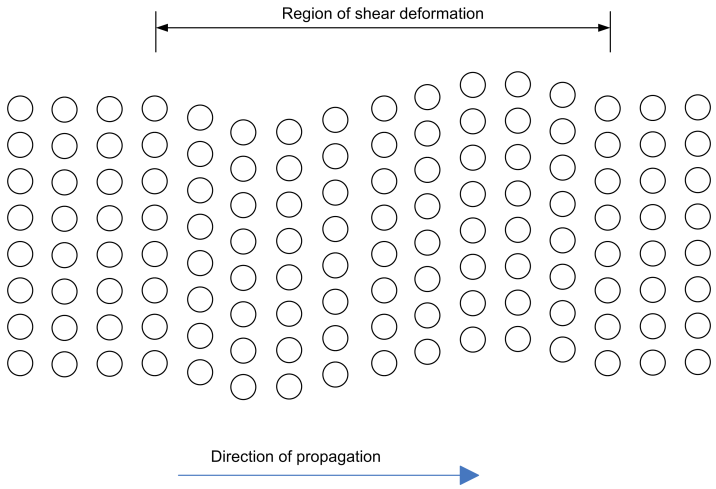

Figure 2.7: Partical motion for distortional or transverse waves waves (Miller and McIntire 1987)

Starting with the wave equation for longitudinal waves, given in equ. 2.11, its solution is

$$u_x = A_1 e^{j(kx-\omega t)} + A_2 e^{-j(kx-\omega t)}. \tag{2.17}$$

The terms A_1 and A_2 correspond to the wave in positive and negative direction respectively. Now considering the wave having an incident angle of $0°$, it can be written as

$$u_x^I = A_R e^{j(k_1 x-\omega t)} \ , \quad k_1 = \frac{\omega}{c_L^{(1)}}. \tag{2.18}$$

The reflected field can be written as

$$u_x^{(R)} = A_T e^{-j(k_1 x-\omega t)} \tag{2.19}$$

and the transmitted field in the second medium is

$$u_x^{(T)} = I e^{j(k_2 x-\omega t)} \ , \quad k_2 = \frac{\omega}{c_L^{(2)}} \tag{2.20}$$

The magnitudes of A_R and A_T are unknown. The amount of energy reflected into A_R and transmitted into A_T respectively is given by the reflection factor

$$R_{12} = \frac{W2 - W1}{W1 + W2}, \tag{2.21}$$

where W is the acoustic impedance of medium 1 and medium 2 respectively. This case of normal incident is relatively simple. No mode conversion occurs, i.e. longitudinal incident waves are reflected and transmitted as longitudinal waves and shear waves are reflected and transmitted as shear waves. However, at oblique incident angles, in analogy to optics, both reflected and refracted waves are produced. The angle of refraction can be calculated knowing the angle of incident θ_1 and the wave velocities c_1 and c_2 of both media (Snell's law):

$$sin\theta_1 c_1 = sin\theta_2 c_2 \tag{2.22}$$

Further complexity is added by the fact that longitudinal waves and shear waves travel with different velocities. A longitudinal wave may therefore be reflected and refracted as longitudinal wave and transverse wave and vice versa. This behavior is called mode conversion and is illustrated for an incident longitudinal wave in Figure 2.8. The refraction and reflection angles are given by a relationship of the form (Meyers 1994)

$$\frac{sin\theta_1}{c_1} = \frac{sin\theta_2}{c_2} = \frac{sin\theta_3}{c_1} = \frac{sin\theta_4}{c_1^{'}} = \frac{sin\theta_5}{c_2^{'}} \tag{2.23}$$

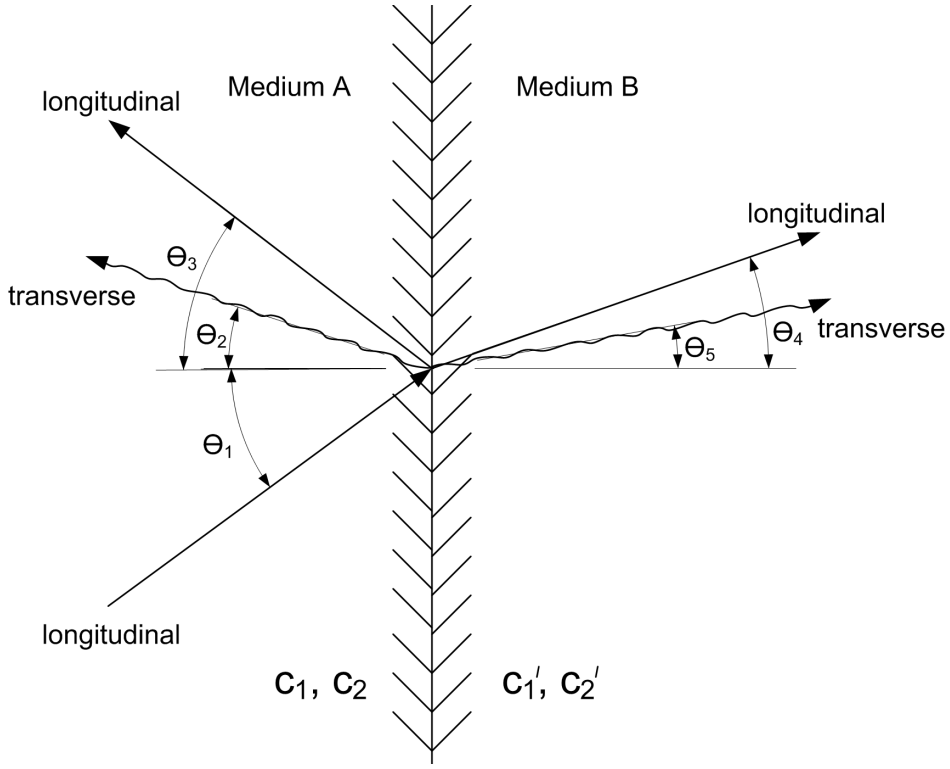

Figure 2.8: Mode conversion for an incident longitudinal wave at a boundary between media A and B. Refracted and reflected waves are produced. c_1 and c_2 are the longitudinal and shear wave velocities in medium A; $c_1^{'}$ and $c_2^{'}$ are the respective velocities in medium B (Meyers 1994).

Incident waves are refracted and reflected differently depending on the media's properties, the angle of incident and the type of wave. Therefore, several cases can be considered by applying boundary conditions on the governing equations. For detailed case studies on this topic, reference is given to Graff (1991).

Apart from mode conversion, another phenomenon adds to the complexity of wave propagation near boundaries: The presence of surface waves. Surface waves decrease rapidly with depth and

their wave speed is lower than that of body waves. The two best known and most important surface waves are the Rayleigh wave and the Love wave. The particles in a Rayleigh wave describe elliptical trajectories, as illustrated in fig 2.9. They are a particular case of interfacial waves which occur when one of the materials has negligible density and elastic wave velocity. Contrarily, Love waves show a behavior where the horizontal component of displacement can be significantly higher than the vertical component (Meyers 1994). This type of wave is important in seismology and may also occur in acoustic emission applications (Miller and McIntire 1987). It is show in Figure 2.10. More details on surface waves can be found in Graff (1991).

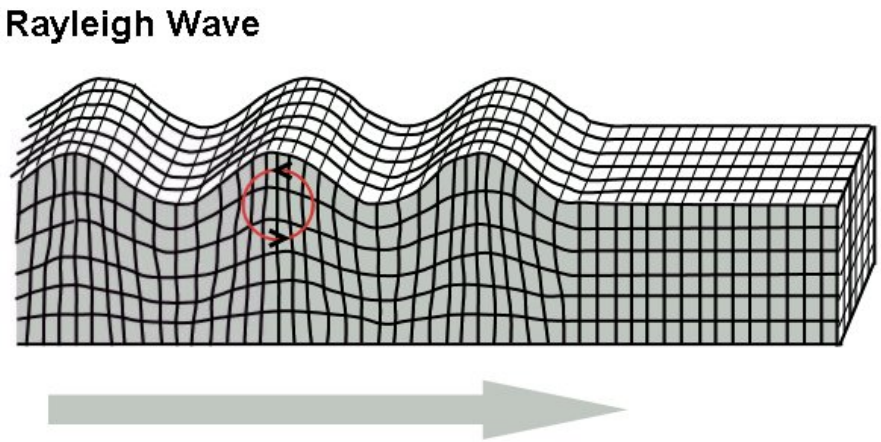

Figure 2.9: Particle motion for a Rayleigh wave.

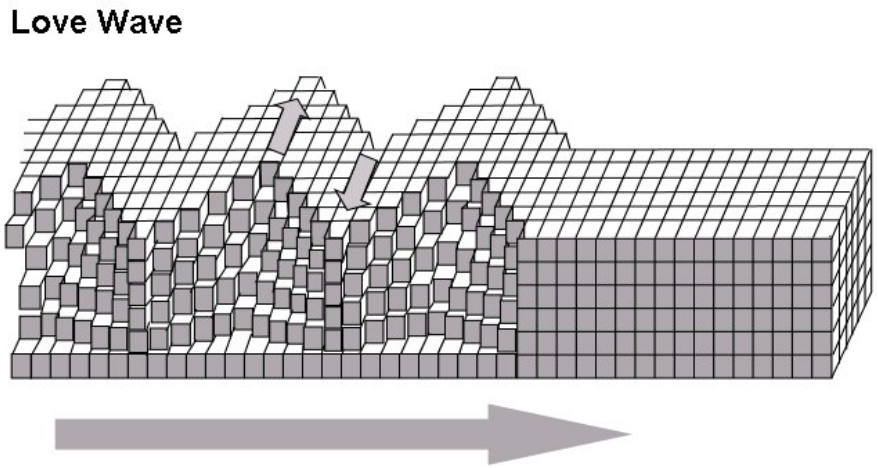

Figure 2.10: Particle motion for a Love wave.

Chapter 3

Snow characteristics and acoustic emission related to snow

In addition to general basics and theory of the Acoustic Emission technique, it is important to consider specific properties of snow and present former work on this topic. The first section will provide some insights into general properties of snow. Its viscoelastic characteristics during loading results in a load rate dependent behavior and is therefore important for the analysis of load-dependent acoustic emissions (St.Lawrence et al. 1973). Thereafter, considerations on acoustic wave propagation in snow are summarized in the next section. Finally the last part sums up conducted research on acoustic emissions of snow.

3.1 Snow characteristics

Obviously, snow is not a persistent material. Once fallen on the ground, it starts a metamorphosis all the way until its melting. Even in well controlled environments in terms of temperature and humidity, like a cold laboratory, metamorphosis takes place. Investigating the material snow thus requires knowledge of at least the most important properties of snow. According to Fierz et al. (2009) these properties are called the primary physical characteristics of deposited snow:

- Microstructure
- Grain shape
- Grain size
- Snow density
- Snow hardness
- Liquid water content
- Snow temperature

- Impurities
- Layer thickness

Amongst these parameters, grain shape, grain size, density, hardness, and snow temperature were used to characterize the snow samples investigated in the present work. In terms of snow acoustics and wave propagation in snow, snow microstructure has significant influence (Maysenhölder et al. 2008). The microstructure of snow refers to the configuration of the ice and the air spaces and cannot be reduced to a single parameter. It is given by a set of parameters, including for example density, porosity, or specific area. Thus, microstructure together with grain shape and size describes the so-called micro scale. Failure at the micro scale is being referred to as snow failure. Conversely, macro scale failure covers a big area, the failure mechanisms affecting this area are referred to as slab failure (Schweizer 1999).

As widely agreed, the release of dry snow slab avalanches requires the existence of a snow slab which is located above a weak snow layer. Most slabs consist of cohesive wind-deposited or well-bounded old snow and have hardnesses in the range of very low to high (McClung and Schaerer 1993). Dry-snow slab release starts with a fracture in the weak layer, which propagates in basal direction inside the weak layer and cause a whole block to be cut out of the snow. The hardness of the weak layer is nearly always very low. Dealing with fracture processes for the release of slab avalanches, the mechanical parameters for slab and weak layer are from spacial importance. Typical values are shown in Table 3.1:

Parameter	Typical value	Range
Slab density: ρ	200 kg m^{-3}	100-300 kg m^{-3}
Slope angle: ψ	$38°$	$30 - 45°$
Poisson's ratio (of slab): ν	0.2	0.1-0.4
Weak layer thickness: d	10 mm	1-15 mm
Slab depth (perpendicular): H	0.5 m	0.3-1m
Tensile strength/weight (slab): $\sigma_t/\rho g$	1 M Pa	0.5-10 M Pa
Young's modulus (slab): E	1 M Pa	0.5-10 M Pa
Peak strength/residual strength: τ_p/τ_r	1.5	1.25 2.0
Shear modulus (slab): G	0.5 M Pa	0.1-5 M Pa
Shear viscosity of slab: η_0	5 x 10^8 Pa s	0.5-10 x 10^8 Pa s
Shear viscosity of weak layer: η_s	0.5 x 10^8 Pa s	0.1-1.5 x 10^8 Pa s
Stiffness/peak stress (fast): G/τ_p	500	300-1000
Stiffness/peak stress (slow): G/τ_p	100	20-200

Table 3.1: Typical average mechanical parameters for slab and weak layer (Schweizer 1999).

Snow is a viscoelastic material. Whether snow shows ductile or brittle behavior depends on the load rate $\dot{F} = \frac{dF}{dt}$. Many laboratory experiments have shown that this load-rate determines the mechanical behavior (e.g. Schweizer 1998). Loading snow at a small rate results in a nonlinear

viscous behavior. At high rates brittle failure occurs, i.e. the elastic properties dominate. The transition between these two states was found by Schweizer (1998) at:

- 1 x 10^{-3} s^{-1} for snow type "small rounded particles", size $\leq 0.5mm$
- 1 x 10^{-4} s^{-1} for snow type "small rounded particles", size $\approx 1mm$

Well consolidated snow shows so-called strain softening, which means that the stress decreases after a certain amount of displacement, either until fracture occurs, or the stress reaches a residual stress (Schweizer 1998). For viscoelastic materials, the fraction behavior can be related to the type of strain. Volumetric strain causes brittle failure, distortion strain causes ductile failure. As pointed out in Chapter 2.5, snow (a solid material) has the ability to absorb both volumetric and distortion strain energy. According to Sentler (1971), the magnitude and relation between these two energy forms depend on the loading conditions.

3.2 Wave propagation in snow

Using equations 2.15 and 2.16 as well as Young's modulus E and Poisson's ratio ν, the speed of sound waves in snow can be calculated analytically. Unfortunately, snow shows a variance in Young's modulus depending on the measurement method and the snow's properties (density, texture,...) of five orders of magnitude (Mellor 1975). This fact is illustrated in Figure 3.1. Additionally, there are actually two media responsible for wave propagation in snow, the ice structure and the air between (Sommerfeld 1982). Especially for low snow densities, analytical and experimental determination of wave speeds becomes quite complex. There is also a lack of data for low-density snow in the literature.

The data shown in Figure 3.1 is valid for well-bounded snow. Young's modulus values for granular snow with low cohesion (typical conditions of weak layers) are even lower. Another way of determining the wave speed is direct measurement by recording the arrival time of a known input signal. In fact, acoustic emission techniques have been used successfully use to determine Young's modulus and Poisson's ratio. Sommerfeld (1982) summarized three sound velocity measurements depending on the snow density form different authors (see Figure 3.2). Apart from measurements, a model for wave propagation in snow was developed by Johnson (1982) according to the Theory of Biot (1962) about acoustic wave propagation in porous media. This model predicts two dilatational waves and one shear wave.

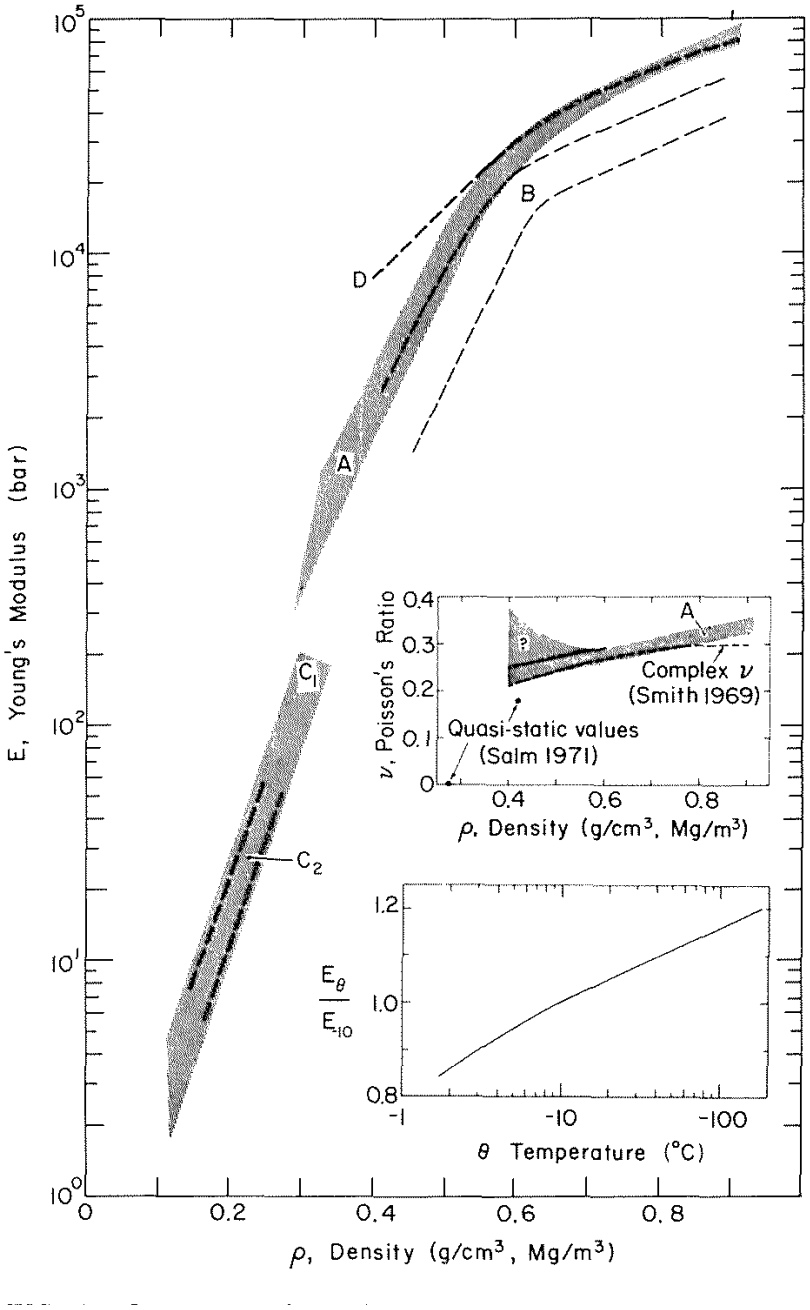

Figure 3.1: Young's modulus for dry coherent snow. (Mellor 1975). Great spreading can be examined depending on different measurement techniques and parameters. For details and citations on the different methods refer to Mellor (1975).

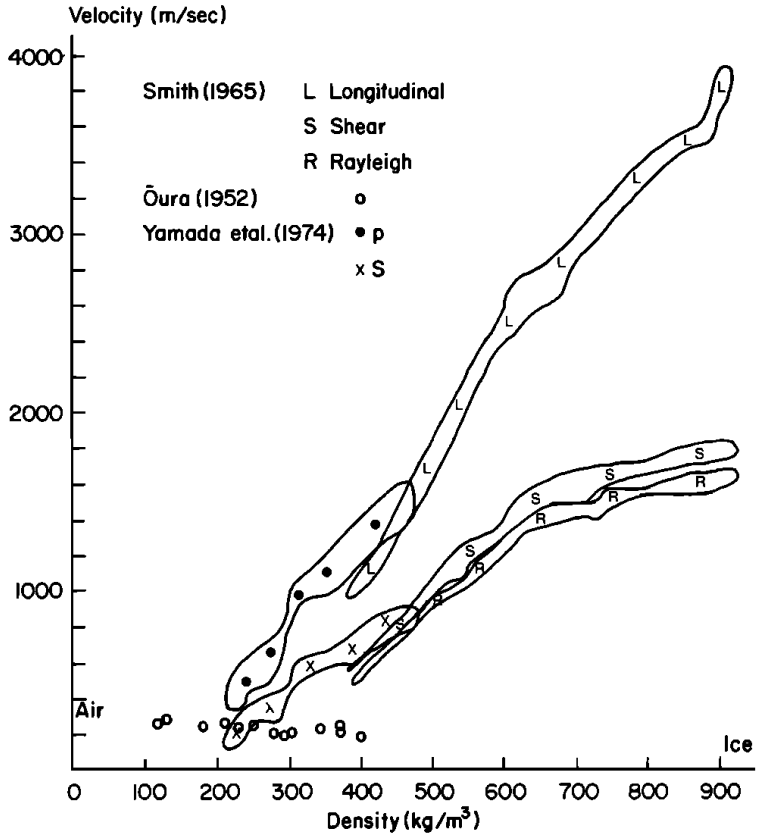

Figure 3.2: Speed of sound in snow (Sommerfeld 1982).

Whether wave transmission in snow is associated with the ice framework or the air seems to be a question of snow density/microstructure and the type of excitation (Sommerfeld 1982; Oura 1952). Whereas Smith (1965) and Yamada et al. (1974) measured motions in the ice framework, the technique of Oura (1952) was to excite and detected pressure waves in the air. As Figure 3.2 reveals, there is a great difference in wave speeds for these two techniques. Buser (1986) chose an approach to determine an acoustic impedance model of snow using an automated resonance tube. With this technique he also introduced and measured sound waves through snow in the air. His results indicated that for this kind of measurement only the air wave in snow can be observed.

In terms of modeling sound wave propagation in snow the measurements shown in Figure 3.2 were done using two different approaches. Snow was either treated as porous media consisting of a rigid ice skeleton or as a continuous elastic or inelastic medium. Both of these approaches do not adequately explain observed wave propagation phenomena in snow (Johnson 1982). Treating snow as a poroelastic material (porous media, consisting of an elastic, fluid saturated skeleton), seems the best way to model wave propagation in snow. The theory on wave propagation in poroelastic materials (e.g. water or oil saturated rocks, soil, tissues, foams), is known as Biot's theory. It was applied on snow by Johnson (1982). This model predicts a fast (first kind) and

a slow (second kind) dilatational wave as well as a shear wave. The first dilatational wave and the shear wave both correspond to measured values in the experiments where the motions of the ice framework were measured. It seems that these two waves travel through the ice skeleton. Interestingly, the slow dilatational wave of the second kind seems to travel through the air pores. Predicted speed of the slow wave and measured speed in experiments where air borne sound is sent through snow samples (Oura 1952; Buser 1986) correspond well. Obviously, an elastic wave caused by an acoustic emission event always excites the ice framework and is detected on the ice framework as well. Therefore, the presence of dilatational waves of the second kind is assumed to be negligible in this present research on acoustic emissions. Recent experiments on acoustic emissions of snow (Ernst 2009) prove this assumption.

3.3 Acoustic emissions of snow

Former research on acoustic emissions of snow can be divided into two main groups: Field experiments and laboratory experiments. The practical reason behind this discrimination is the highly frequency-dependent attenuation of snow. Therefore field experiments basically deal with low frequency signals, while the high frequency signals can be examined in laboratory experiments. Fundamental work in field experiments has been done by St.Lawrence et al. (1973), Sommerfeld (1977), Sommerfeld and Gubler (1983) and Bowles and St.Lawrence (1977). A field site instrumented with geophones has been deployed in the swiss alps since 2008. Six geophones are buried inside the snow in an avalanche release zone, one reference sensor is placed on the ground. Preliminary observations from three winters and details at the setup can be found in van Herwijnen and Schweizer (2011). Extensive laboratory work was done by St.Lawrence et al. (1973), St.Lawrence (1980), Bradley and St.Lawrence (1975) and more recently by Scapozza et al. (2004), Reiweger et al. (2010) and Ernst (2009). The latter constructed and used a special shear apparatus for load-controlled loading of snow samples. This apparatus was also used for this present research and is described in detail in Chapter 4.4.

Main concern of the field experiments was to solve the question if there is an acoustical precursor prior to avalanche release and how this precursor can be monitored without being masked by noise originating from various environmental sources. The basic parameter for signal discrimination in this context is the AE signal's frequency. Sommerfeld (1977) and Sommerfeld and Gubler (1983) worked with geophones resonant at 28 and 150 Hz respectively. In his preliminary observations Sommerfeld (1977) proposes that periods before and during avalanches were associated with high noise, while periods of known stability were associated with low noise. Conversely, Bowles and St.Lawrence (1977) observed that quiescent periods are also an indicator for snow-slope instability. As St.Lawrence (1980) summarizes, one is faced with contradictory observations indicating the same result, a problem which is similar in nature to the problem with earthquake prediction. Swarms of smaller precursor events may be followed by a large earthquake but large earthquakes also occur without any precursor. Mathematically spoken, acoustic emission activity

is basically neither a necessary nor a sufficient requirement for avalanche release. In order to increase knowledge about the processes inside the snow pack, emphasis was placed on discrimination of the acoustic emission signals. In the very low frequency range of 1-30 Hz, Sommerfeld and Gubler (1983) discriminated the acoustic emission into two groups:

1. Type I signals: Spikes that originate from macroscopic cracks
2. Type II signals: Signals that may originate from differential movement on shearing planes

This type of discrimination was already known from seismic investigations of glaciers (Dewart 1968) and also previously observed in snow (St.Lawrence and Bradley 1977). St.Lawrence (1980) covered a wider frequency range and related low frequency signals to general instability. Fractures indicated by these signals can lead to major failure, but if they do not, they locally reduce the strain energy available for fracture (strain softening). This is an explanation for the contradictory observations described above. Signals in the ultrasonic frequency range (>20kHz) are said to indicate fracture at a scale which involves single grains, similar to processes observed in polycrystalline ice (Gold 1960). An interesting practical point ha been worked out by St.Lawrence (1980) concerning the relationship of frequency range, size of failure and detectable scale. The higher the signal's frequency, the smaller the fracture size and the smaller the distances where acoustic signals can be measured. Therefore the investigation of the ultrasonic signals is still restricted to laboratory scale and the connection between micro- and macro scale (i.e. laboratory and field experiments) is a great challenge.

As pointed out in section 3.1, from the mechanical point of view strain and stress (loading) rates are the most decisive factors determining if ductile or brittle failure of snow occurs. Catastrophic failure without any acoustic emission precursors is evidence of a purely brittle fracture. The transition region between ductile and brittle behavior is the investigated region in former laboratory research. The most recent experiments of Reiweger et al. (2010); Ernst (2009) as well as those of this work examine stress induced behavior, Scapozza et al. (2004) carried out strain induced experiments and St.Lawrence (1980) derived the first models for both stress and strain induced strain based on the form:

$$N = N(\sigma, \epsilon, T, s) \tag{3.1}$$

N is the number of acoustic emissions per unit volume of material, σ is stress, ϵ is strain, T is temperature and s is a variable related to the structure or texture of the snow. Emphasis was placed on getting insight into slope stability and acoustic emission response. In this model, ultrasonic acoustic emission activity generally indicates stability. Only if avalanche activity is associated with an accelerating creep phenomenon this may not be true. Accordingly, major failure can take place if the stress on a snow slope exceeds some critical value and is held on this level.

In terms of failure mechanisms, it seems quite certain that a major failure leading to avalanche release is associated with brittle failure. Recent laboratory measurements by Scapozza et al.

(2004) also indicate this relationship. He reports that brittle failure is characterized by low-frequency acoustic emissions, produced by large crack formation originating in material flaws. His spectral analysis of acoustic emission waves with various sensors showed that AE signals show energy in a wide frequency range, depending on the type of failure. Peak frequencies of 500 kHz were observed during ductile deformation and can thus be associated with bond breaks. During brittle failure, peak frequencies were spread over a range of 30 to 100 kHz.

Chapter 4

Experimental setup

Having covered theory and basics of AE, this Chapter describes how the particular experiments were carried out. The first section provides general information on the complete setup. Snow and process parameters will be discussed in section two and three. The fourth section presents the shear apparatus before finally the acoustic emission measuring system is described.

4.1 General information

All the measurements were taken in the cold laboratories at the WSL Institute for Snow and Avalanche Research SLF in Davos. The temperature in the laboratory was set to $-5°$. Problems with a transient spike-like noise produced by a valve in former research at the institute (Scapozza et al. 2004; Ernst 2009) were avoided by transferring the apparatus and peripheral devices into a different cold chamber. Still, artefacts in the data by measuring extrageneous noise always have to be considered. Parameters influencing the mechanical processes inside the snowpack and subsequently the acoustic emission response are given either by the snow sample's properties or the setup of the apparatus. Therefore these parameters are distinguished into snow parameters and process parameters. Output of the shear tests are also process parameters (displacements) and the AE parameters (see Figure 4.1).

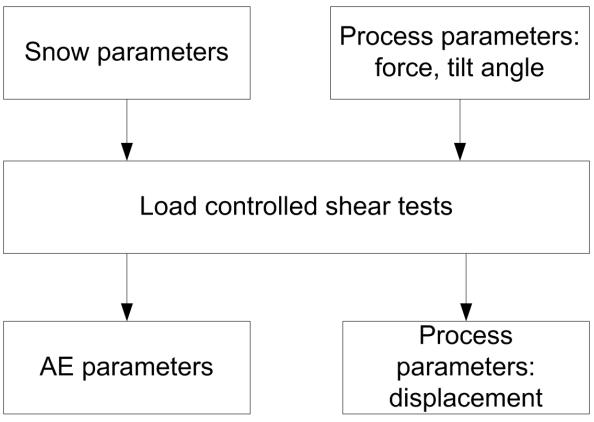

Figure 4.1: Load controlled shear tests, input and output.

A schematic of the complete test setup is shown in Figure 4.2. Pressure is applied on snow samples mounted on a ground plate with adjustable tilt angle, simulating natural loading mechanisms of snow (force F). The tilt angle controls the magnitude of shear stress inside the snow sample. The displacement in x- and z- direction were measured with potentiometric displacement transducers. The data set is divided into process parameters $(F, \phi, \Delta x, \Delta z)$, classical AE parameters (amplitude, energy, duration etc.) and frequency parameters (peak frequency, centroid etc.). Additionally, snow parameters like density or hardness determine the most pregnant snow properties.

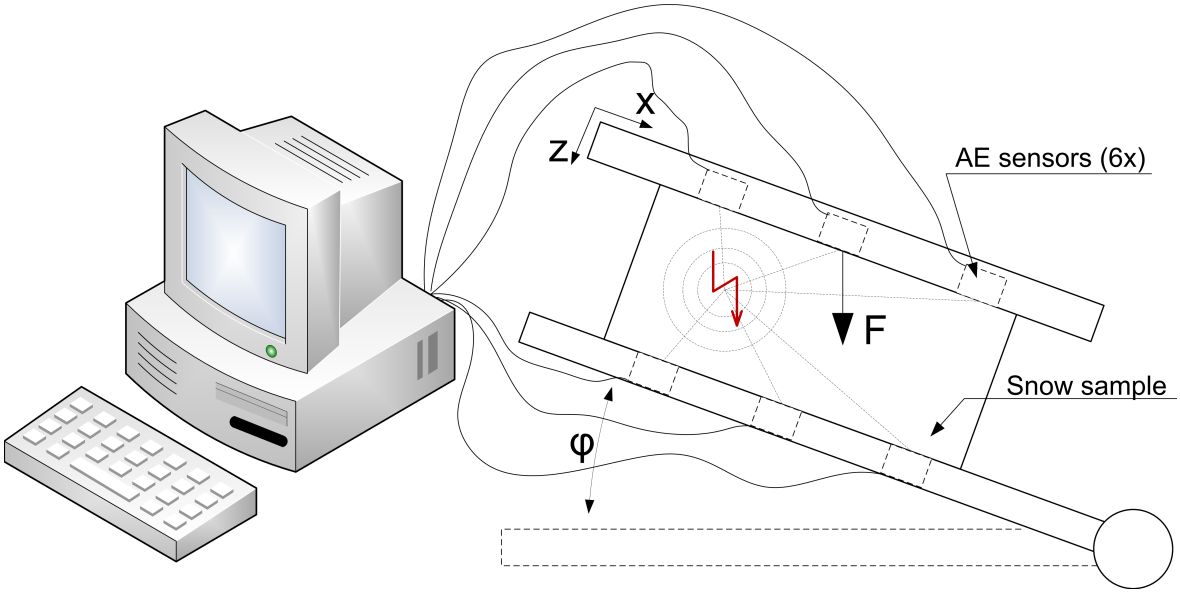

Figure 4.2: Schematic test setup. A snow sample is placed between two plates with six acoustic emission transducers which have direct contact to the snow surface. The tilt angle ϕ determines the shear stress inside the snow sample. Process parameters (force F and displacement in x- and z-direction) and acoustic emissions were recorded and analyzed on a measurement PC.

4.2 Snow samples, preparation and parameters

The experiments took place during winter, so natural snow from outside could be used for the sample preparation. In terms of snow structure two basic types of snow samples were investigated:

Homogeneous snow samples: These were samples with uniformly distributed mechanical and acoustical properties. The natural snow was sieved into a wooden box in the cold laboratory. After that it was compacted and left to sinter for several hours to days, depending on the desired hardness. Homogeneous snow is rarely present in nature, since a natural snowpack always reflects precipitation periods and metamorphosis. These natural processes produce various layers with different properties of great spatial and temporal variability. Obviously, for basic research this behavior creates complex problems of unknown wave propagation

characteristics. Therefore, it was convenient to start research with homogeneous samples.

Layered snow samples: This type of samples consisted of a weak layer between two relatively dense top and bottom layers (Figure 4.3). The weak layer contained large faceted crystals with low hardness. This structure is similar to natural weak layers, responsible for dry-snow slab avalanches. The top and bottom layers were produced similarly to the homogeneous snow samples described above. The weak layer was produced in two different ways:

1. By applying a strong vertical temperature gradient (Fukuzawa and Narita 1992; Reiweger et al. 2010). These samples are in later section denoted as DHA (depth hoar artificial). This technique is close to nature and produces very soft weak layers. The drawback for AE testing is the very high acoustic damping of the resulting snow structure (very large faceted crystals with high porosity). This was especially a problem for the localization experiments, since it was hard to receive proper signals on the minimum required four sensors.
2. By taking natural depth hoar (DHN) and placing it manually between the two outer layers. The layers are by far not as weak as the DHA layer. The faceted crystals lose their dangerous arrangement and sinter quite fast, gaining stability. Still, they represent a significantly weaker zone and the acoustic damping is reduced. Localization experiments were therefore carried out with DNH samples.

One basic step in the snow sample preparation was common for all types of samples: As mentioned above, samples were never cut out of a natural snow pack and tested directly because the exact stratification remains unclear in this case. Instead, the snow was sieved through a 2 mm grid sieve into special wooden boxes before applying uniform pressure on the snow. This pressure causes the snow to sinter similar to a natural snowpack. The advantage is highest possible isotropic and uniform mechanical character of the samples, which is a vital requirement to produce meaningful measuring results. Apart from that, the resulting snow density and hardness can be controlled quite easily by varying the pressure and sinter time. Higher pressure increases density and hardness. Additionally, the longer the sinter process, the more bonds can form, which increases stability.

4.3 Process parameters

The parameters described in the last section refer to the properties of the used snow samples as variable input parameters. According to Figure 4.1, process parameters are partly input into the system (force F and tilt angle ϕ) and partly output (displacements in x and z direction). Applying a force and observing the resulting displacement is the nature of load-controlled tests. Compared to the opposite technique where given displacement is the input and the load is measured, this is closer to real loading of snow in nature. The load was increased either until the sample ruptured or until certain values where reached. In this case, also the distribution of AE activity and displacement could be examined for example holding a constant force. The tilt angle ϕ (compare

Figure 4.3: From the mountains into the cold lab: (top) dry-snow slab avalanche (Totalphorn, photo: R. Pajarola), (bottom left) natural weak layer (photo: I. Reiweger), (bottom right) artificial weak layer produced in the cold laboratory.

Figure 4.2) controlled the amount of shear stress in the sample. A tilt angle of 0° means that no shear component is present inside the snow, hence it refers to compressional tests. Apart from that, tilt angles were varied up to 30°, producing considerable shear stress. The exact magnitude of shear stress on the sample can be derived by multiplying the applied vertical stress with $\sin(\phi)$ (Reiweger et al. 2010).

The load was measured continuously by means of a load cell with analog output. The displacements were also measured continuously by using potentiometric displacement sensors driven with a DC supply voltage. The output voltage was amplified and mapped to the sensor's displacement range (0-80mm). For details on sensor placement and recording see Chapters 4.4 and 4.5.2.

4.4 Shear apparatus and sensor coupling

The shear apparatus used for this experiments has been designed and built at the institute SLF (Ernst 2007). Figure 4.4 shows a schematic of the loading apparatus and a photograph of a snow

sample in the apparatus form previous research (Reiweger et al. 2010). The sample is placed between a bottom and a top plate. The top plate is the element which applies an equally distributed load on the snow sample, similar to the mass of new snow lying on older snow. In order to constantly increase the load, the top plate is pulled down vertically by a water tank attached to the plate via wire ropes. This tank corresponds to the schematic mass in Figure 4.4. By opening a valve, a fluid runs down into the tank increasing its mass. The aperture angle of this valve thus determines the loading rate on the snow sample.

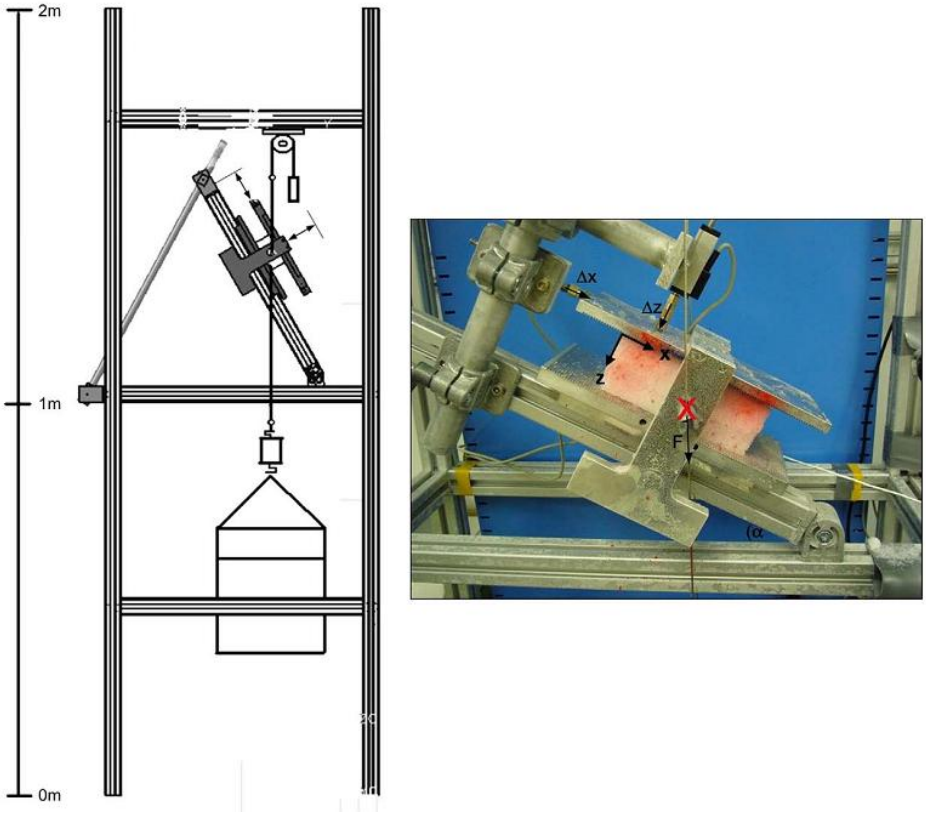

Figure 4.4: Schematic of the loading apparatus and photograph of a snow sample in the apparatus. α denotes the slope angle, F is the force acting on the snow sample, and Δz and Δx denote the compressive and shear displacement of the upper plate (Reiweger et al. 2010).

Intensive research and modifications were performed on the design of bottom and top plate, later in this section also called pressure plates. In the beginning of this study, experiments were conducted with metal plates, similar to earlier work with the apparatus. An advantage of these plates was that closed linkage between snow sample and plates was achieved easily by slightly warming the plates as well as the sensors. Especially for tests with large slope angles, this linkage is very important in order to not measure noise from friction between plates and snow sample.

However, tests on three-dimensional localization with the metal plates yielded suboptimal results, which were assumed to be related to the metal's low acoustic impedance (see Chapter 5.3). Therefore, plates made of polystyrene and a rigid foam plastic were tested and yielded much better results. These plates are shown in Figure 4.5, including the six sensors for three-dimensional localization. Using three sensors each in the bottom and top plate was a compromise between feasibility and performance. Best localization performance would have been achieved by placing one sensor on each of the six sides of the sample. The test setup with oppositely arranged sensors also showed good performance and was much less time-consuming. Slightly worse results in terms of localization and accuracy were especially observed for AE emission events occurring in regions near the samples face sides.

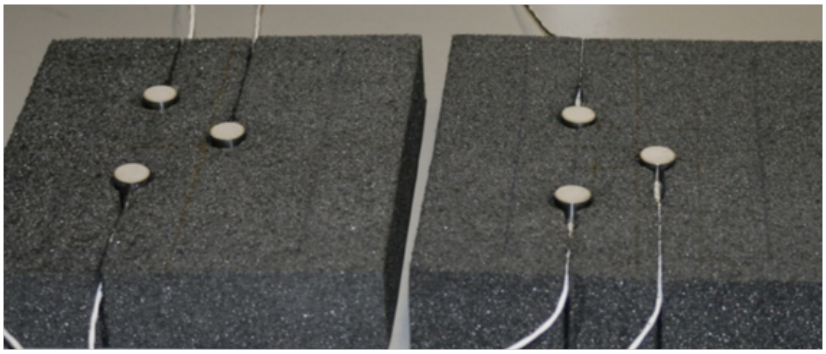

Figure 4.5: Foam plates designed for three dimensional localization tests. Three sensors were bedded inside each plate and had contact to the snow sample with decent pressure.

Apart from the sensor position in the plates, also the way of bedding the sensors inside the plates was subject to several variations. Fig 4.6 (a) shows the basic design from earlier research at the institute. The sensors were placed in a drill hole with slightly bigger diameter than the sensors and held in place with a fixing screw. However, the resulting direct low-impedance connection from the snow to the sensor housing via plate and screw could lead to systematic errors, especially for localization algorithms (Joachim Sell, Physical Acoustics Corporation, personal communication). A first improvement was done by widening the drill hole's diameters and placing pieces of foam between plate and sensors in order to achieve proper decoupling (Figure 4.6 (b)). Still it was necessary to hold the sensors in place with a screw, which again was assumed to be a possible low-impedance acoustic path and thus a short-circuit for the acoustic waves. The production of a new type of plates made of a rigid foam material allowed for bedding the sensors directly inside the plates (Figure 4.6 (c)) which improved sensor coupling.

Sensor coupling is a delicate part in acoustic emission testing. For snow, a special technique for the coupling of acoustic emission transducers was used successfully in previous research (Scapozza et al. 2004; Reiweger et al. 2010). This technique involves two steps. First the sensors are heated slightly above 0° C by means of an industrial hot air gun. After that, the sensors are pressed

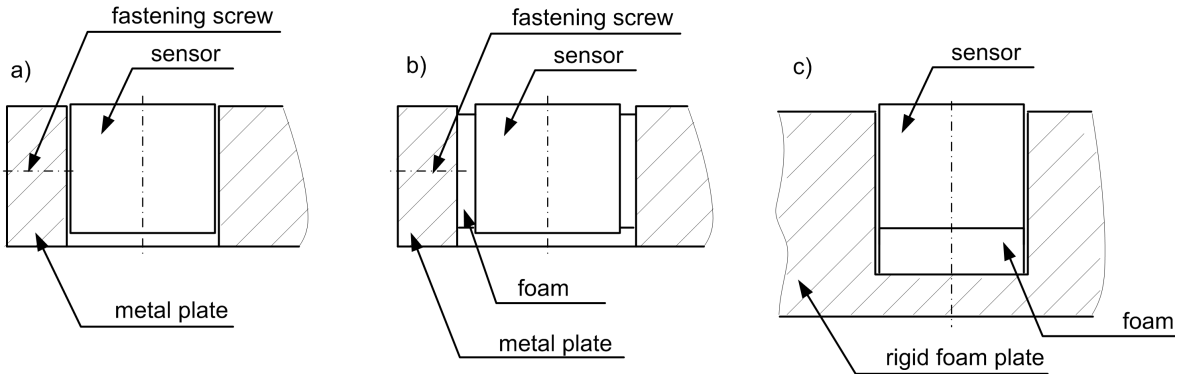

Figure 4.6: Variation of pressure plates and sensor bedding. (a) metal plates, sensors directly in contact with the plate and fixed with a screw. (b) metal plates with sensors decoupled by foam and fixed with a screw. (c) plates made of rigid foam material. The sensors are bedded elastically inside the plates.

decently on the snow surface . A thin ice layer develops between sensor and snow surface, ensuring a mechanically rigid low impedance connection. As mentioned above, the placement of the six sensors inside the pressure plates was a practical consideration. Sensor positions are well defined within the plates and by placing the snow sample between bottom and top plate, the sensor coupling is done automatically. In the metal plates, the sensor's wear plate surface was aligned with the plate's surface. Problems with this design arose when snow samples were not completely in touch with the sensor plate. Air between snow surface and sensor of less than 1 mm was enough to destroy proper coupling. For the foam plates, this problem was solved by bedding the sensors elastically (4.6 (c)). The positive effect of this technique is depicted in Figure 4.7.

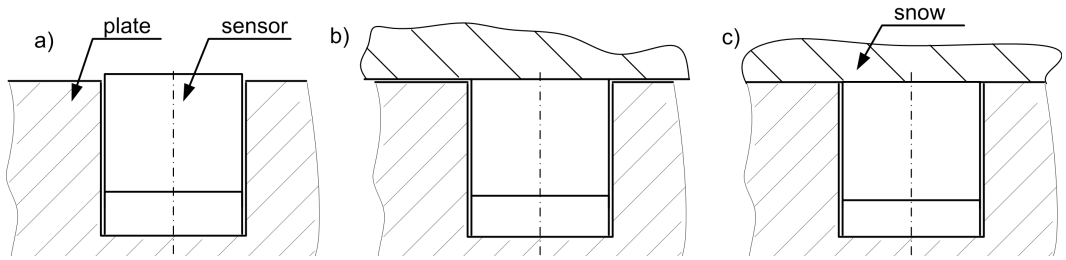

Figure 4.7: Sensor in the foam plate: (a) initial state without snow sample. (b) snow sample not resting on the plate properly producing air space between plate and and snow. The elastic bedding design still ensures connection between sensor and snow. (c) snow sample resting properly. Sensor and plate are aligned.

4.5 The acoustic emission recording system

The measurement's central element besides the loading apparatus was a six channel acoustic emission measurement system supplied by Physical Acoustics Corporation. The system consisted

of wide band piezoelectric AE transducers, preamplifiers, a personal computer and the recording- and analysis software AEwin. The recording devices (three 16 bit 40 MSamples PCI2 A/D cards) allowed for real time waveform acquisition and feature extraction. Apart from the six AE channels, additional process signals could be recorded with the help of four parametric analog inputs. The sampling frequency for the AE channels was set to 5 M Samples/s, since the expected AE signal frequencies were not higher than 1 MHz. According to Shannon's sampling theorem, a sampling frequency of 5 MS/s is well within the criterion, but not too high in order to keep the amount of data low. The band pass parameters in the analog front end were comprehensibly set to 20 kHz and 2 MHz. The analog gain for the preamplifiers was set to the maximum value of 60 dB, ensuring adequate amplification of the very low level signals. During the end of the experiments, also tests with 40 dB gain were carried out successfully. Fig 4.8 shows a basic block diagram of the AE system along with the chosen parameters.

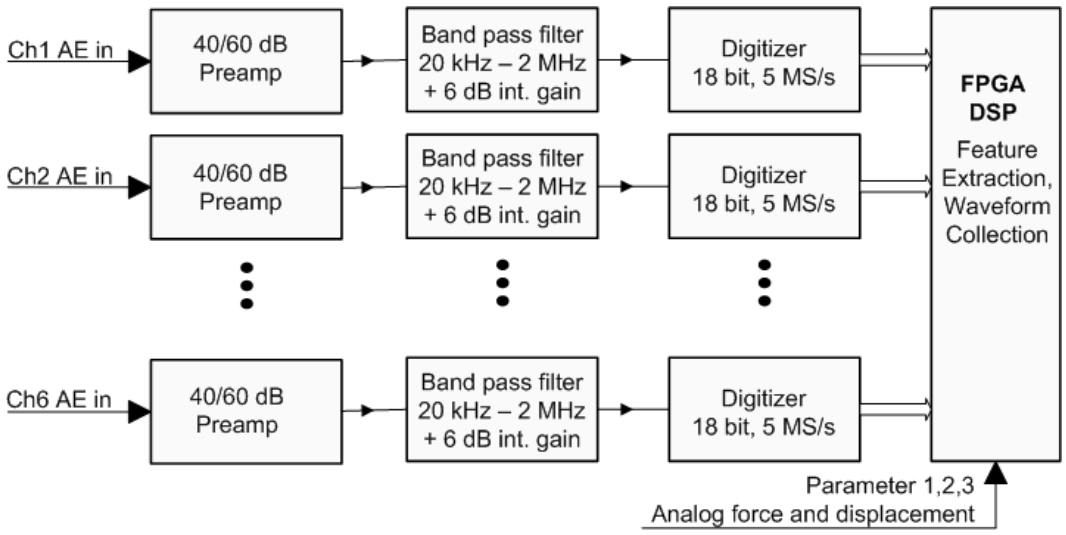

Figure 4.8: Six channel acoustic emission measurement system, basic block diagram description.

The maximum input voltage for the analog-to-digital converter (ADC) is 10 V. Physical Acoustics standard is to declare a maximum signal amplitude U in dB relative to a reference voltage of 1 μV and preamplifier gain G of 40 dB:

$$U(dB) = 20\,log\,(\frac{U_{max}}{1\mu V}) - G \tag{4.1}$$

Accordingly, Physical Acoustics documentation refers to a maximum signal amplitude of 100 dB AE and 99 dB ASL. The 6 dB internal gain on the DAQ cards was added to the preamplifier gain on Physical Acoustics recommendation. Hence, the maximum signal amplitudes reduces to 93 dB ASL and 73 dB ASL for 40 dB and 60 dB respectively.

4.5.1 Sensors and preamplifiers

Signal-based acoustic emission analysis requires sensors with frequency characteristics as wide and flat as possible (Grosse and Ohtsu 2008). As pointed out in Chapter 2.4.1, it is not possible to design transducers with a completely flat frequency response. The best compromise between flatness and sensitivity for signal-based AE analysis was found for the Physical Acoustics Corporation WD sensors. These sensors have an operating frequency in the range of 100 - 900 kHz and peak sensitivities of 55 [1] or -62.5 [2] dB respectively. The operating temperature ranges from -65 to 70°C. Figure 4.9 shows the frequency characteristics of the Physical Acoustics WD sensor. The specific characteristics of all the six sensors can be seen in appendix A. Although they are quite similar especially in terms of resonances, there are some significant variations which cannot be avoided. Therefore each sensor is calibrated before shipment and comes with its own certificate.

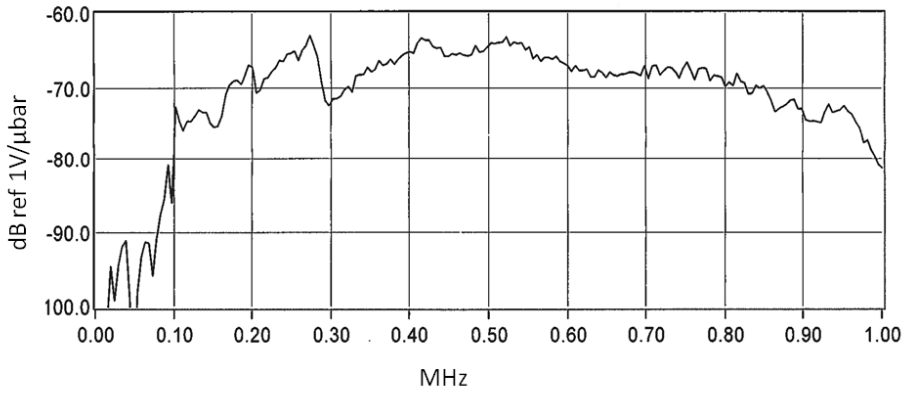

Figure 4.9: Frequency characteristics, AE transducer WD (Physical Acoustics Corporation).

4.5.2 Data acquisition unit and software

The following listing summarizes the main components and technical data of the AE system:

Transducers Physical Acoustics Corporation WD transducer. Dimensions 18(dia) x 7(height). Operating temperature -65 to 177°C. Operating frequency 100-900 kHz.

Preamplifiers Physical Acoustics Corporation 2/4/6 voltage preamplifier. Gain 20/40/60 dB (switch selectable). Output signal up to 20 V_{pp} into 50 Ω.

Recording the AE parameters

Signal-based acoustic emission techniques implement recording and storing entire AE wave forms. These wave forms may contain high frequencies, a fact which requires high sampling rates. With the used AE emission recording system, sampling rates of 15 MSamples/s can be realized. As

[1] Denotes response to surface waves (angle of incidence transverse or parallel to face of sensor).
[2] Denotes response to plane waves (angle of incidence normal to face of sensor).

stated in the beginning of this section, a sample rate of 5 MSamples/s was set for this present experiments. In combination with excellent resolution of 18 bit, huge amount of data is produced. Therefor it is vital to detect and store only the significant wave forms. A basic parameter determining start and end of recording is the threshold level, described in Chapter 2.2.1. The maximum time possible to record is determined by sampling rate and length of sampling window. Since brittle rupture processes in snow produce long AE signals, the maximum length l of 15 k (k = 1024) samples was chosen. Thus, the maximum recording time is derived by

$$t_{max} = \frac{l}{f_s} = \frac{15 \cdot 1024}{5 \cdot 10^6 s^{-1}} = 3.072 \cdot 10^{-3} s \tag{4.2}$$

Beginning of recording is triggered with the first positive or negative threshold crossing. Earlier termination of recording before the maximum value is controlled by three timing parameters in combination with the threshold level (PAC 2007):

1. Hit definition time (HDT). Correct HDT ensures that one recorded hit exactly corresponds to one AE event. One does not want to record several events as one hit, neither is it intended to record one AE event as several hits. HDT starts with every threshold crossing in the signal and only terminates when no threshold crossing is detected during the HDT period. This also terminates recording and defined the end of the signal.

2. Peak definition time (PDT): The function of PDT is to enable determination of the time of true peak of the AE waveform. It is triggered by new signal maxima and terminates recording when no new maximum is detected during the PDT period.

3. Hit lockout time (HLT): The HLT inhibits the measurements of reflections and late-arriving parts of the AE signal, hence, data from wave arrivals can be acquired at a faster rate.

Recording the process parameters

Apart form the acoustic emission signals, external process parameters could be recorded via several analog inputs on the data acquisition card. The voltage input range was between 0 and 1 V. The signals could be scaled and compensated with an offset value in order to derive the physical value from the voltage signal. Assuming linear behavior for the load cell as well as the potentiometric displacement sensor, the scaling was done by several comparative measurements. External process data could be recorded either hit-driven or time-driven. Hit-driven means that every recorded acoustic emission hit triggers sampling of an external parameter. Time-driven data is sampled at constant time intervals between 10 ms and 1s. For this present experiments, time-driven sampling was chosen at a sampling rate of 100 Hz.

Chapter 5

Results and discussion

This chapter is divided into three sections. The first section on signal classification will concentrate on occurrences and properties of both the "classical" parameters and the frequency related parameters. Signal patterns in both categories are combined in order to draw a picture on classifying different AE signals and their origins. Thereafter, load-displacement-AE relations are shown versus test time and results on the three-dimensional localization experiments are presented.

5.1 AE parameters and Signal classification

5.1.1 Overview

In order to give an impression of the range of the significant AE signal parameters, this section will show histograms which show the distribution of the most common classical and signal-based parameters. The data is taken from four measurements with different snow properties, tilt angles and load rates (see Table 5.1). Emphasis will be placed on the numbers of hits and counts along with their amplitudes and energies, because these values are often used as the first criterion for material failure (e.g. Miller and McIntire 1987). In addition, signal parameters like duration or rise time are investigated, since they are very useful to distinguish different source mechanisms (Pollock 2008). The spectral parameters (peak frequency, frequency centroid) are mainly assessed in combination with the classical parameters. Especially for materials which are hard to characterize and of time-variant nature, this is important to avoid misleading conclusions.

Meas.	Snow	ϕ	$\dot{\sigma}$	Amp.	Rupt.
Hom1	Homogeneous 200x46x120 mm, ρ = 378 kg/m^3, RGlr 0.5 - 1 mm, hardness 4 (hard, pencil)	10°	89.58 Pa/s	40 dB	No
Hom2	Homogeneous 120x40x90 mm, ρ = 262 kg/m^3, RGlr 0.25 - 0.5 mm, hardness 4 (hard, pencil)	0°	73.15 Pa/s	60 dB	No
Hom3	Homogeneous 120x50x90 mm, ρ = 196 kg/m^3, RGlr (DFdc) 0.5 - 1 mm, hardness 3 (medium, 1 finger)	20°	18.52 Pa/s	60 dB	No
DHN1	Layered 200x66x120 mm, Outer layers: ρ_{ol} = 417 kg/m^3, RGlr 0.5 - 1 mm, hardness 4 (hard, pencil). Weak layer: ρ_{wl} = 200 kg/m^3, FCxr (DHxr) 2 - 3 mm, hardness 2 (soft, 4 fingers)	20°	104.58 Pa/s	60 dB	Yes

Table 5.1: Set of displayed measurements for signal classification with Details on snow and process parameters: Samples' dimensions are given in the form length x height x width. The codes for the morphological snow classifications are in accordance with Fierz et al. (2009): RGlr means "large rounded grains", DFdc stands for "partly decomposed precipitation particles", FCxr for "rounded faceted particles" and DHxr for "rounding depth hoar". In case there is a second grain type in brackets, the first one is the primary and the one in the brackets the secondary type. The code for the grain type is followed by the crystal's diameter. ϕ denotes the tilt angle and $\dot{\sigma}$ the normalized load rate corresponding to the sample areas , given in Pa/s. The right column indicates if the sample ruptured or not.

Table 5.1 includes details of the four measurements with both snow parameters and process parameters varying. The goal of this approach was not to obtain statistically significant findings, but to show a wide section of different measurement progressions and the associated AE parameters. The load and displacement characteristics for the four chosen measurements are shown in Figure 5.1. The displacements in x- and z- direction are geometrically combined in a resulting displacement in order to reduce complexity.

5.1.2 "Classical" signal parameters

Counts and hits versus amplitude/energy

AE hits and counts display the general acoustic emission activity (compare Chapter 2.2.1). First, the distributions of hits and counts versus signal amplitude are compared from a high strength homogeneous snow sample (Hom1) and a low strength weak layer sample (DHN1) which ruptured during the test. The corresponding three figures (5.2 to 5.4) concentrate on the distribution of hits and counts versus signal amplitude. No obvious time and load relationship can be examined. However, the impact of catastrophic failure on AE parameters is showed by presenting different periods of the same measurement. The upcoming figures on counts and hits versus signal am-

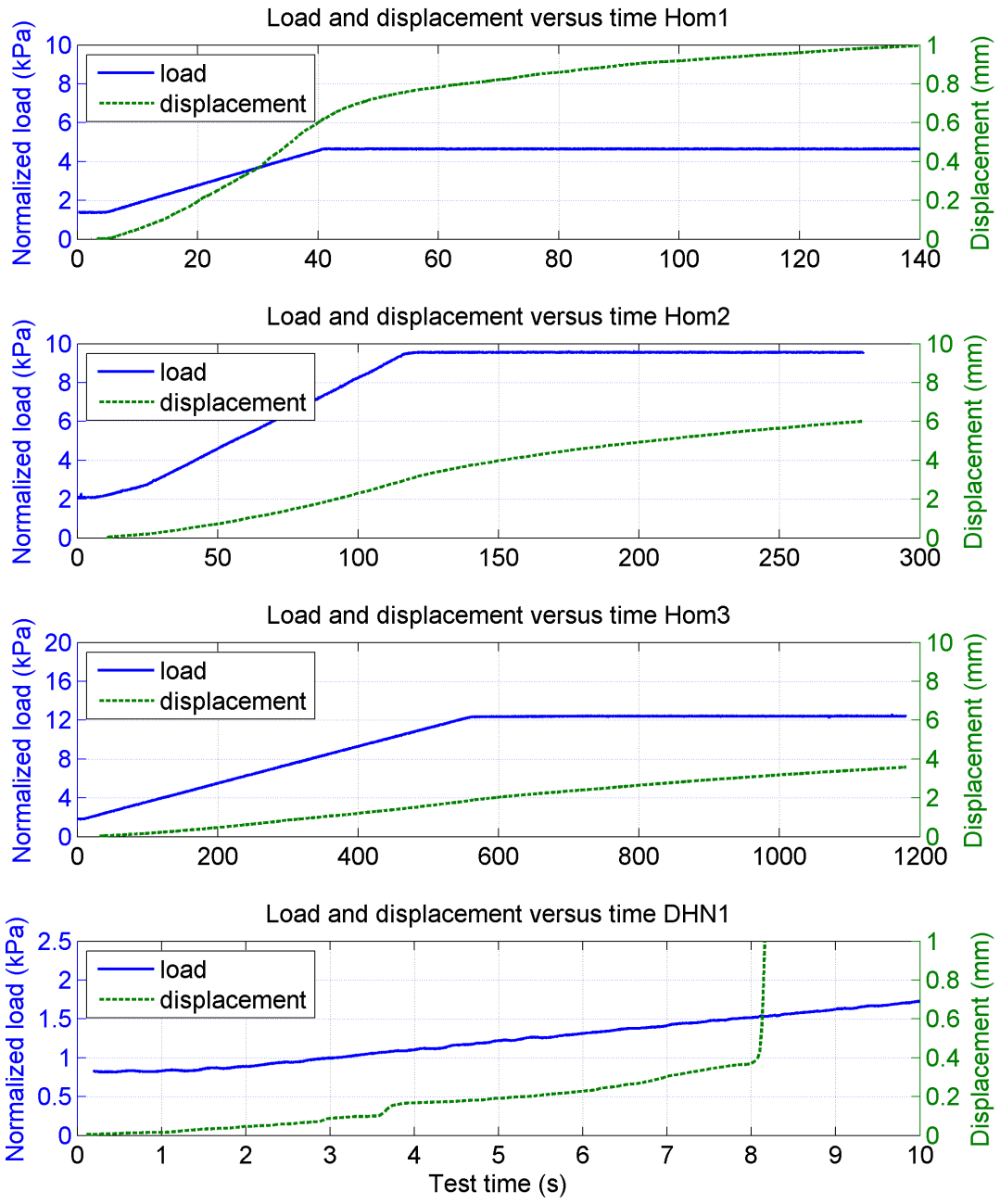

Figure 5.1: Set of displayed measurements for signal classification: Load and displacement characteristics.

plitude are equally assembled: The top plot is a point plot where one point represents one hit at the corresponding values "number of counts" and "amplitude". The advantage of this type of diagram is that dominant hits can be seen and examined easily. The obvious drawback is that no information about the frequency of occurrence can be extracted for the areas with many hits. Therefore, the same data is presented as a histogram in the middle plot, where the height of each bar corresponds to the number of counts at each discrete amplitude level. Finally, the bottom plot is as well a histogram, showing an equally constructed distribution of the number of hits for each amplitude level.

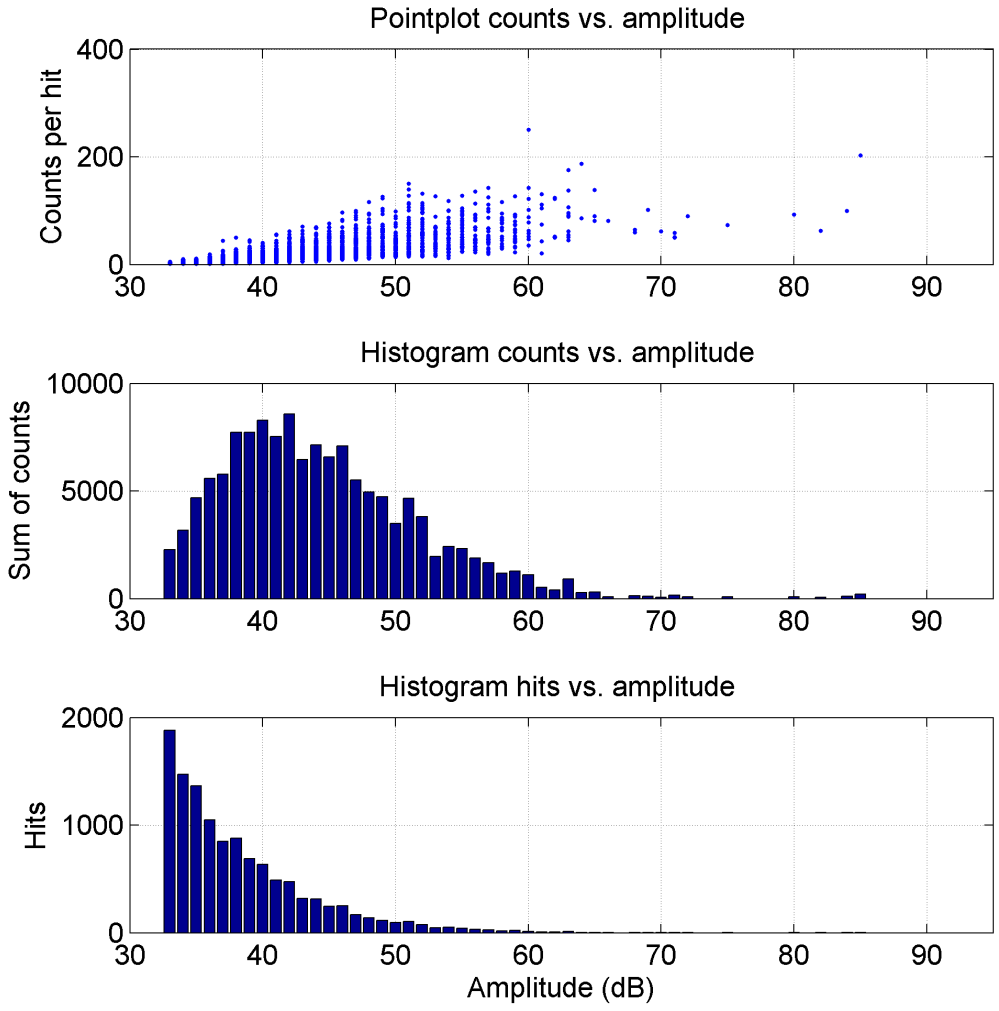

Figure 5.2: Counts and hits versus amplitude distribution for measurement Hom1. No catastrophic failure occurred.

Figure 5.2 shows a shear test at slightly tilted angle ($10°$). The high density snow was homogeneous, thus did not show any weak spots and showed great strength. Neither catastrophic failure, nor visible breaking processes occurred. Conversely, the second representative measure-

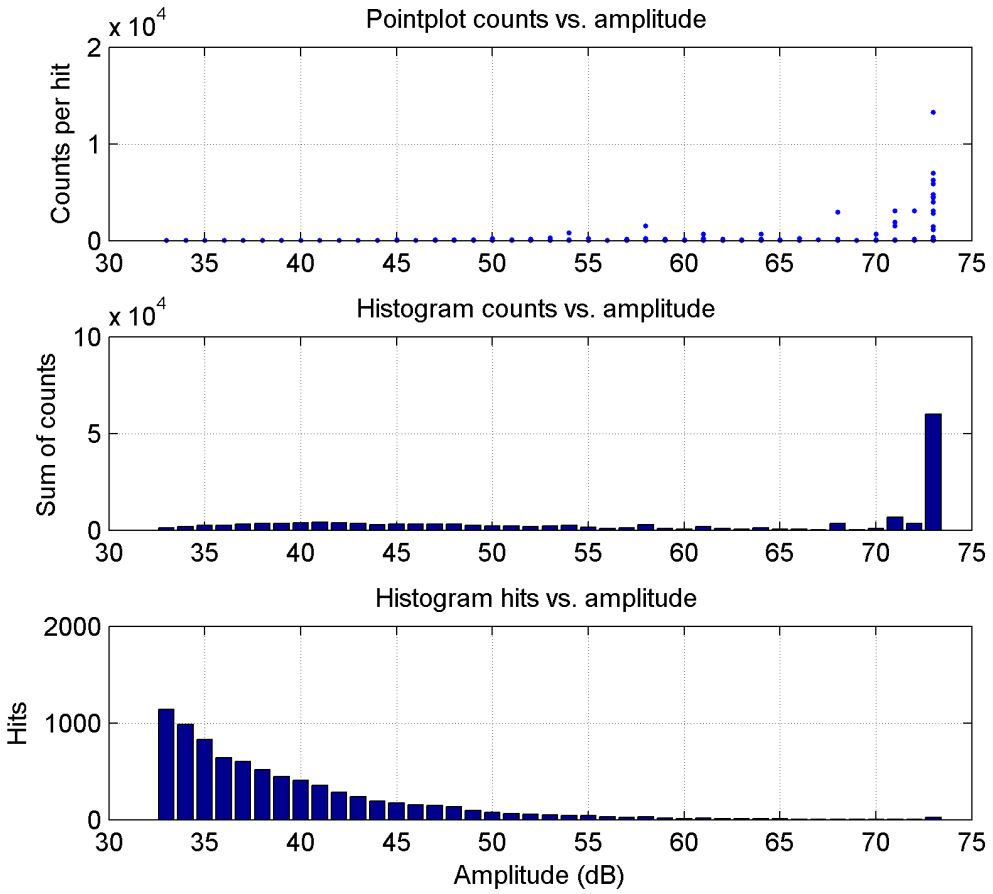

Figure 5.3: Counts and hits versus amplitude distribution for measurement DHN1. Catastrophic failure occurred.

ment (Figure 5.3 and 5.4) was carried out with a layered snow sample containing a DHN weak layer (depth hoar naturally grown, see Chapter 4.2). This weak zone caused catastrophic failure, preceded by a failure process with smaller amplitude but distinct nature. Figure 5.3 displays the entire AE activity of this test, including the catastrophic failure. Catastrophic failure processes produce an extremely large number of counts at high amplitude levels, a fact that somewhat hampers the diagram's interpretation. Therefore, Figure 5.4 shows the same test results, but with the data cut in time before the catastrophic failure event (after 8 seconds, see Figure 5.1 bottom plot). Note that the number of counts at 73 dB is reduced by the factor of 60 compared to Figure 5.3.

Taking a closer look at the three diagrams, the distinct character of catastrophic failure events can be examined clearly by observing the number of counts. Figure 5.2, which displays the measurement for the high strength homogeneous snow sample, shows that the "counts per hit"- points in the upper plot increased in level with increasing amplitudes, but no real outlier would indicate a critical event. The histograms show the missing information about the distribution of hits and counts. While the majority of hits occur at low amplitudes, the maximum count numbers - i.e.

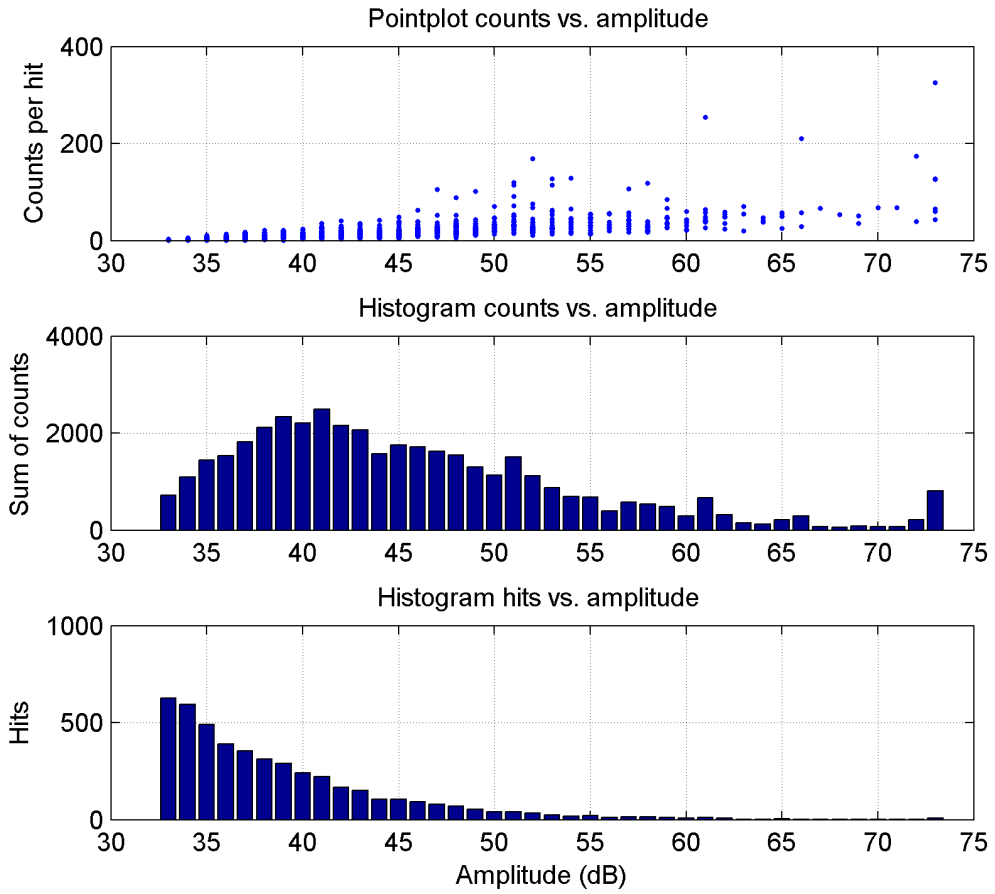

Figure 5.4: Counts and hits versus amplitude distribution for measurement DHN1. Data cut before catastrophic failure at test time 8 seconds (see Figure 5.1 bottom plot).

threshold crossings of the transducer output voltage - are found in the region between 40 and 45 dB. Examining Figure 5.3, the data from the weak layer snow sample experiment shows a completely different picture. The distribution of hits in fact is quite similar to above. However, the point plot and histogram concerning counts show huge values for the highest amplitudes. Figure 5.4 proofs that these hits with many counts occurred when the catastrophic failure occurred. Here the data before the catastrophic failure was cut. The distributions in this case are again similar to Figure 5.2. The remaining hits with high count numbers at the 73 dB level arise in a possible precursor event 4 seconds before the catastrophic failure. These time and load related issues will be stressed in more detail in Chapter 5.2.

The observations on counts and hits versus amplitude are completed by Figure 5.5 and Figure 5.6 which show the measurements for the other two homogeneous samples Hom2 and Hom3 respectively. Attention is drawn to the maximum amplitudes in each measurement in Table 5.2. Preamplifier gain of 60 dB limits the maximum signal amplitude which can be measured without overdriving the analog-to-digital converter to 73 dB, 40 dB gain results in a maximum amplitude of 93 dB (see Chapter 4.5). Catastrophic failure events, especially those leading to complete sample

damage, often evoke signal amplitudes which are too high for the 60 dB preamplifier gain. This seems to be the case for the DHN1 measurement as well. Still, overdrives during rupture might be accepted in order to increase sensitivity for the time before. The decreasing maximum signal amplitude for the homogeneous samples might be explained by the decreasing density (increased attenuation) and load rate with each measurement (compare Table 5.1). Unknown variables, first and foremost the quality of sensor coupling, certainly have influence too.

Hom1	Hom2	Hom3	DHN1
85 dB	70 dB	65 dB	73dB

Table 5.2: Maximum signal amplitudes for the four shown measurements.

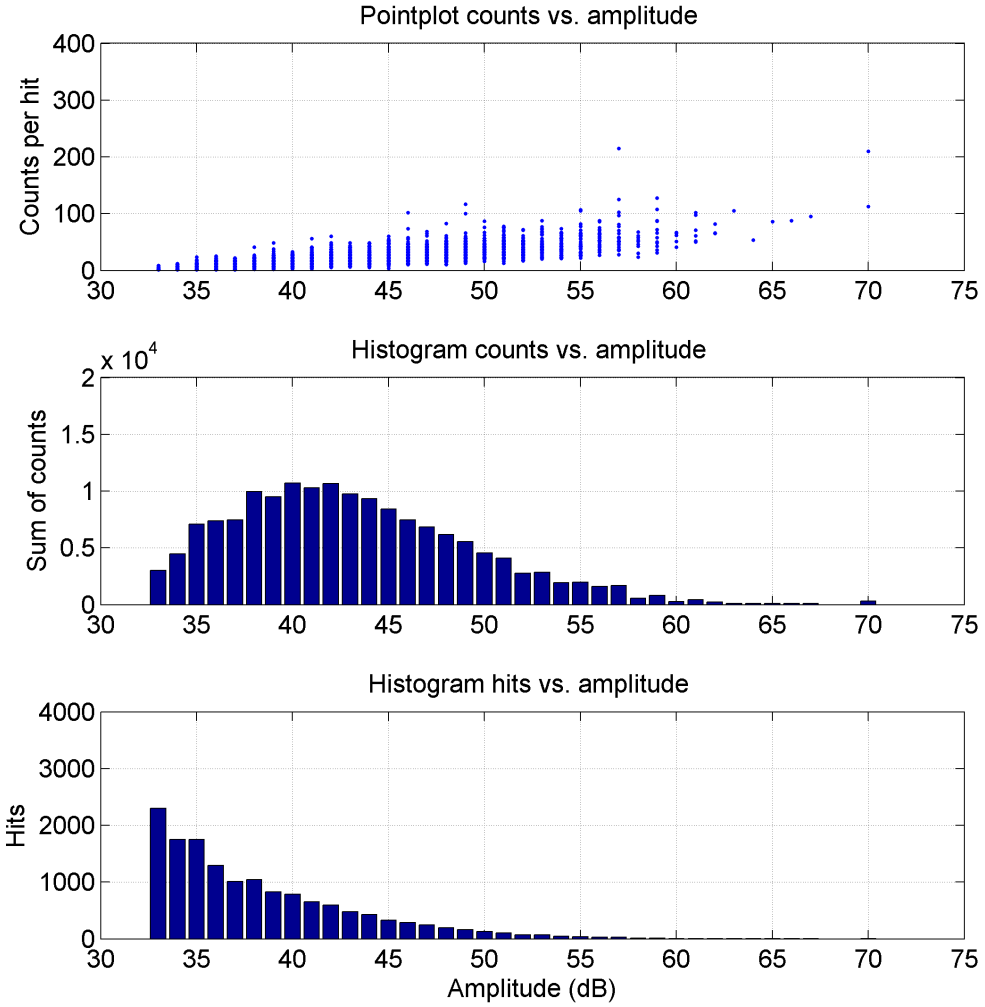

Figure 5.5: Counts and hits versus amplitude distribution for measurement Hom2. No catastrophic failure occurred.

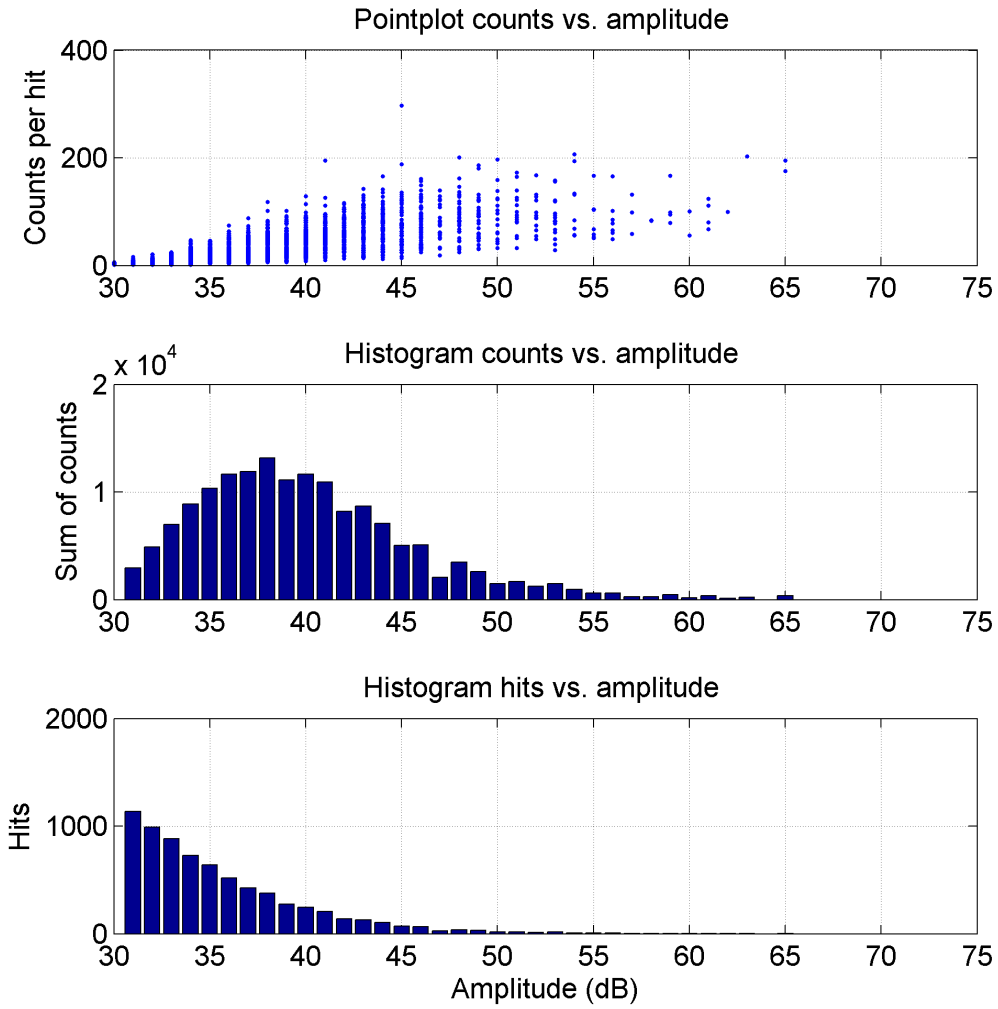

Figure 5.6: Counts and hits versus amplitude distribution for measurement Hom3.

It is not surprising that the highest signal amplitudes occur in times of catastrophic failure. Since signal amplitude is a decibel value, its logarithmic nature only partly reveals significances in the data at first glance. Regarding signal energy as another important AE signal parameter, a much larger range of values arises. This can be seen clearly by plotting the number of counts per hit versus signal energy instead of amplitude. This is shown in Figure 5.7(b) and (c), where the homogeneous sample Hom1 is compared with the ruptured layered sample with and without displaying the rupture. The high energy events during catastrophic failure have a 30 times higher energy than the high energy hits for the same data with the catastrophic failure being cut off.

Duration and rise time versus amplitude

Among the various AE parameters, duration and rise time are from special importance in signal discrimination (Pollock 2008). As described in Chapter 2.2.1, duration means the length of an AE hit, i.e. the time from the first to the last threshold crossing.

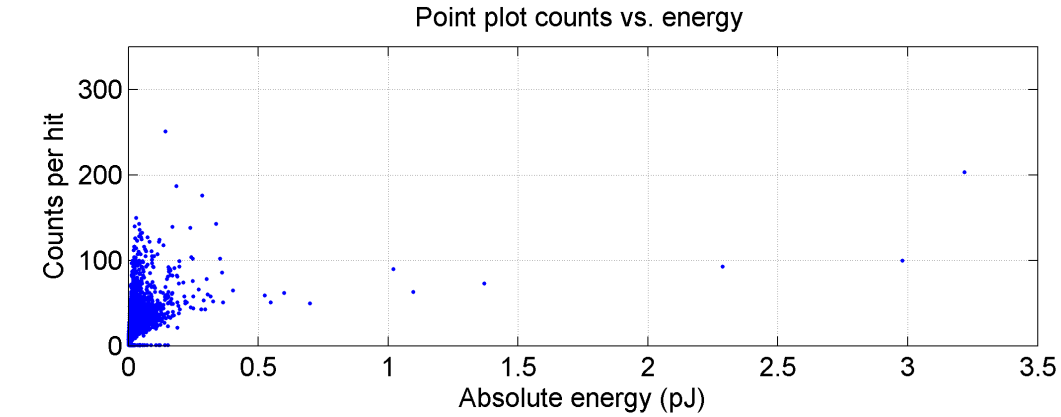

(a)

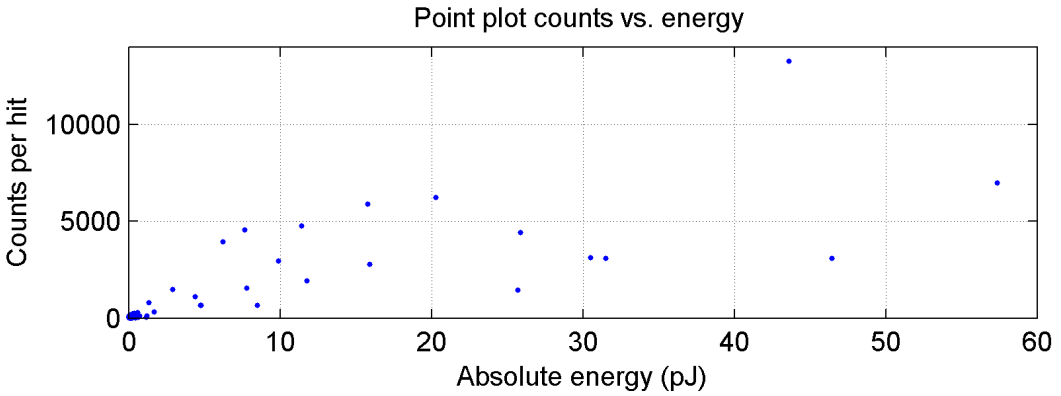

(b)

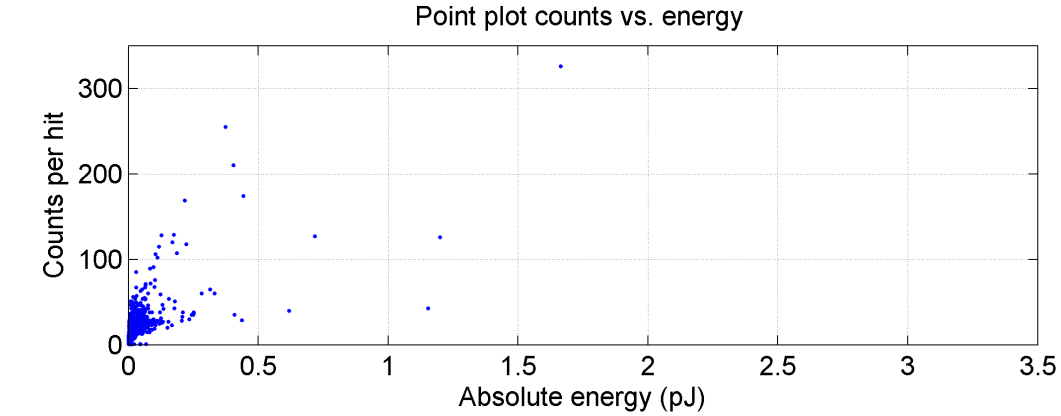

(c)

Figure 5.7: Counts per hit versus energy: (a) high strength snow sample, (b) weak layer snow sample including catastrophic failure, (c) weak layer snow sample with data cut before catastrophic failure.

Rise time is the time from the first threshold crossing until the point of maximum signal amplitude. The distributions of these parameters show a similar behavior to the "number-of-counts" distributions. Indeed, if the signal frequency was constant, the number of counts would

be proportional to the signal's duration. Figure 5.8(a) and (b) show the parameters duration and rise time versus signal amplitude for the measurements Hom1 and Hom2. The distributions are similar, still it can be noted that both duration and rise time in measurement Hom2 only have approximately half the amount of the Hom1-values. Again, as known from previous plots, a drastic difference in the values can be seen for the ruptured layered sample Lay1 for duration and rise time depending on including the rupture in the data or not (Figure 5.9(a) and (b)).

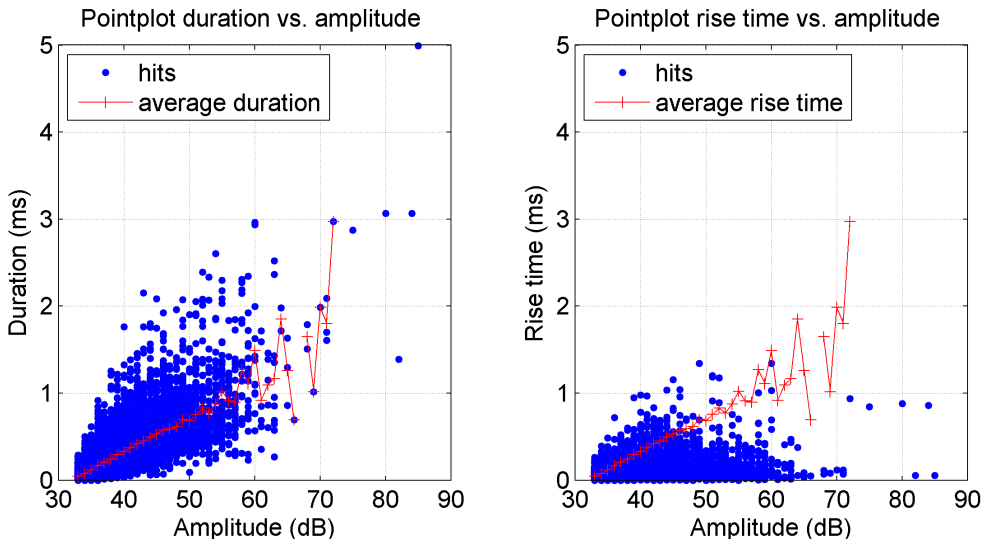

(a)

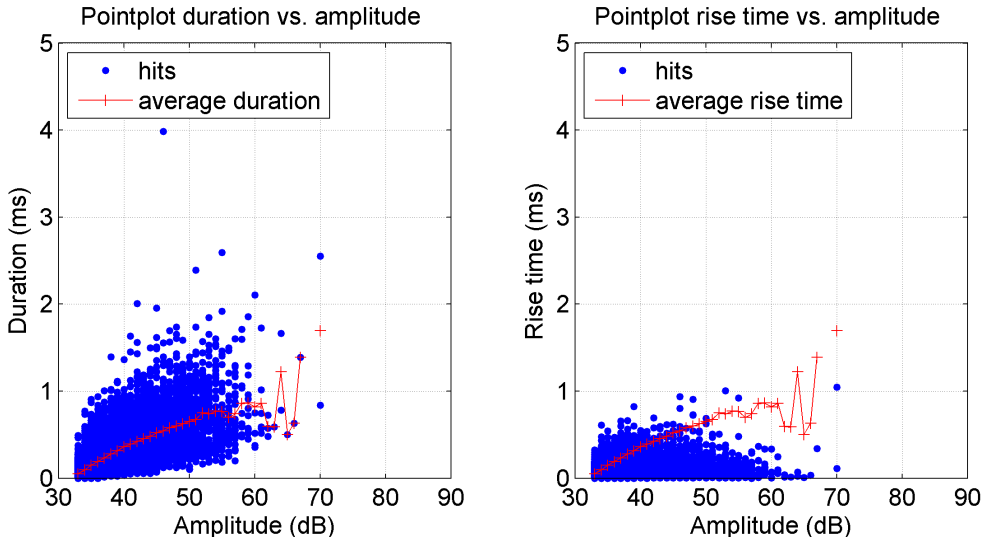

(b)

Figure 5.8: Duration and rise time per hit versus energy, homogeneous snow samples: (a) homogeneous snow sample Hom1, (b) homogeneous snow sample Hom2.

Obviously, signal frequencies vary in a wide range, as the next section about frequency related parameters will show. Still, as Figure 5.10 shows, there is a significant relationship between num-

ber of counts and duration for the measured hits. Hence, also the parameters duration and rise time - along with "number of counts", amplitude and energy - are capable of indicating fracture inside a snow sample. Furthermore, it will be shown in the following that these parameters also provide valuable input for signal classification.

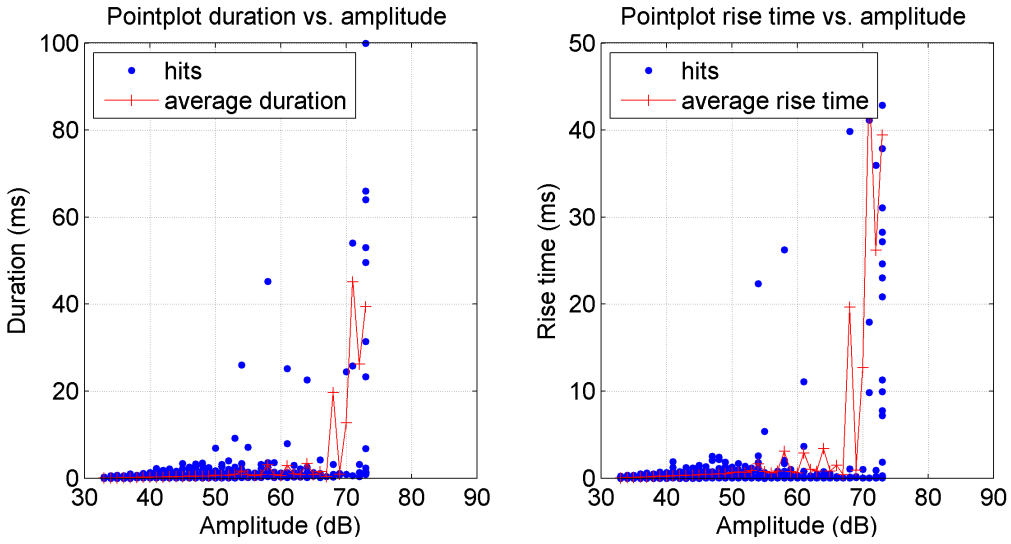

(a)

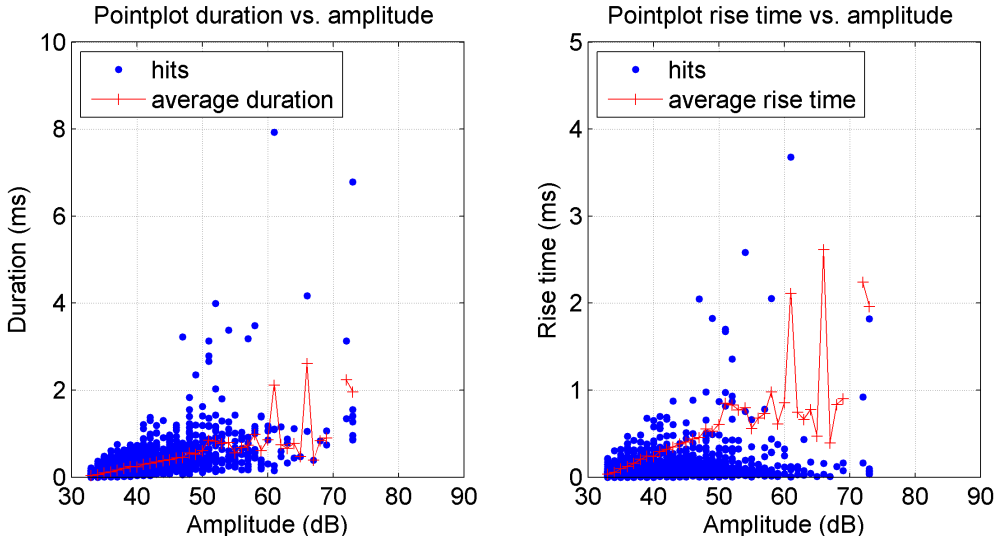

(b)

Figure 5.9: Duration and rise time per hit versus energy, layered snow sample: (a) Weak layer snow sample DHN1, including catastrophic failure, (b) DHN1 with data cut before catastrophic failure. Both duration and rise time exhibit approx. ten times larger maximum values during the catastrophic failure.

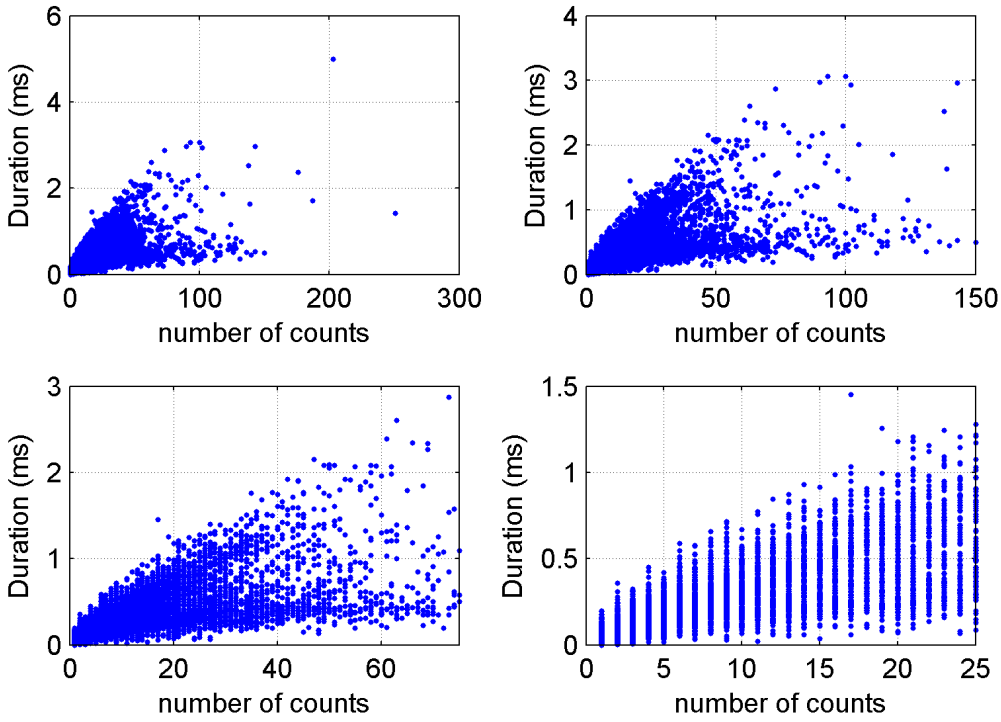

Figure 5.10: Duration versus number of counts at four different zoom levels for the measurement with the high strength snow sample.

5.1.3 Frequency related parameters

Along with waveform streaming of the AE hits, various possibilities arise for analyzing the signal's frequency content. One of these is the automatic extraction of frequency parameters, more precisely the parameters peak frequency and frequency centroid, which was an included feature of the measurement system. This section will have a closer look on these two parameters. Figures 5.11 to 5.15 show typical distributions for frequency centroid and peak frequency and are equally constructed: The two top plots show the distributions of frequency centroid and peak frequency as histograms. The height of each bar corresponds to the number of hits within bands of 10 kHz. At the bottom, the parameter's distributions regarding signal amplitude are depicted as point plots. The red line in the bottom right plot indicates the average frequency centroid for each discrete amplitude level.

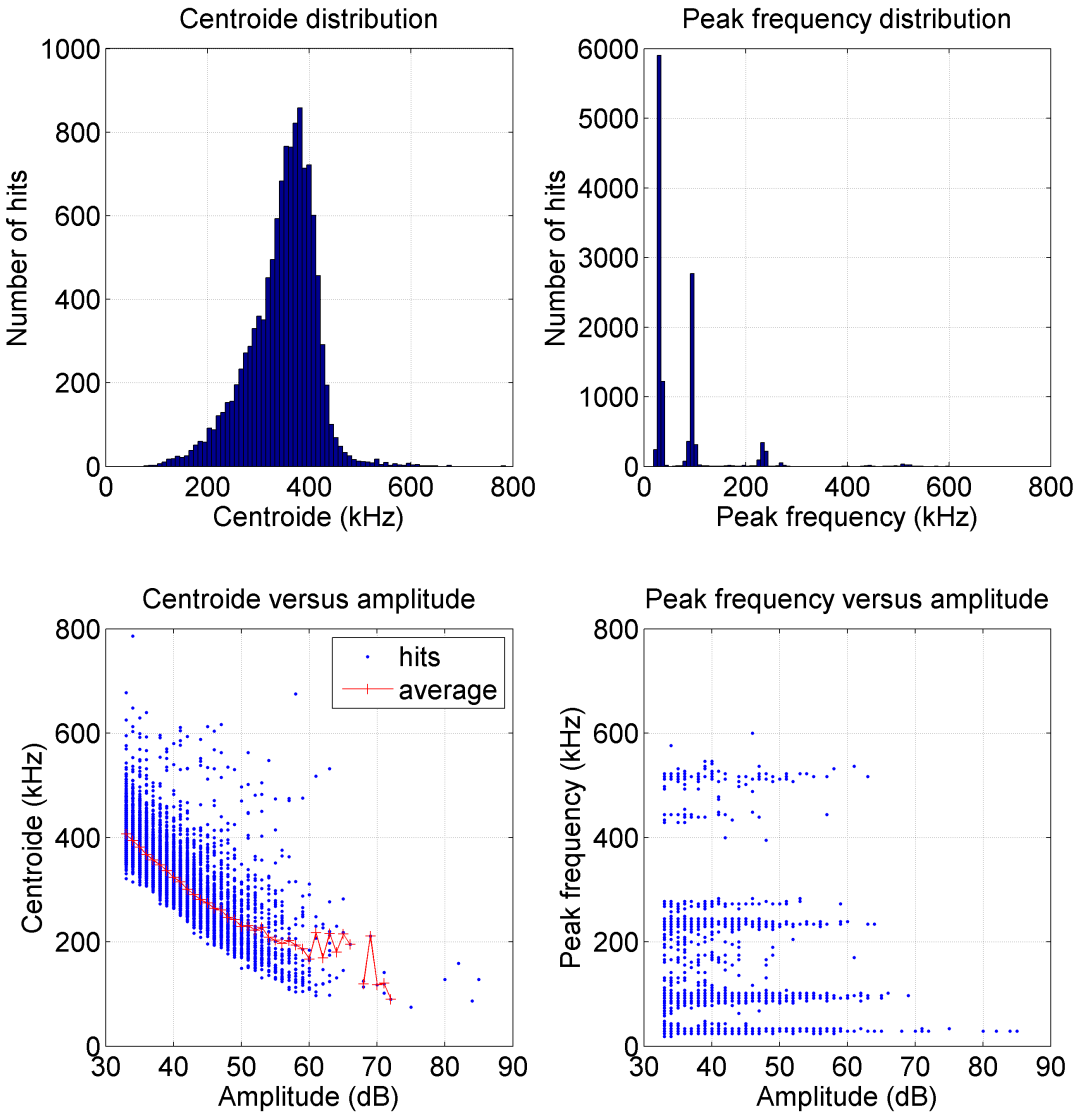

Figure 5.11: Distribution of centroid and peak frequency (Hom1): The upper plots show the number of hits for constant ranges of centroid and peak frequencies. Note the distinct accumulations of hits versus peak frequency, caused by the sensor resonances. The lower plots show point plots of the two parameters versus amplitude. Again, the resonances can be clearly identified (bottom right plot). The bottom left plot shows an interesting feature, present in all measurements: Centroid decreases with increasing signal amplitude.

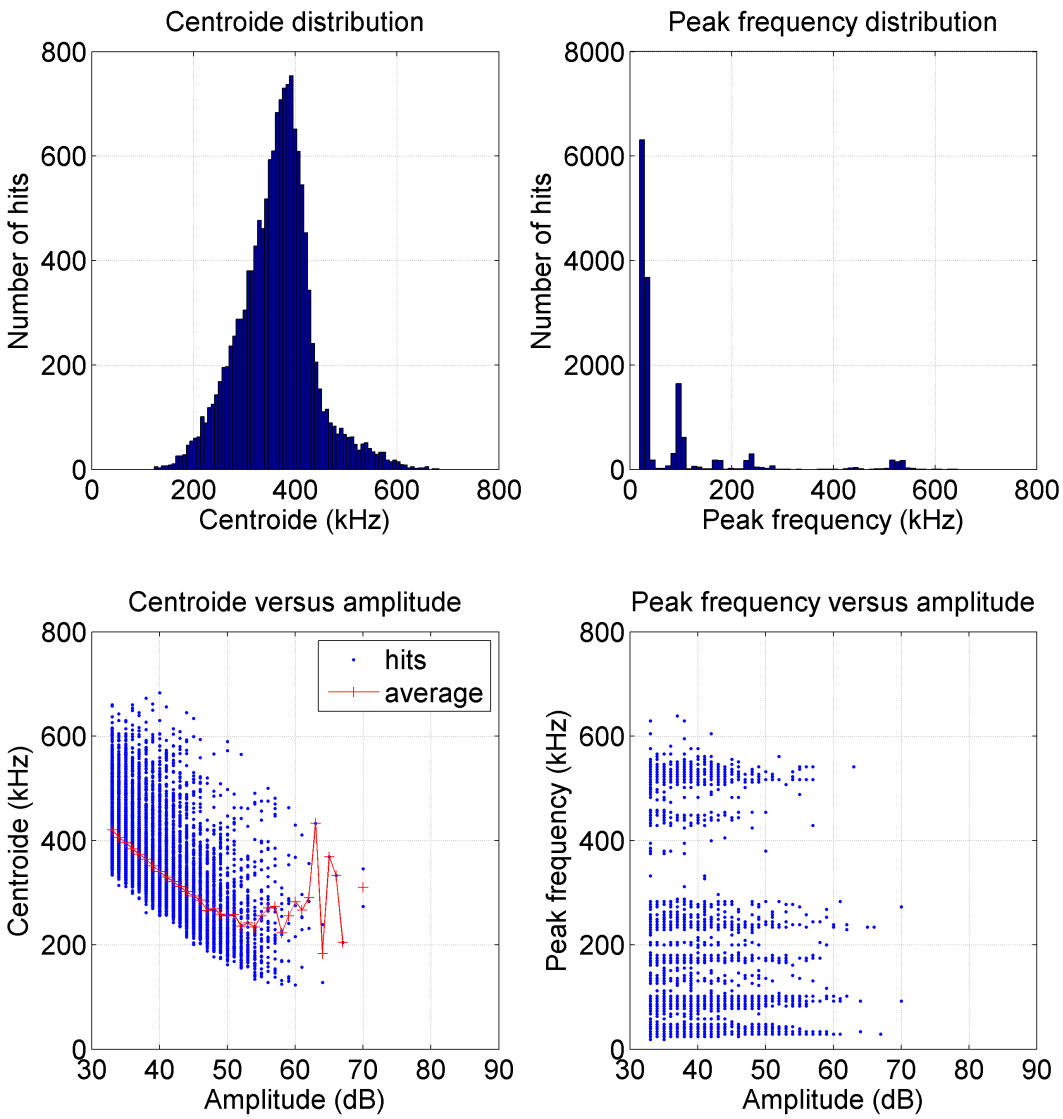

Figure 5.12: Distribution of centroid and peak frequency (Hom2).

Regarding the distributions, measurements Hom1 (Figure 5.11) and Hom2 (Figure 5.12) show a similar picture: A slightly asymmetric centroid distribution has its peak around 400 kHz. The peak frequencies display clearly the transducer's resonances. Most of the hits have their peak frequency in a region around 30 kHz, about the quarter to half amount at around 100 kHz and a third accumulation can be seen at 230 kHz. Only very few hits have peak frequencies at 450 and 520 kHz respectively. The measurement with the low density snow sample Hom3 (Figure 5.13) exhibits a slightly higher peak in the centroid distributions and relatively more hits with peak frequencies around 100 and 230 kHz. This is remarkable, since the low-pass filter character of snow is assumed to increase with decreasing density. It will be pointed out later in this section, that high AE frequencies are assumed to be related with microscopic failure, hence, such a distribution might be an evidence for dominantly ductile deformation. Displaying the values of

centroid and peak frequency for each hit as point plot versus amplitude (bottom plots) shows an interesting behavior valid for all measurements. The higher the signal amplitude, the lower the average frequency centroid. The huge number of hits with low peak frequencies (around 30 or 100 kHz) occur at every amplitude level. The high amplitude (and also the high energy) signals have their peak frequencies exclusively in the low regions.

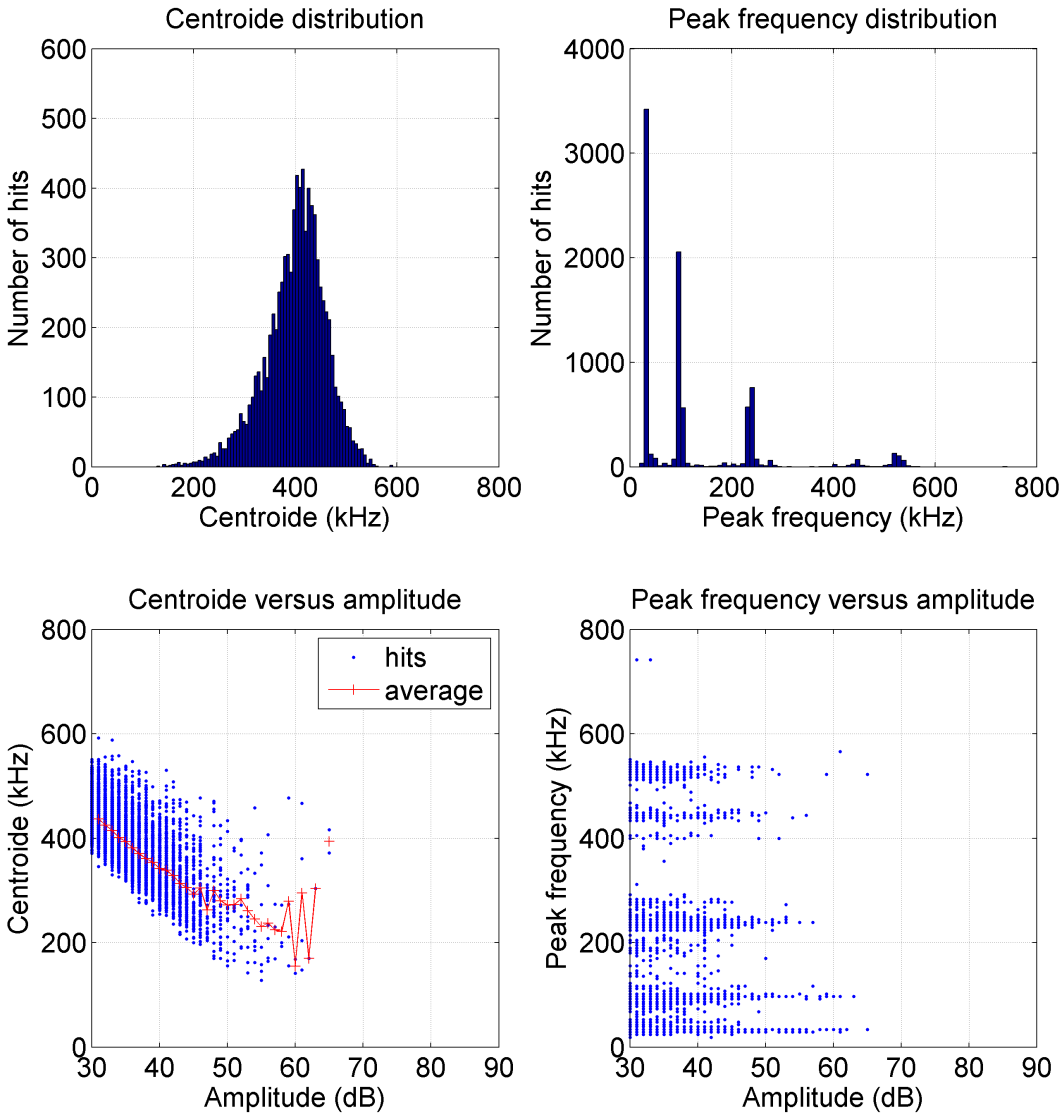

Figure 5.13: Distribution of centroid and peak frequency (Hom3).

Figure 5.14 and 5.15, displaying the weak layer sample DHN1, show that both centroid and peak frequencies are basically lower compared to the homogeneous samples. Other measurements with weak layer samples partly showed the same behavior, but also distributions similar to the measurements with the homogeneous samples could be examined. Hence, no indication for im-

minent fracture or reliable information on the type of failure (brittle-ductile) can be concluded by only viewing the signal's frequency content. An approach on signal classification combining the frequency parameter peak frequency and the classical parameter duration is shown in Figure 5.16. It seems that the type I signals (spikes) can be basically associated with ductile failure (bond breaks), whereas type II signals (noise) indicate brittle failure. No experiment included periods where one signal type occurred exclusively.

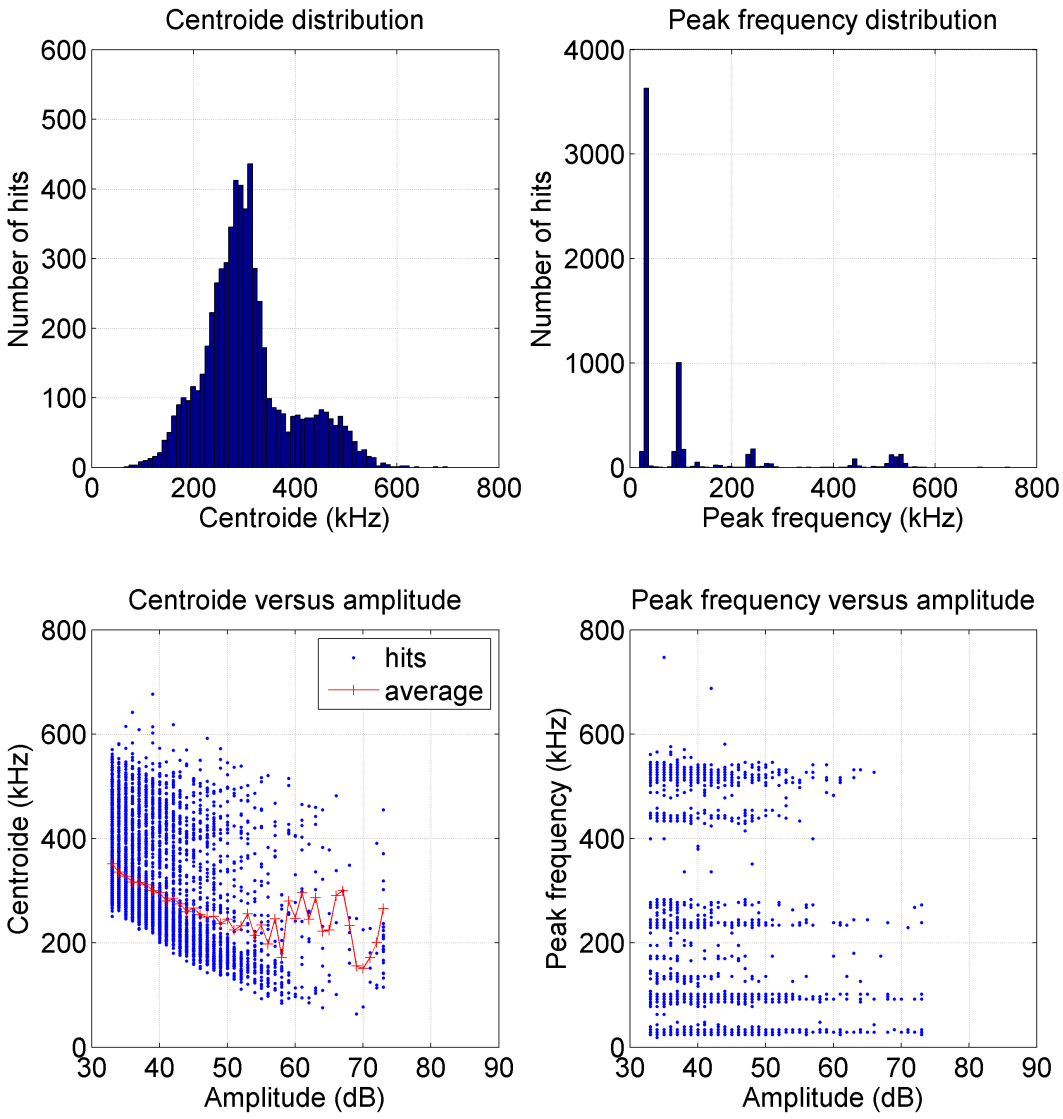

Figure 5.14: Distribution of centroid and peak frequency (DHN1), including catastrophic failure

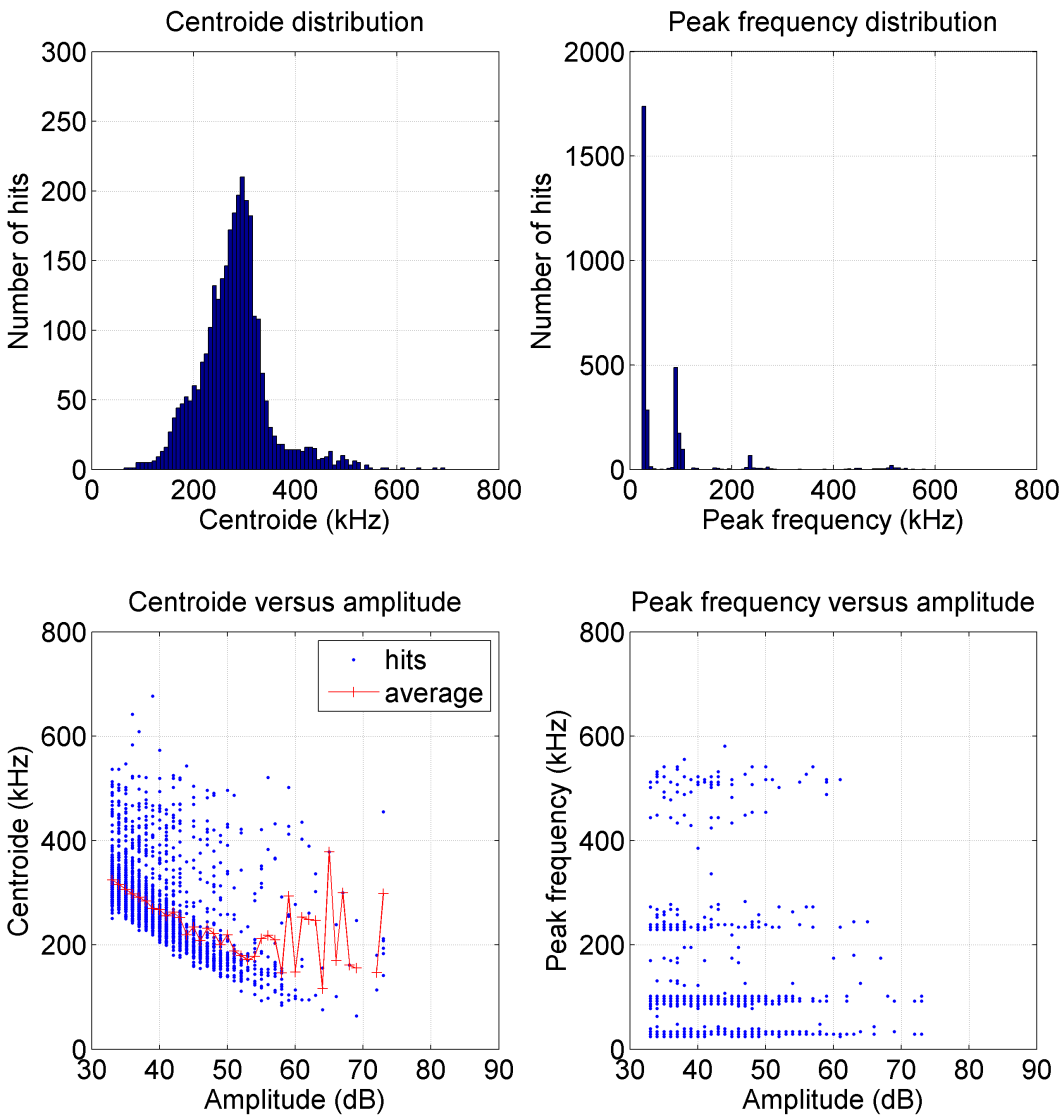

Figure 5.15: Distribution of centroid and peak frequency (DHN1), data cut before catastrophic failure.

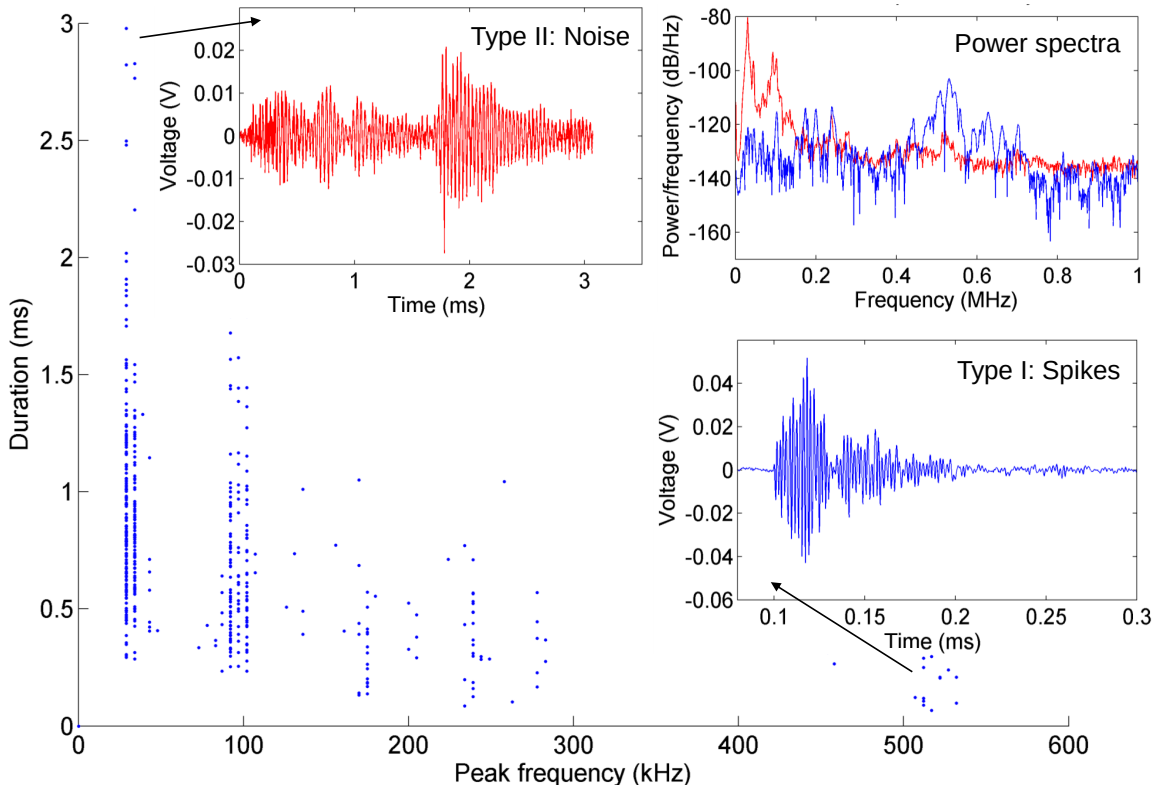

Figure 5.16: Signal classification approach combining the "classical" AE parameter signal duration and the frequency parameter peak frequency: Signal type I (spikes) is characterized by high frequency and short duration, signal type II by low frequency content and longer duration. The top right plot shows the power spectra of the two example signals.

5.1.4 Discussion

A practical remark should be given to the classical AE parameters, since they already provide great insight into different failure processes inside a snowpack. Obviously, with respect to field experiments, they can be derived with much less effort compared to the frequency parameters. AE events with significant character are indicated by several classical parameters. Significant character can mean signs of ductile failure as well as signs of brittle failure. Brittle failure of considerable size always goes along with local displacements. Compared to the rapid energy release originating during microscopic bond breaks, it was assumed from the beginning on that brittle failure (larger scale) produces long-lasting AE events, resulting in high count numbers and long durations and rise times. Indeed, AE hits characterized by long durations and rise times seem to be related to large displacements (Figure 5.9). Not only long durations, but also highest energy values are a sufficient and necessary sign for brittle failure. However, the signal's amplitude level does not indicate which kind of breaking process was the origin of the observed AE hit. Spike-like signals

originating from failure processes on the micro scale may also have high amplitudes, especially if the distance between source and sensor is short (compare Figure 5.16).

In order to increase reliability of signal classification, the frequency parameters represent great additional information. The signal's frequency is inversely proportional to the size of failure. This property has been proved in the macro scale (Sommerfeld 1982) and seems to apply on the micro scale as well (Scapozza et al. 2004). A drawback resulting from the unavoidable sensor design with several piezoelectric elements is the complex frequency response. In terms of peak frequency only some discrete frequencies are present, which reduces the resolution in distinguishing various failure mechanisms. The frequency centroid is well suited to indicate trends in the signal's frequency content, but observing a single centroid does not lead to any reliable conclusion about a particular signal (see Figure 5.11). The sensor's frequency characteristics may be compensated digitally by filters containing the inverse impulse response of the sensor (Grosse and Ohtsu 2008). However, modeling the impulse response of a wide band AE transducer needs a huge number of filter coefficients and is not simple to derive. Still, also an approximation might already lead to better results but was out of scope within this thesis. As far as laboratory research is concerned, further approaches on signal classification with the help of frequency parameters seems highly promising. An important question for upcoming field research will be which parameters should be observed. Frequency related parameters require recording of the entire waveform, which is therefore at the moment difficult to realize in the field. Amongst the classical signal parameters, the counts activity is the probably mostly used parameter. It is fairly easy to extract with the help of a simple analog circuit (Scapozza et al. 2004). Also the energy parameter suits the field requirements quite well.

Very important considerations at the beginning of any AE research have to be made on the signal amplitude in order to set the threshold correctly. For laboratory experiments the threshold could be possibly increased to a level of 40 to 50 dB without loosing important data. For field applications, the proper threshold may be lower because of the larger distances from source to sensor. Therefore, the threshold value has to be reconsidered in every new testing environment. The right choice of the threshold level is important for two reasons. Firstly, a too low threshold can cause the AE system to overload in times of high AE activity and secondly, the amount of data is reduced by increasing the threshold level. Obviously a threshold which is set too high causes the loss of important data.

Overloading of the recording system is a serious problem, because it results in non-reconstructible errors in parameter extraction and waveform recordings. Unfortunately, this happened during some of the measurements within this research, an example can be seen in fig 5.17. It shows the parameter "absolute energy" versus signal amplitude for measurement on the homogeneous high strength snow sample Hom1. The AE hits at 33 dB having high energy values are artefacts. Whether this events actually did not occur at all or just the extracted parameters are wrong can-

not be said afterwards (Manuel Löhr, Physical Acoustics Corporation, personal communication). Only some datasets are concerned though, affected by decreasing the timing parameters in order to optimize recording quality (see Chapter 4.5.2). How badly exactly the data is affected by these errors could not be determined, therefore an absolute reliability on the measurement data cannot be assured. Still, it has been agreed on presenting the data in order to show ways of interpreting the AE data in general, as it was the main target of this research.

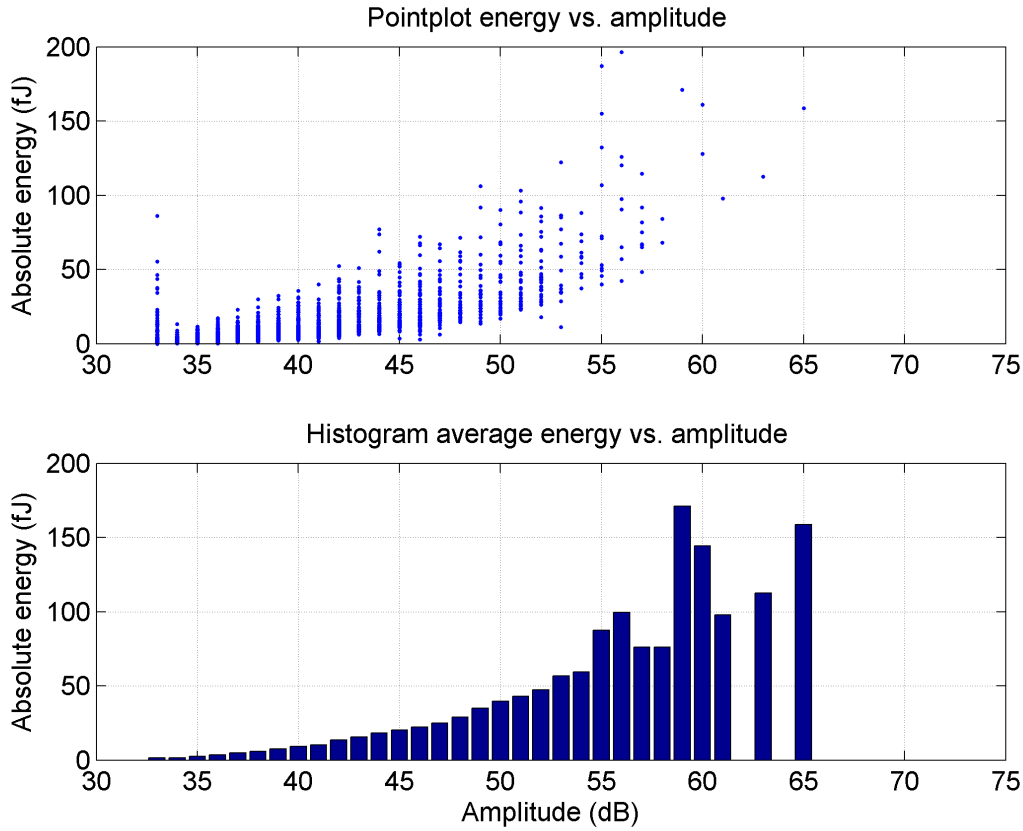

Figure 5.17: Average absolute energy versus amplitude level. Homogeneous snow sample: density 378 kg/m^3, large rounded particles (0.5-1 mm), hardness 4 (hard, pencil). Significant hits occur only at amplitudes higher than 55 dB.

5.2 Load/displacement/AE relations

5.2.1 Overview

The interaction of load, displacement and acoustic emissions is important in order to understand the temporal processes inside a snow pack. Methodical tests on that issue were carried out parallel to the experiments within this thesis, concentrating on varying tilt angles and load rates. Within this thesis, emphasis is placed on presenting general possibilities of data analyzing rather than presenting statistically significant results. The series of plots (Figure 5.18 to Figure 5.24) show data from the previously illustrated measurements Hom1, Hom2, Hom3 and DHN1 (see Table 5.1

and Figure 5.1). A second measurement with a weak layer sample was chosen to be displayed in addition. This sample contained a DHA (depth hoar artificial) layer, details on the measurement are given in Table 5.3.

Meas.	Snow	ϕ	$\dot{F}$	Amp.	Rupt.
DHA1	Layered 120x75x90, outer layers: ρ_{ol} =260 kg/m^3, RGlr (FCxr) 0.5 - 1 mm , hardness 3 (medium, 1 finger). Weak layer: ρ_{wl} = 150 kg/m^3, DHxr (FCxr) (1 - 1.5 mm), hardness 2 (soft, 4 fingers)	30°	37.04 Pa/s	60dB	Yes

Table 5.3: Additional presented measurement DHA1: Details in snow and process parameters. For explanations on the abbreviations see Table 5.1.

The Figures contain three plots: The top plot shows the characteristics for load and displacement, similar to Figure 5.1. The middle plot illustrates the acoustic emission count activity as point plot, which means that every point represents one hit with its number of counts indicated on the y-axis. The bottom plot shows the cumulated number of counts in intervals of either 1 s or 0.1 s, hence the load rate or 10 times the load rate per second. This division was necessary in order to increase the resolution for short test scenarios. Additionally, the bottom plot shows the average count rate (blue solid line) and the displacement velocity (green dashed line). This value was derived by low-pass filtering (noise reduction), deviating and averaging the displacement data. In this section, the AE count rate was chosen to be presented as the representative AE parameter. Evolutions of other AE parameters can be seen in Appendix B.

5.2.2 Homogeneous snow samples

Figures 5.18, 5.19 and 5.20 show the measurements with homogeneous snow samples (Hom1, Hom2, Hom3), introduced in section 5.1.1. No catastrophic failure occurred during these measurements but attention is drawn to the behavior of count rate and displacement velocity. In order to observe how these parameters develop during increasing stress and constant stress, the load was held at a constant level after reaching a certain maximum value, This maximum value was determined by the available fluid able to run down in the tank (compare Chapter 4.4) and was between 110 and 140 N. The high-density snow sample Hom1 (Figure 5.18) shows a similar behavior for count rate and displacement velocity: Both values increase strongly during the increasing load before diminishing drastically with the beginning of the constant-load phase by factors of approximately 10 and 5 for count rate and displacement velocity respectively. Measurement Hom2 (5.19), characterized by lower snow density and load rate, shows the count rate decreased by a factor of around 10, while the displacement velocity is only reduced to half the maximum rate. Finally, measurement Hom3 (5.20) featuring even lower snow density and load rate still shows a notable reduction (approx. by a factor 5) in the count rate, while the displacement velocity only

reduces slightly. Such observations might be an interesting approach for distinguishing between "dangerous" micro structural processes leading to snow instability and resintering processes which increase snow strength (compare Chapter 1). Assuming the period of the increasing load being the "dangerous" one (or at least more dangerous) compared to the constant-load period, the AE count rate indicates the transition between the two states very well.

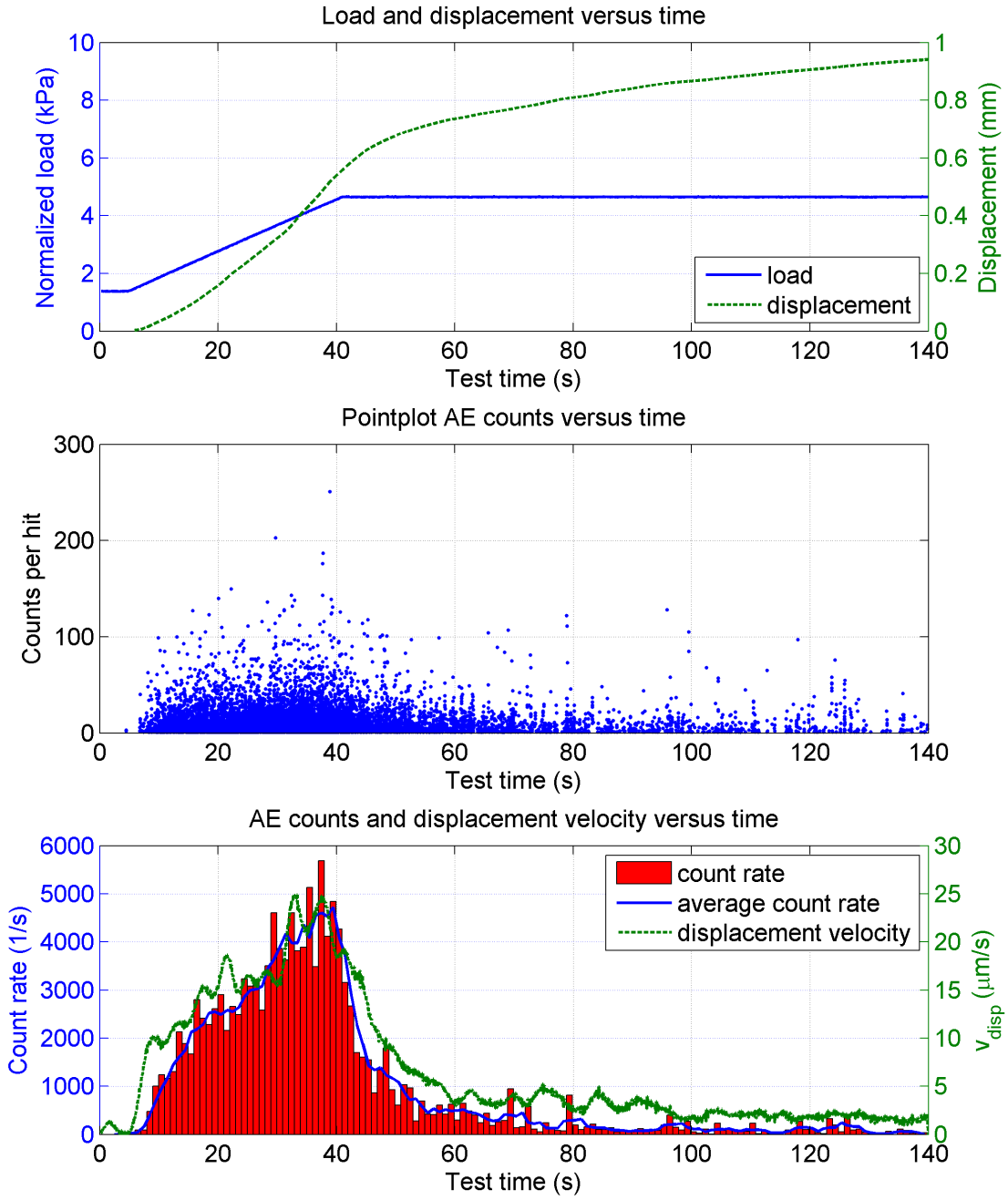

Figure 5.18: Load, displacement and acoustic emissions relations for measurement Hom1.

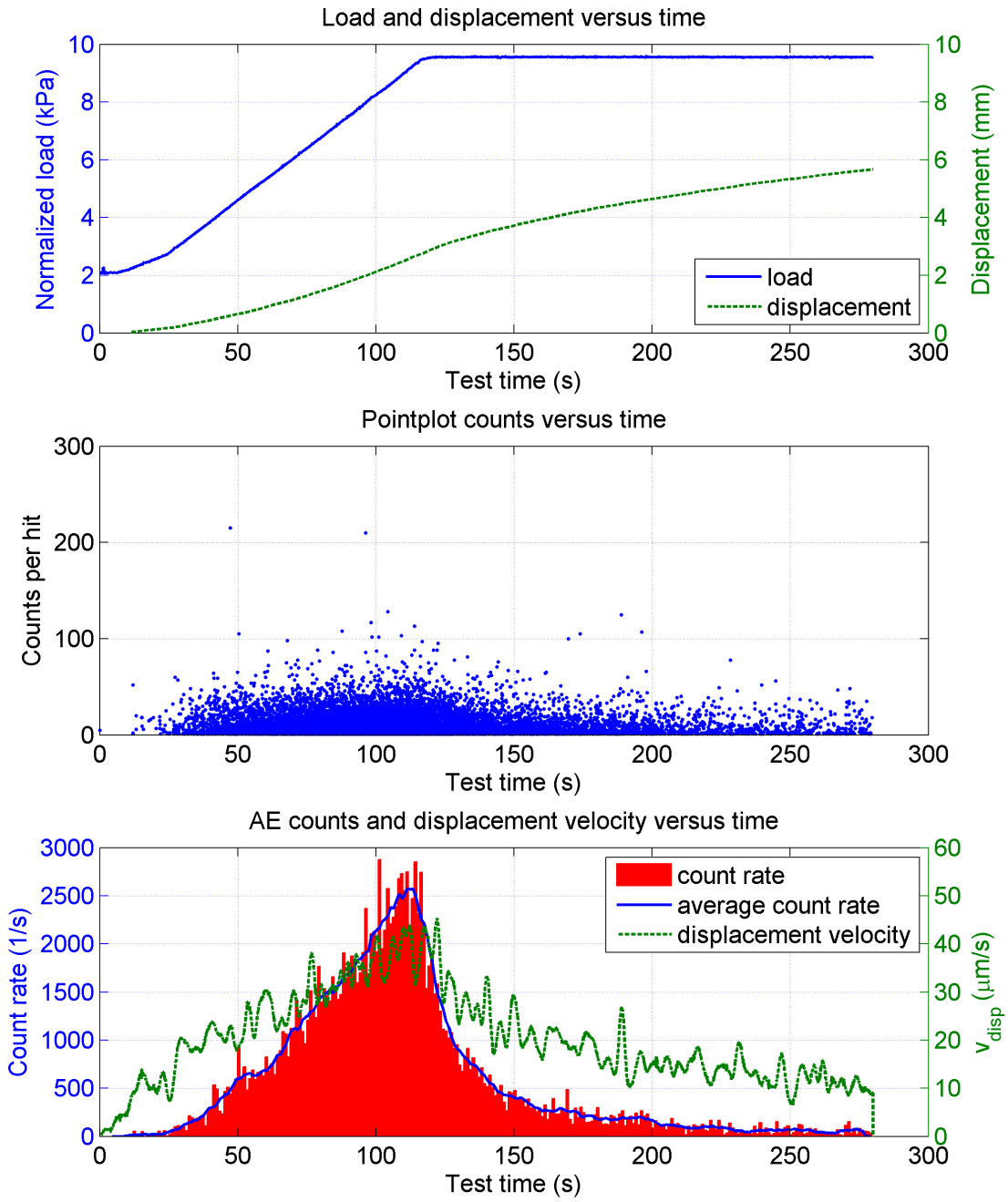

Figure 5.19: Load, displacement and acoustic emissions relations for measurement Hom2.

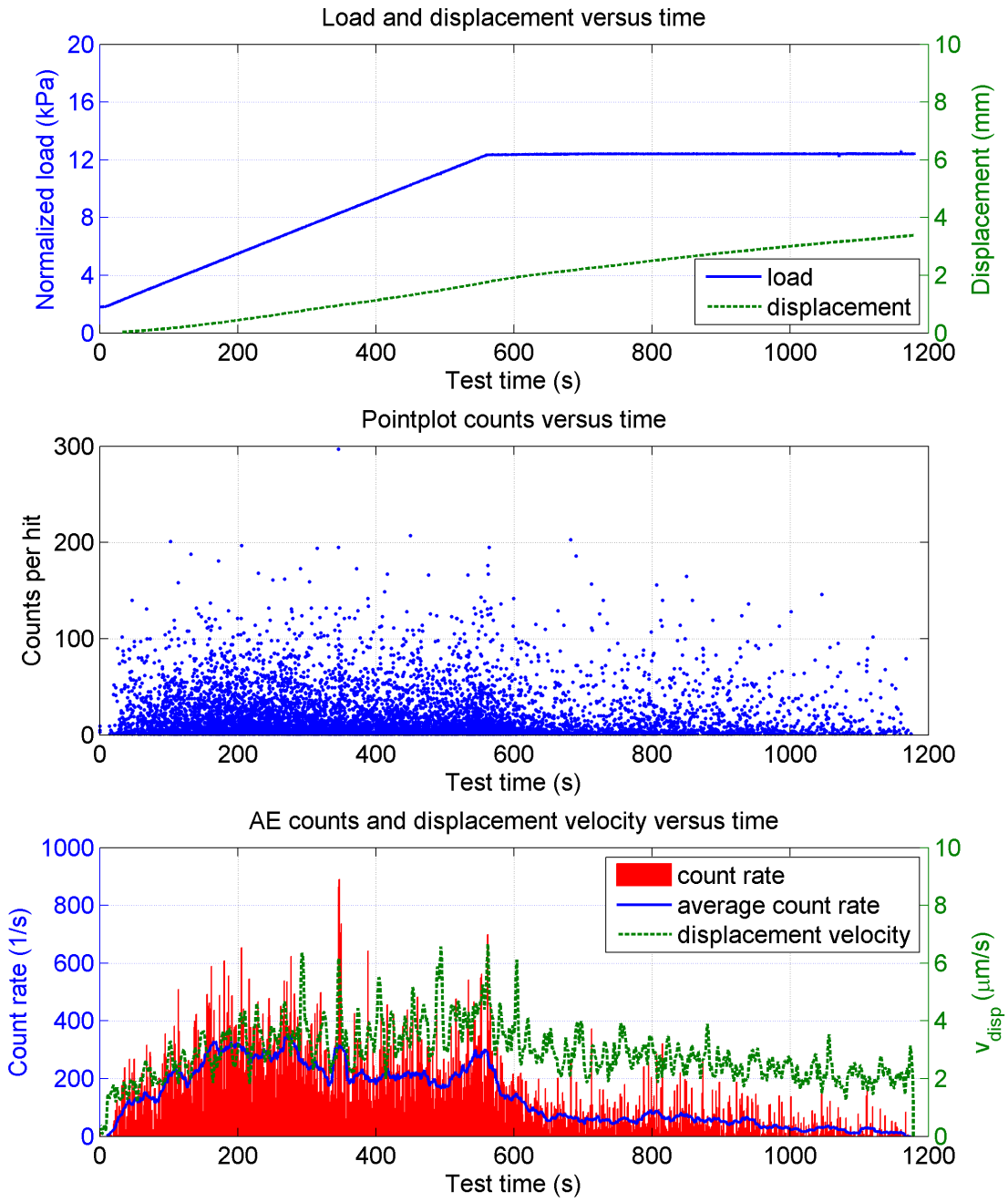

Figure 5.20: Load, displacement and acoustic emissions relations for measurement Hom3.

5.2.3 Layered snow samples

In this section, two representative measurements with weak layer snow samples are shown. Figure 5.21 shows a test with a DHN sample (DHN1, depth hoar natural, see Table 5.1) and Figure 5.22 a test with a DHA sample (DHA1, depth hoar artificial, see Table 5.3). The count rates are extremely high during rupture, hence not much information on the period before is provided observing the entire data. However, a smaller rupture can be seen in measurement DHN1 at 3.7

seconds, which did not cause complete damage yet. For better visualization, Figure 5.23 and 5.24 show the measurements with differently scaled y-axis.

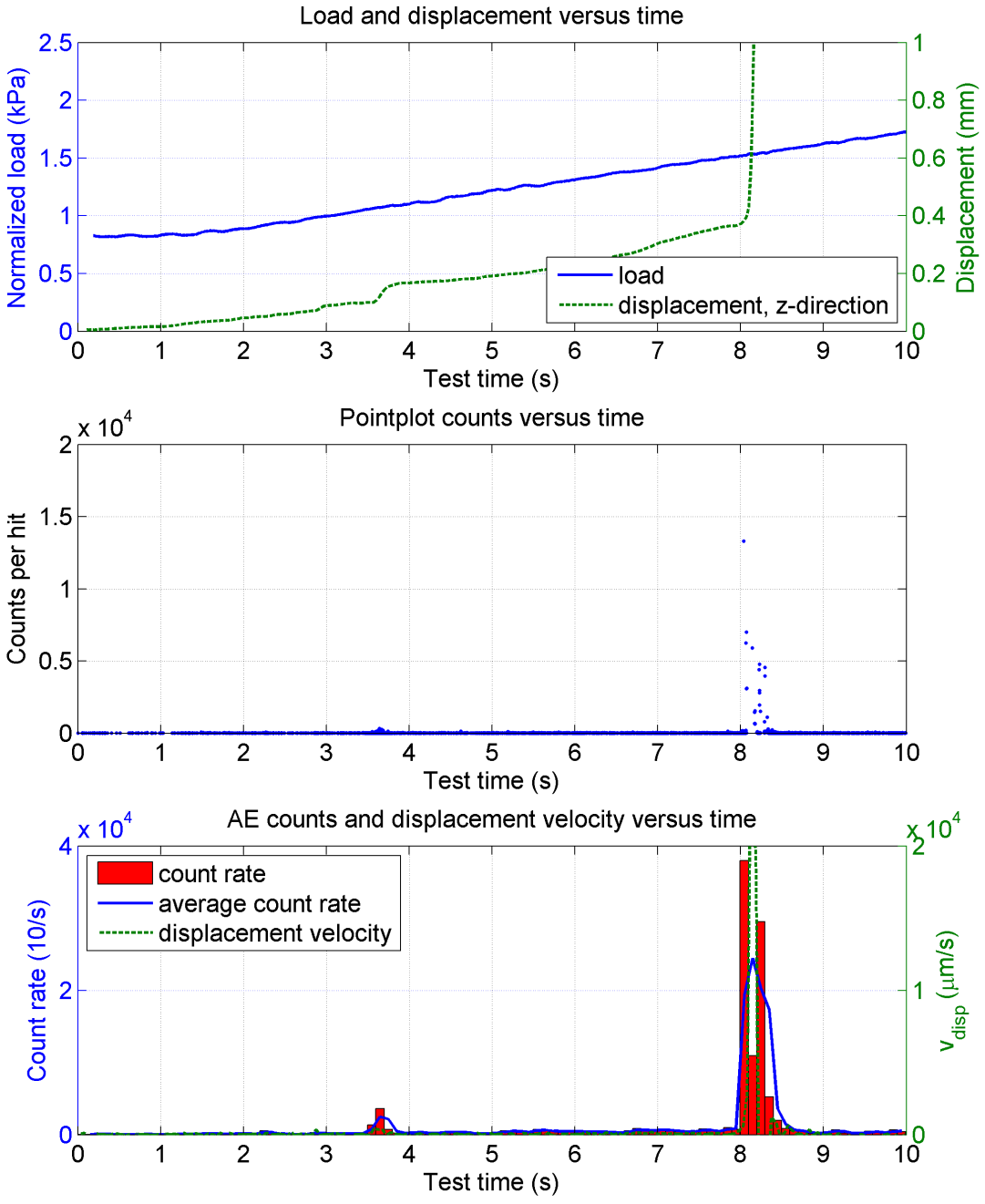

Figure 5.21: Load, displacement and acoustic emissions relations for measurement DHN1.

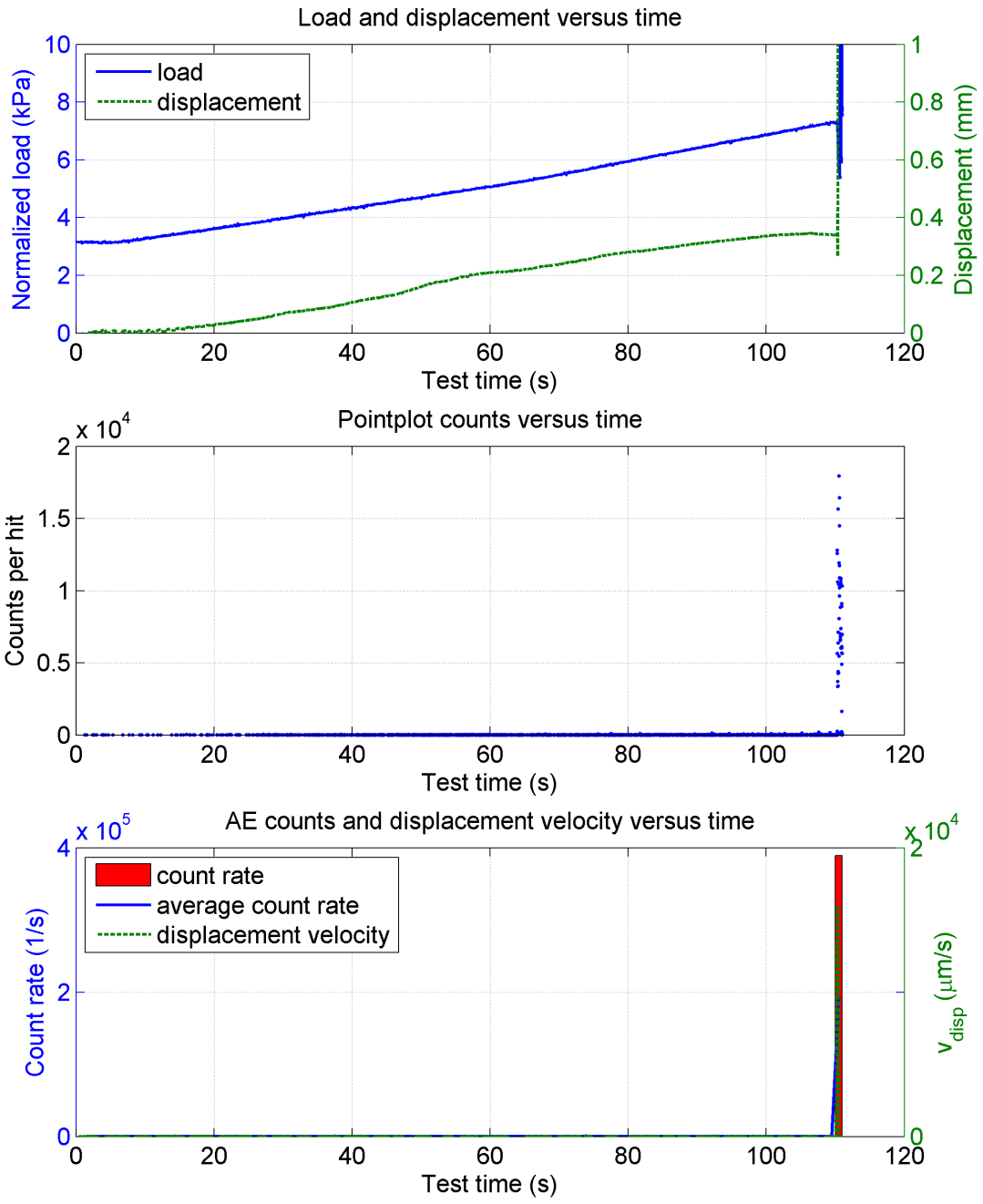

Figure 5.22: Load, displacement and acoustic emissions relations for measurement DHA1.

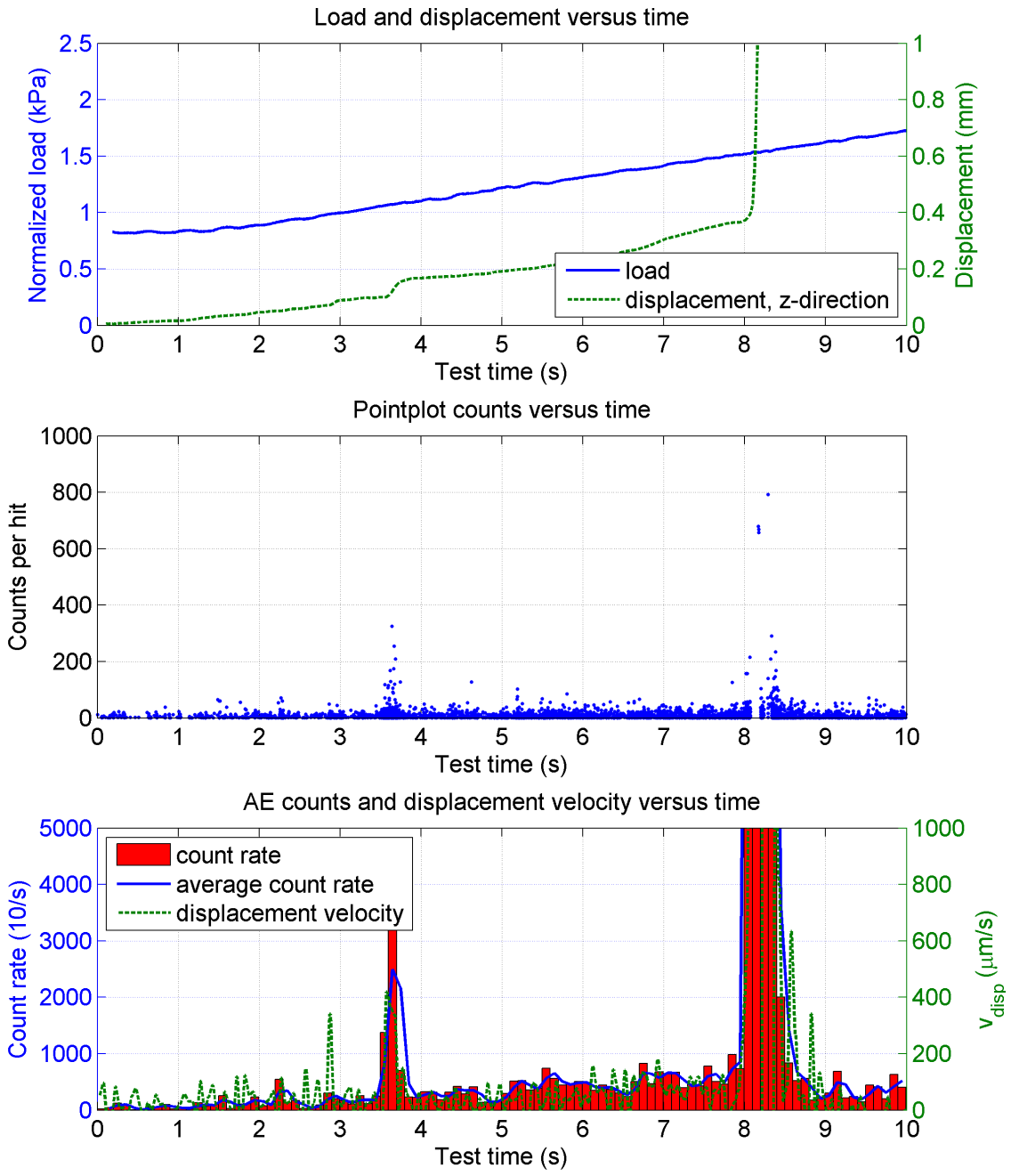

Figure 5.23: Load, displacement and acoustic emissions relations for measurement DHN1, zoomed.

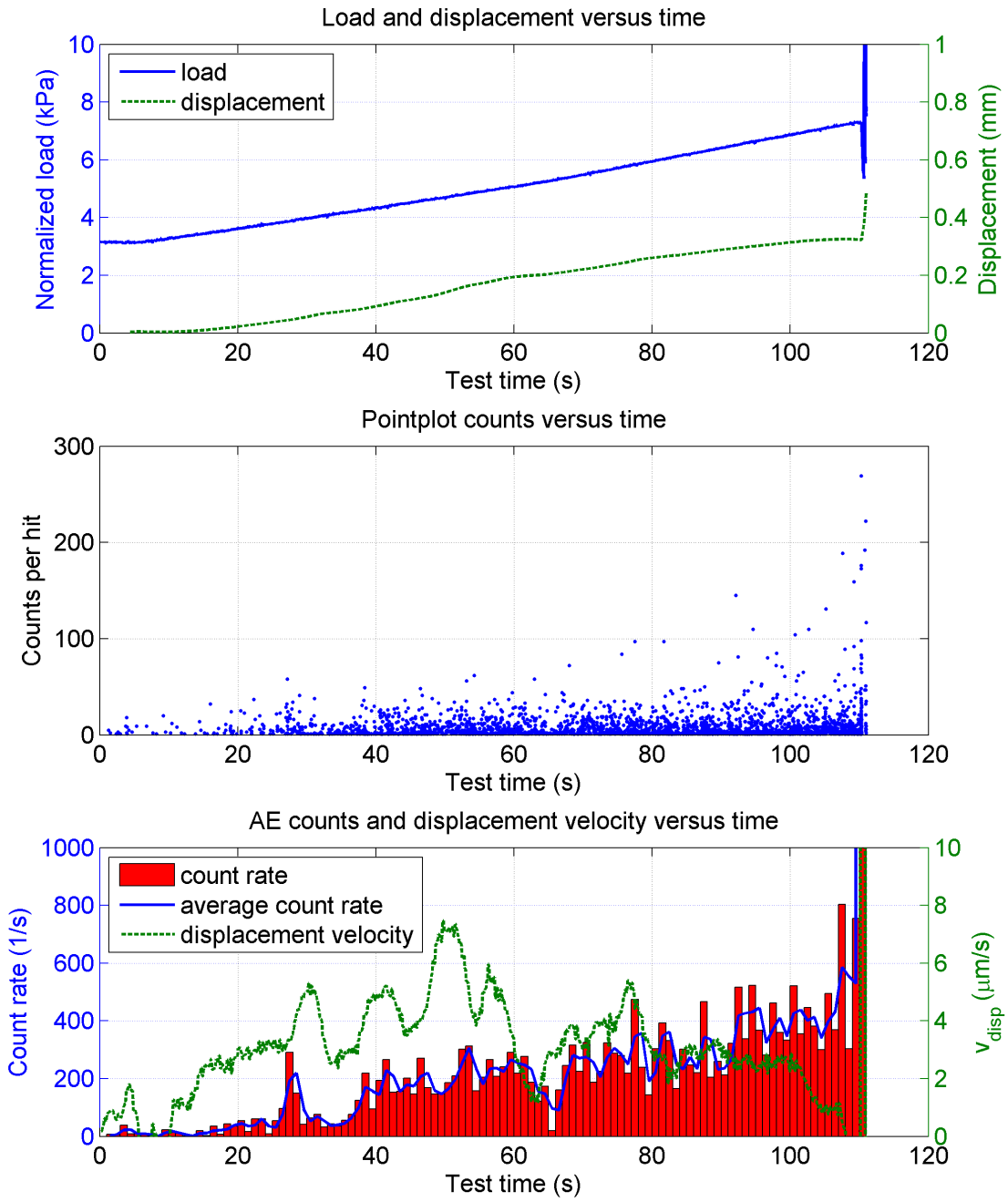

Figure 5.24: Load, displacement and acoustic emissions relations for measurement DHA1, zoomed.

5.2.4 Discussion

Displaying AE activity along with process parameters versus test time is promising and full of various analyzing methods. Comprehensive coverage of several measurements including all the significant AE parameters is a complex task. A selection of measurements with concrete considerations on snow, process, and analyzed AE parameters should be aimed. All the discussed

signal parameters in Chapter 5.1 are capable of displaying AE activity versus test time. Which parameter is best suited should be worked out for every particular application. Especially for field experiments, practical considerations may play a huge role in this process. As far as this thesis was concerned, the count parameter seemed to show all important features. Apart from that, similar count behaviors compared to other AE parameters like for example signal energy or duration were observed (see Chapter 5.1).

Load-controlled tests with snow samples on different tilt angles is probably as close to nature as it gets in the cold laboratory. Still, higher load rates are needed in the laboratory to cause catastrophic failure, and test times of around tens to hundreds of seconds do not correspond to nature. This being the situation, reliable insight into precursory processes inside a snow pack on a laboratory scale with respect to field conditions might remain illusive. Combining field and laboratory experiments seems to be a highly promising approach though. One step towards modeling nature even closer in the laboratory might be special long term experiments, where a sample is monitored while its strength is being reduced. This could be done equally to the technique used to produce weak layer snow samples, i.e. applying a temperature gradient. At the same time, pressure on the sample could be increased occasionally and the acoustic emission response measured continuously.

5.3 Source localization

An integral feature which arises with a multichannel AE recording system is the ability of event source localization. Chapter 2.3 provides theoretical basics. More than when simply analyzing data on single AE channels, three dimensional localization algorithms require high standards on consistent instrumentation conditions and wave propagation properties (Grosse and Ohtsu 2008). Therefore, the localization performance was first evaluated with simulated AE events at known coordinates. After approaches simulating AE sources with piezoelectric sparks failed, evaluation was carried out by applying mechanical stress in small areas within a homogeneous snow sample. It turned out that reproducibility was difficult to obtain, mostly because of varying sensor coupling quality. Reasonable localization performance in terms of accuracy and reproducibility could finally still be achieved.

All figures on the localization experiments consist of two plots. The left hand plots show a two-dimensional section of the snow sample. The green dots indicate the sensor positions, the red dots show localized AE events, i.e. one dot corresponds to one event. The figures' left hand plots depict the energy distribution of all localized events depending on the sample height. The first results presented show a validation experiment (Figure 5.25). The cross denotes the location of the simulated source, surrounded by the measured AE events (red dots). The dot's wide spreading is probably caused to some extent by the indistinct nature of the applied stress. The hypo center localization as a function of sample height via energy distribution shoes a quite

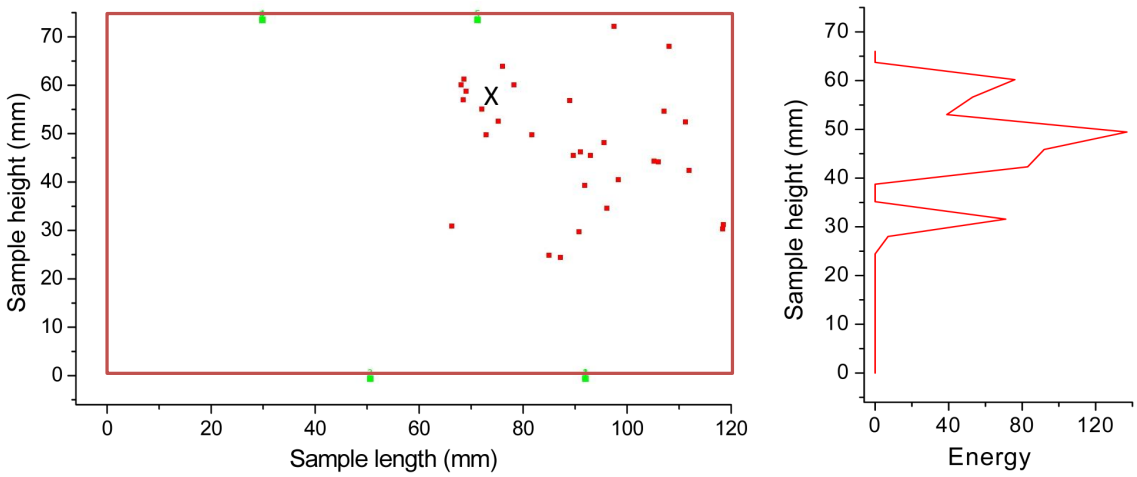

Figure 5.25: Evaluating localization performance by applying mechanical stress at known coordinates. Localized events spread considerably, a distinct hypo center as function of sample height is shown via energy distribution in the left hand plot. The deviation for this measurement was about 7 mm.

distinct point of origin with a deviation of about 7 mm. Accuracies in that range were rated fair enough to continue with the main parts of the experiments, which was to localize AE events in homogeneous and layered snow samples during load controlled compression tests.

A representative measurement with a layered snow sample is shown in Figure 5.26. Acoustic emission activity was assumed a priori to be concentrated in the weak layer. This hypothesis could be proved, especially regarding the AE event's energy distribution. The event distribution (left hand figure) was subject to considerable spreading, similar to what was experienced in the evaluation phase. Distinct energy distribution as a function of sample height reflects the explicitly higher AE activity in the weak layer. Manual inspection of the signal types involved in the localization algorithm revealed that only the type II signals (low frequencies) and more precisely only signals with peak frequencies in the 30 kHz region were part of the localization process. This fact is also true for the comparative measurements on homogeneous snow samples. An example of such a measurement is shown in Figure 5.27. Energy distributions in homogeneous samples were rarely uniform. Mostly energy peaks formed in the regions near the sample surfaces on the top and bottom side respectively. There are several possible explanations for this behavior: On the one hand, events near the sensor are possibly rather recognized by the minimum of the four required sensors. On the other hand, stresses inside a homogeneous snow sample might be unevenly distributed, decreasing towards the snow sample's center. Such a behavior would be certainly amplified by varying sample flatness resulting in spatial difference of pressure application by the pressure plate.

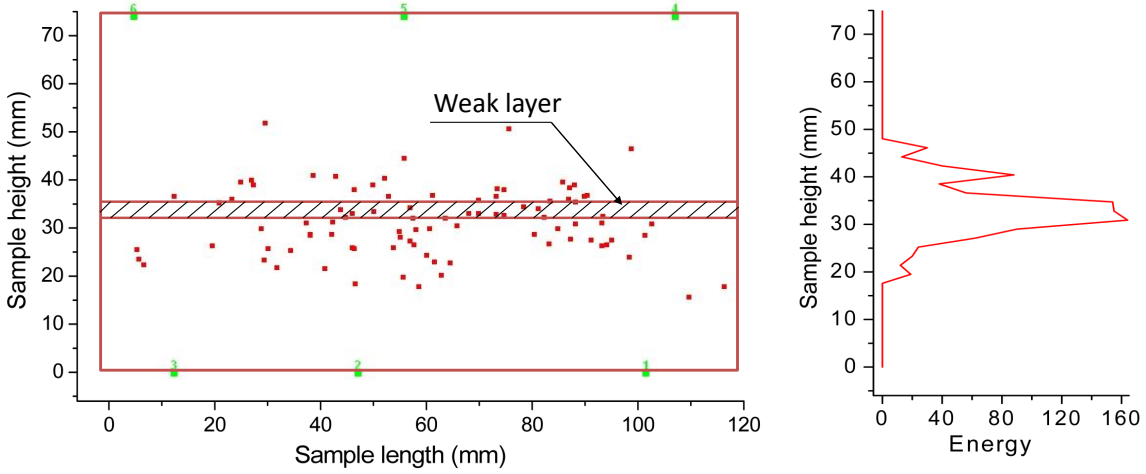

Figure 5.26: Localization experiment with a layered snow sample. Energy distribution versus sample height shows a clear AE activity in terms of energy release inside the weak layer.

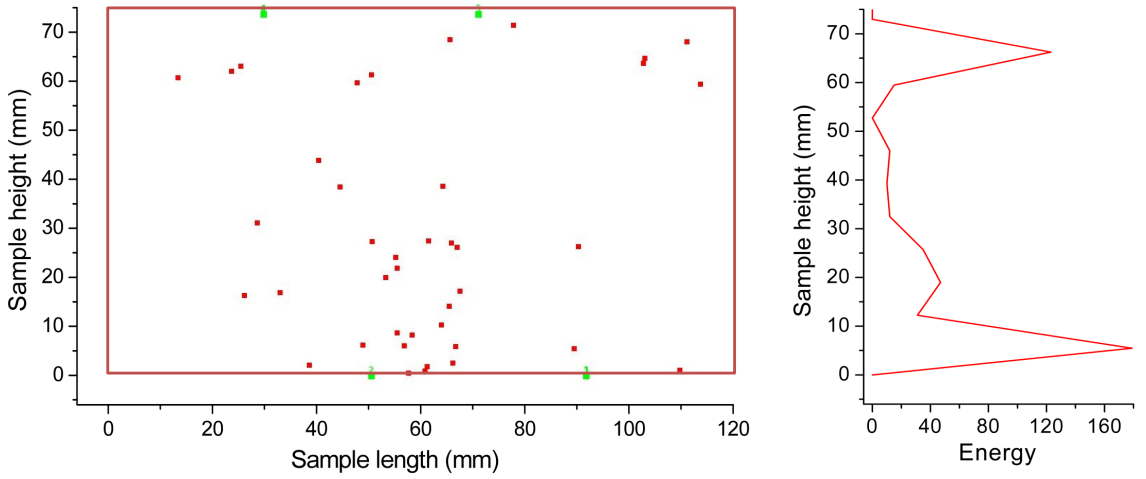

Figure 5.27: Localization experiment with a homogeneous snow sample.

Localizing AE events, especially with a complicated material like snow is a challenging part. It is common sense to evaluate a system's localization performance before carrying out the actual experiments. While for most materials (e.g. concrete, metal, rock, etc.) the test event is produced by a Hsu Nielsen source, also known as pencil lead fracture (PLF) (Grosse and Ohtsu 2008), this is not possible on a soft material like snow. The big advantage behind the Hsu Nielsen source is its well defined nature: Exactly one transient impulse with high energy is released when breaking a pencil lead on a test specimen. Additionally, the source area is very small which allows for high accuracy evaluation test results. Not surprisingly, attempts to break pencil leads on the snow surface mostly failed, even with hard snow samples. Therefore, very rough pretests inside the load apparatus were carried in out in an early stage by applying pressure at only one side

of the sample with results indicating a considerable source of systematic error. It was strongly believed that distortions in wave propagation through the sample holders were responsible for the bad results. This assumption was assured by carrying out localization tests outside the apparatus as shown in Figure 5.28.

In the localization tests without metal plates surrounding the snow sample, no systematic errors, as it was the case for measurements in the load apparatus, did occur. Source simulation attempts were made with piezoelectric sparks and pencil lead breaks on a screwdriver, introducing the signal into the snow. Neither of both techniques turned out to be sufficient in terms of required energy amount released. Only some events could be localized with minimum signal energies, some were not localized at all. Tests applying mechanical stress at certain spots inside the snow with the help of a cranked wrench key turned out to deliver satisfactory results. Good reproducibility was derived, however considerable spreading of the introduced AE events had to be accepted.

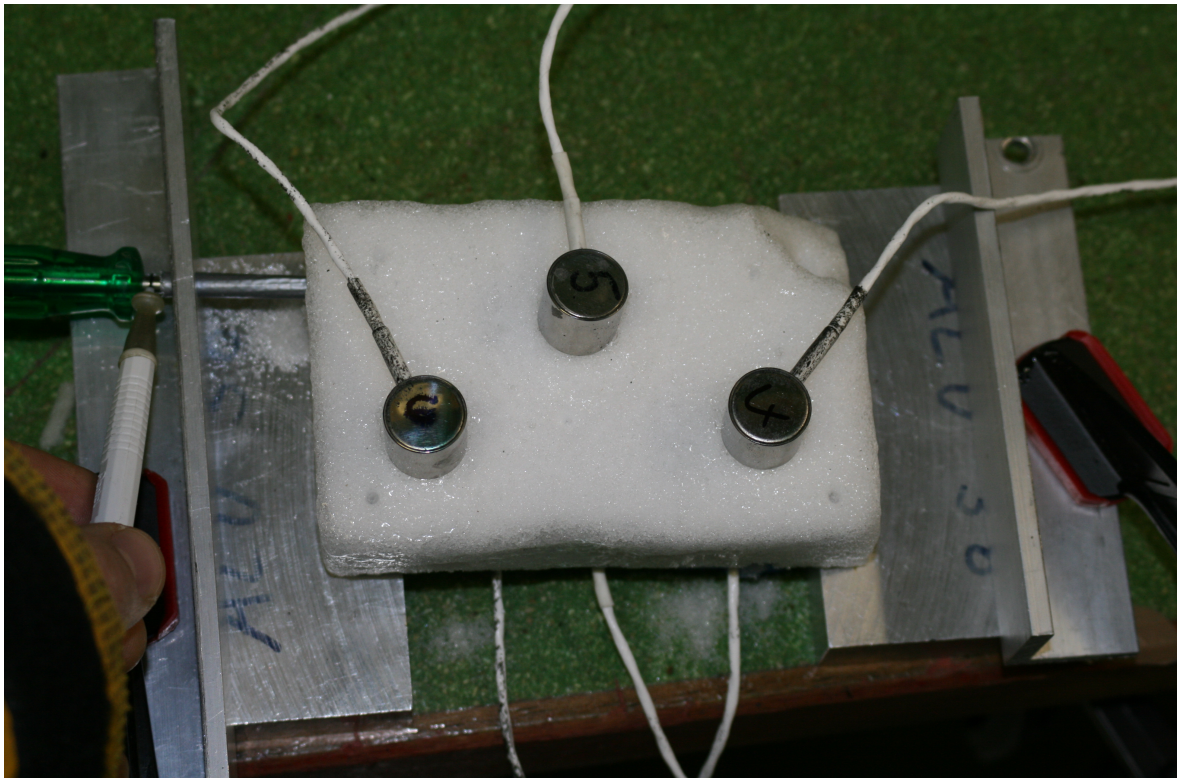

Figure 5.28: Localization test outside the apparatus. A source was simulated by a PLB break introduced into the snow via a screw driver.

A concluding note on AE events localization in snow should be finally given regarding snow sample size. The reported measurements were conducted with quite small snow samples. Signals which were part of the localization algorithm showed high energy values. This fact would allow for increased sample sizes in terms of signal attenuation which would offer interesting possibilities.

On the one hand, crack propagation could be traced properly in space and time. On the other hand, decent sample size would possibly allow for a discrimination of P- and S-wave, which would improve localization performance (Grosse and Ohtsu 2008) and increase knowledge of wave propagation in snow. Last but not least, increasing sample size in the laboratory would gain knowledge needed for deploying a test site in the field.

Chapter 6

Conclusions and outlook

The laboratory work performed within this thesis was an important step towards understanding acoustic emission processes in snow. AE signals could be recorded in high quality and were analyzed paying particular attention to various parameters. Great insight into micro scale failure processes inside the snow pack could be gained. Approaches on signal classification were worked out by investigating the classical signal parameters as well as the signal-based frequency parameters. Most reliable conclusions on different signals and their possible mechanical formation can be drawn by combining both types of parameters. Inversely proportional behavior of failure size and signal frequency, as reported from Sommerfeld (1982) at the meso and macro scale, seem to be the case at the micro scale as well. Precursor signals prior to catastrophic failure were sometimes observed as short periods of significantly higher count rates, energies and durations. However, samples also ruptured without exhibiting such precursory patterns. Finally, three-dimensional source localization was carried out successfully. For layered snow samples, acoustic emission activity was concentrated in the weak layer. Limitation in terms of accuracy and feasibility had to be accepted.

Suggestions for further research on this topic emphasize on approaches both in laboratory and field. Since it was the first time that acoustic emissions of snow were investigated with a professional signal-based recording system, there was an extremely large number of possible ways to analyze the data. As it can be seen in Chapter 5, this was done systematically by investigating the various signal parameters. In terms of snow and process parameters with high influence on the acoustic emission response there was not much room for systematical variation. This should be part of further research in the laboratory with main concerns on reproducibility.

As far as the measurement system is concerned, highest attention should be drawn to preamplifier gain, threshold level and timing parameters. Highest possible amplification might lead to overdrive and wrong parameter extraction in times of large failures. On the other hand, high preamplifier gain provides the best sensitivity for experiments concentrating on very low level signals (e.g. present in low density snow, during tests with low load rates or large samples).

Threshold level and timing parameters have to be considered in combination: A low threshold level can cause the recording device to operate at full capacity. More precisely, huge failure processes, which produce very long and strong AE signals, can block the signal processing on the data acquisition cards in such a way that dramatic errors occur in parameter extraction. Increasing the timing parameter diminishes these problems, because the system "blocks itself" for a longer period, assuring the time needed for correct data processing. Since measurements with a preamplification gain of 60 dB tended to cause overload problems, it is suggested to continue the laboratory scale experiments at a gain of 40 dB.

On the hardware side, sensor coupling is an important issue to deal with and having the sensors integrated in the system's actuator, i.e. the plate applying the force on the sample, can be a source of systematic error. An alternative way of applying stress on a sample would be the so called three point bending test, already applied on snow samples by Sigrist (2006). This test is widely used in non-destructive testing including acoustic emission testing (e.g. Gallego et al. 2010) Also, *b*-value analysis and improved *b*-value analysis, like carried out for rock by Rao and Lakshmi (2005) or concrete (Shiotani et al. 2001) could be included. This material science approach is certainly not that close to natural loading of snow but the advantages would be:

- Standardized technique with extensive research in various materials
- Easier visual inspection of the sample during the test
- Easier sensor placement and reliable decoupling of sensors and loading force.
- Possibility of increased sample size

As the laboratory results show, the high damping of snow makes it impossible to monitor bigger samples or even real slopes in the field without managing to increase the detectable ray path length. This ray path length could be increased using waveguides which receive stimuli from somewhere in a snow pack and carry the resulting wave with low losses to acoustic emission sensors. An approach which includes waveguides is for example used in soil science in order to find precursors for landslides (Cohen et al. 2009). Having the same goal to find and use acoustic precursors for the prediction of avalanches and landslides respectively, cooperation between these research fields is already strong and will hopefully be even more extended in the future. Besides increasing the detection radius, practical issues like power supply and data management have to be considered for field application. A field site monitoring seismic signals with geophones in the Swiss Alps (van Herwijnen and Schweizer 2011) already provides good infrastructure.

The laboratory research for the thesis consciously placed emphasis on signal-analysis by recording entire waveforms (signal-based AE technique). This approach works well in laboratory with manifold applications. However, for field experiments a classical AE approach (i.e. extracting signal parameters by analog circuits) might be sufficient and would drastically reduce complexity and error-proneness. In terms of sensor selection, it is suggested to concentrate on the region

around 30 kHz where obviously high energy is present in the acoustic emission signals. In accordance with assumptions made within this thesis and by Scapozza et al. (2004), sensitivity would be highest for brittle failure mechanisms at the micro and meso scale. Resonant sensors in the frequency range around 30 kHz could be used to improve the signal-to-noise ratio.

The most efficient and promising way of monitoring processes inside the snowpack at every scale seems to be the combination of low frequency analysis (seismic signals by geophones) and high frequency acoustic emission monitoring. Influences on geophones from low frequency noise produced by surrounding ski areas or aircrafts (van Herwijnen and Schweizer 2011) should be far less dominant in the 30 kHz region. To monitor big areas and big-scale acoustic emission phenomena, geophones are the best choice. On the other hand, effects at the meso scale like for example water flow and the quality of local displacements represent vital additional information. Combining the two data sets in the analysis could be a very important point in using acoustic precursors for avalanche prediction. Further promising improvement could be achieved by not only combining different acoustic emission data but also including well known mechanical tests at the same field site. Ongoing research at the SLF already correlates data from fracture propagation tests (PST, propagation saw tests) and automatic snow profiles from the SMP (snow micro penetrometer) (Johnson and Schneebeli 1999; Schweizer et al. 2010). It would be interesting to include acoustic emission data in these observations. In this context, also the acoustic emission response during and after mechanical input would be an interesting research topic. An acoustic snow penetrometer working on this principle in the micro scale has already been developed (Staack 2004). At a larger scale, responses to defined mechanical input could be observed with a geophone and provide information of great practical value on the snowpack's condition.

Despite various challenges, acoustic emission techniques applied on snow certainly seem to have great potential. Highly promising practical applications in the field of avalanche formation and forecasting could be complemented by a deeper theoretical insight into wave propagation in snow. How acoustic waves exactly propagate in snow depending on their frequency is still not clear. It would be interesting to see experiments exclusively concentrating on this point. Snow density is an important parameter in the context of wave propagation, but certainly not the only one. The complex parameter snow texture seems to involve concise information on how acoustic waves travel through snow. Investigations on snow texture on a micro scale with the help of micro computer tomography (μCT) is an outstanding research field at the WSL Institute for snow and avalanche research SLF (e.g. Schneebeli 2004). Probably μCT pictures and the corresponding values can help to understand the wave propagation in snow and establish a proper model. Last but not least reliable signal classification could be aided by pattern recognition techniques, which is a core competence of the JOANNEUM Forschungsgesellschaft.

Appendix A

Sensor characteristics

This chapter shows the original sensor calibration certificates, supplied by Physical Acoustics Corporation.

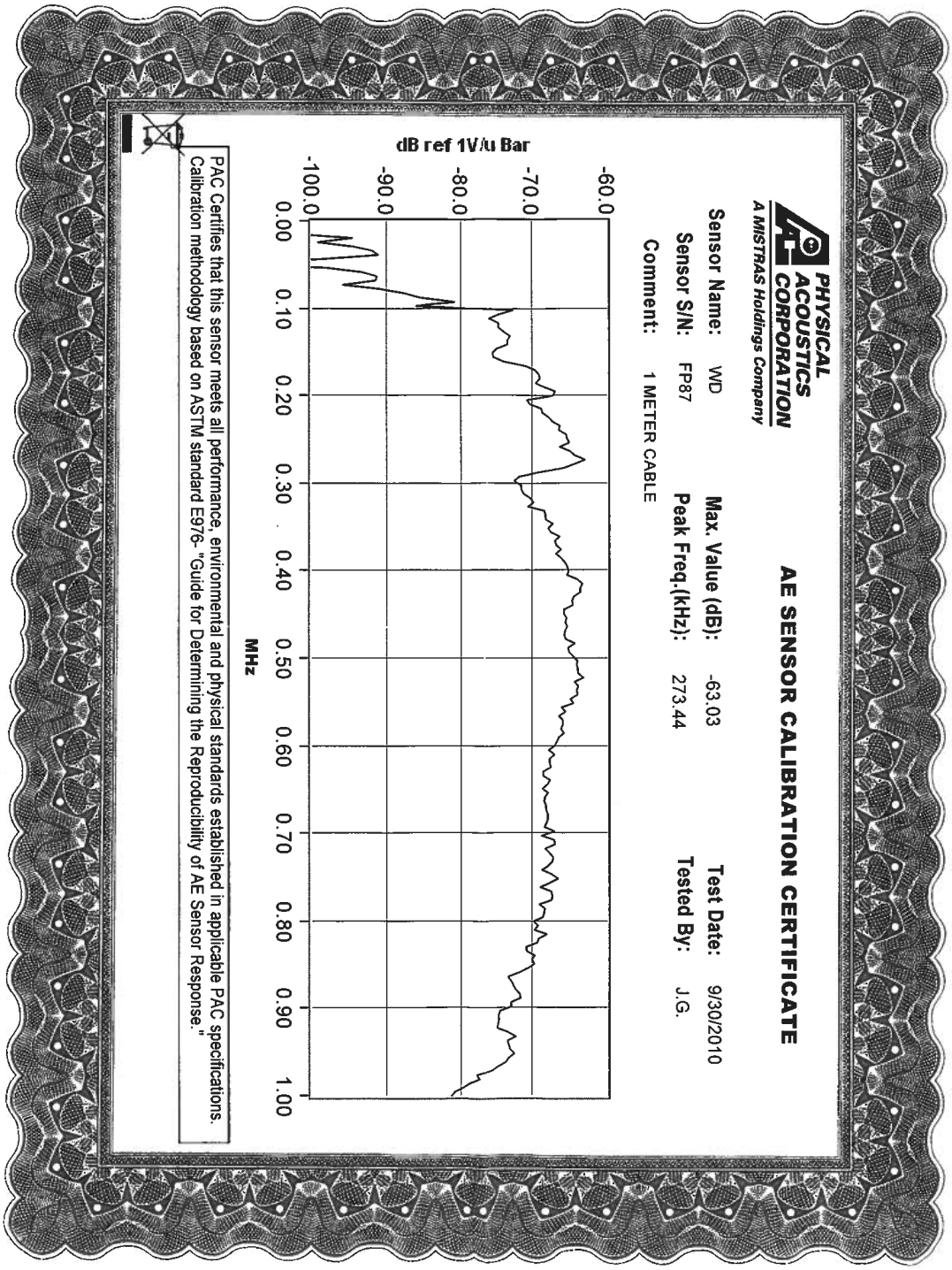

Figure A.1: Calibration certificate, sensor PAC WD FP87

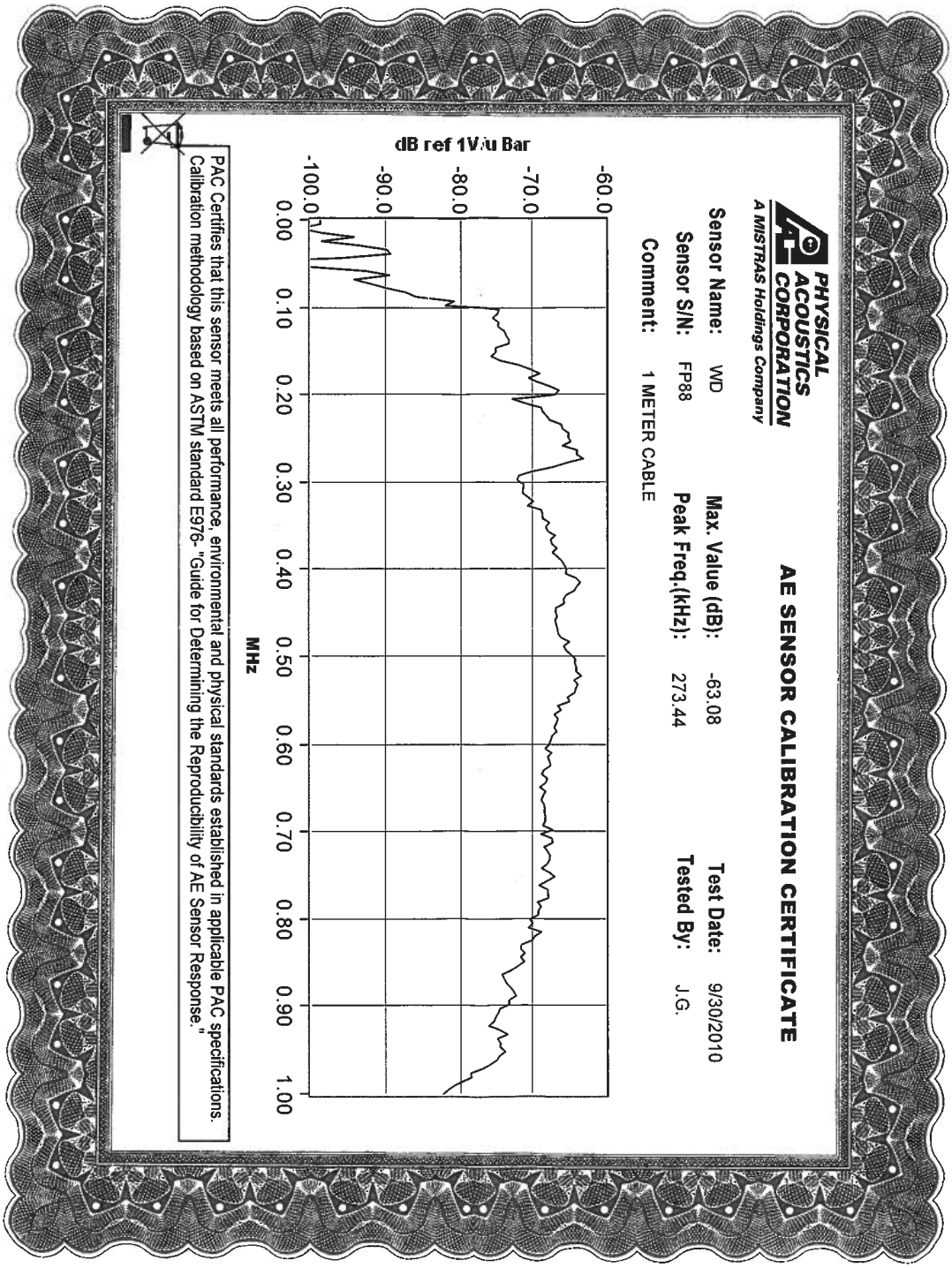

Figure A.2: Calibration certificate, sensor PAC WD FP88

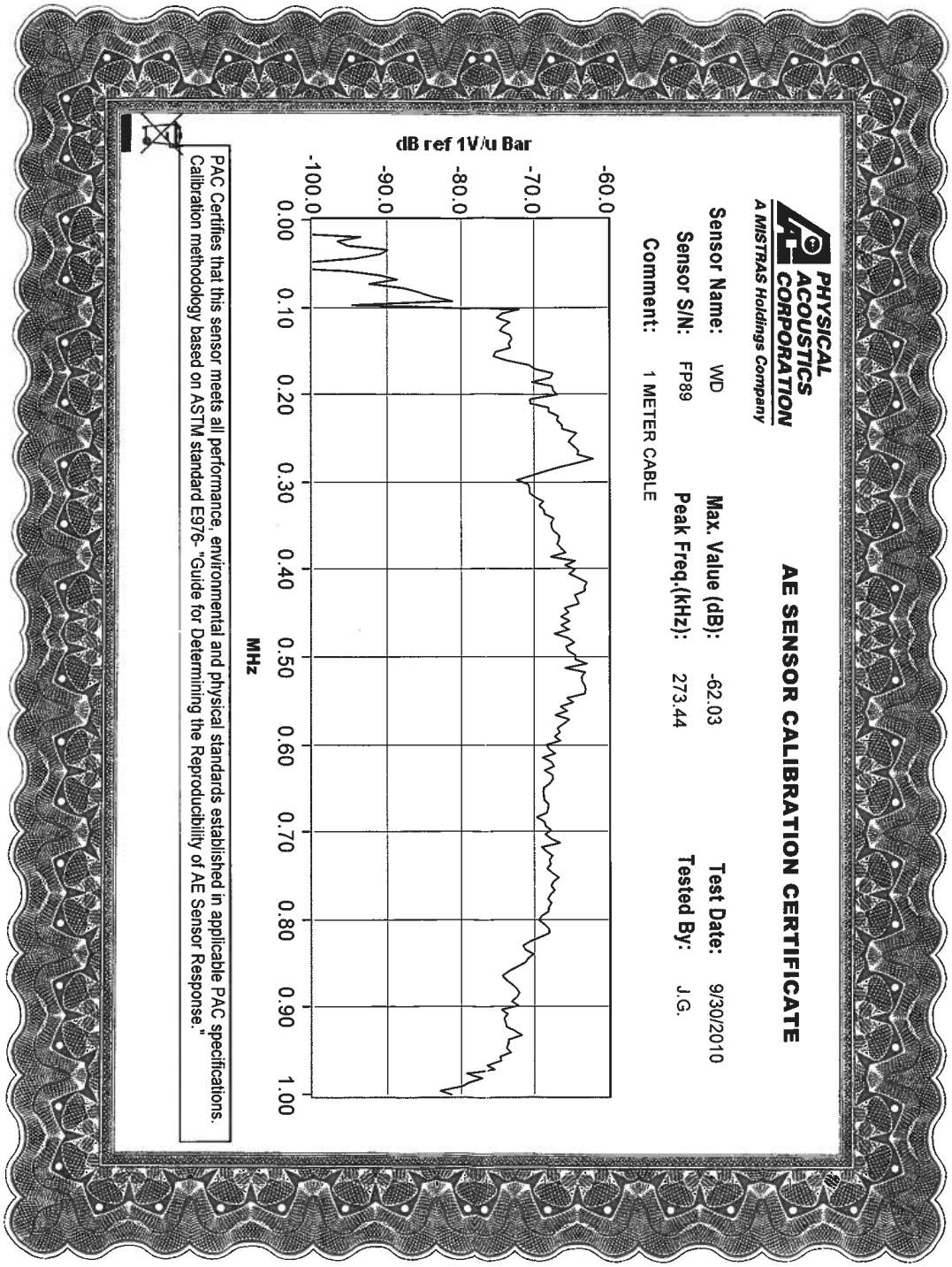

Figure A.3: Calibration certificate, sensor PAC WD FP89

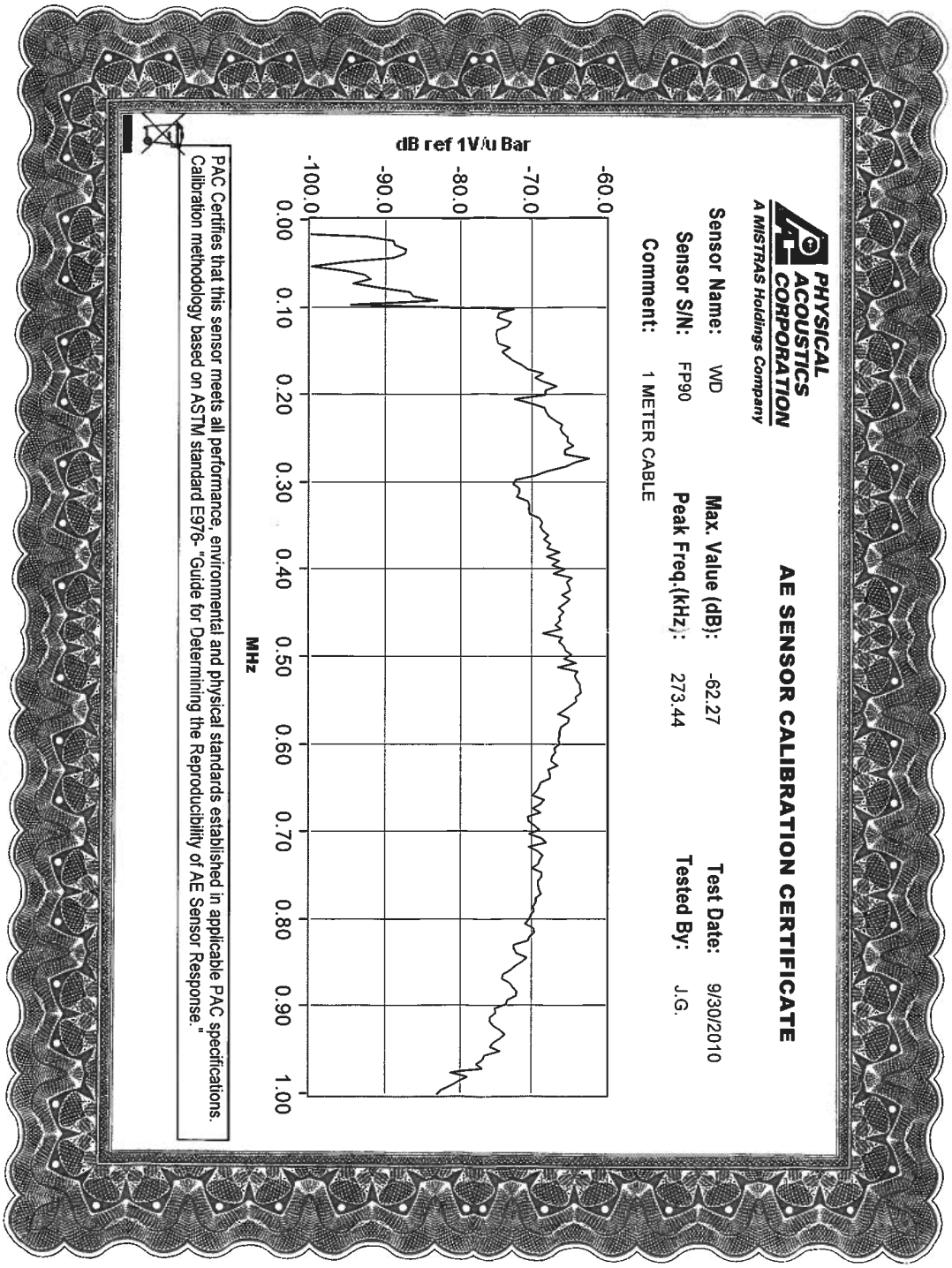

Figure A.4: Calibration certificate, sensor PAC WD FP90

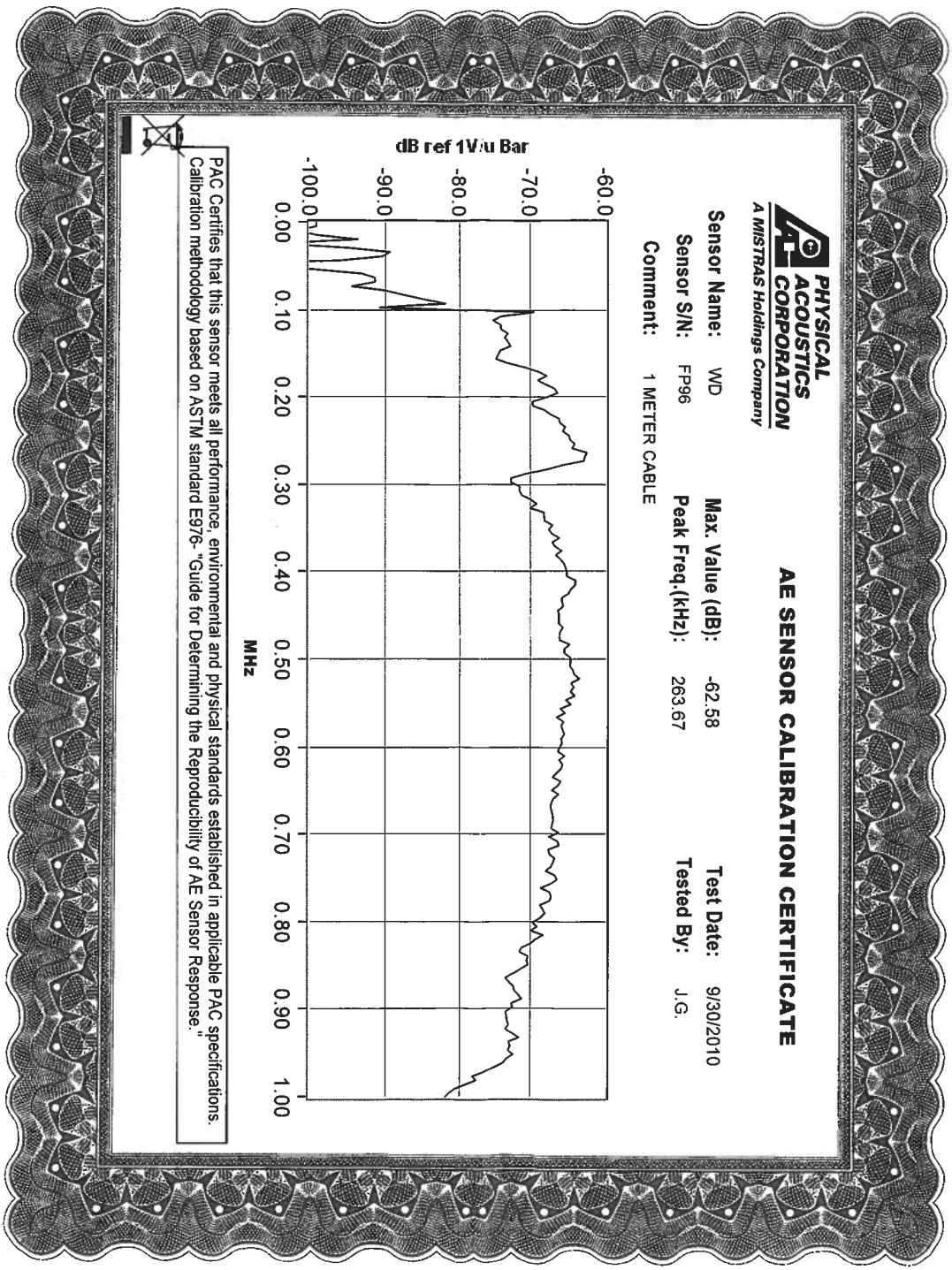

Figure A.5: Calibration certificate, sensor PAC WD FP96

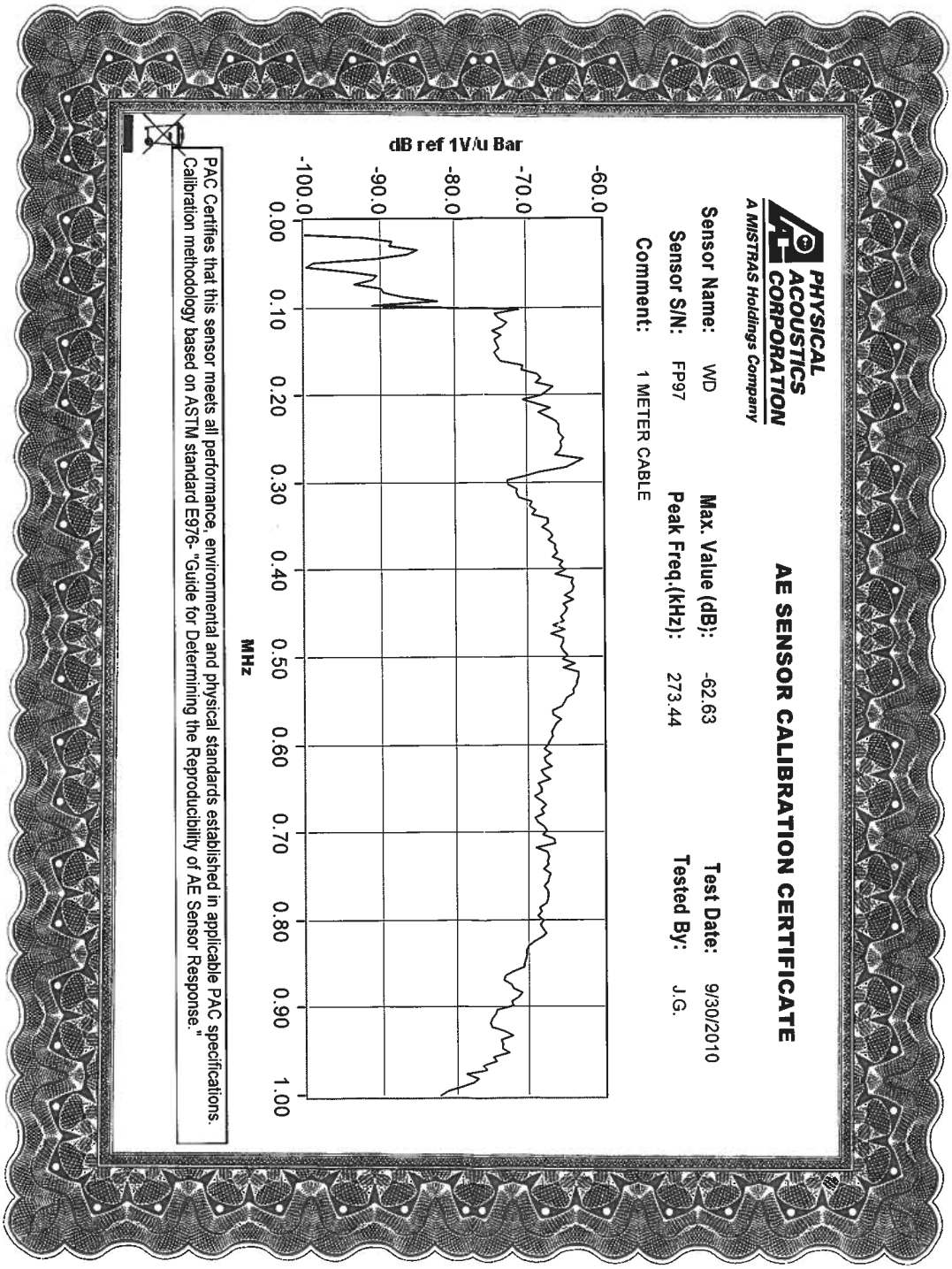

Figure A.6: Calibration certificate, sensor PAC WD FP97

Appendix B

Various AE parameters versus test time

This chapter shows additional measurements with layered DHA (depth hoar artificially grown) snow samples. Measurements details are given in Table B.1. Compared AE parameters are count rate, absolute energy and rise time.

Meas.	Snow	ϕ	$\dot{\sigma}$	Amp.	Rupt
DHA2	Layered 120x73x90 mm, outer layers: ρ_{ol} = 192 kg/m^3, RGlr 0.5 mm, hardness 2 (soft, 4 fingers). Weak layer: FCxr (RGlr) 0.75 mm, hardness 1 (very soft, fist)	10°	392 Pa/s	60 dB	Yes
DHA3	Layered 120x73x90 mm, outer layers: ρ_{ol} = 192 kg/m^3, RGlr 0.5 mm, hardness 2 (soft, 4 fingers). Weak layer: FCxr (RGlr) 0.75 mm, hardness 1 (very soft, fist)	10°	113 Pa/s	60 dB	Yes
DHA4	Layered 120x73x90 mm, outer layers: ρ_{ol} = 192 kg/m^3, RGlr 0.5 mm, hardness 2 (soft, 4 fingers). Weak layer: FCxr (RGlr) 0.75 mm, hardness 1 (very soft, fist)	10°	387 Pa/s	60 dB	Yes
DHA5	Layered 120x73x90 mm, outer layers: ρ_{ol} = 192 kg/m^3, RGlr 0.5 mm, hardness 2 (soft, 4 fingers). Weak layer: FCxr (RGlr) 0.75 mm, hardness 1 (very soft, fist)	10°	226 Pa/s	60 dB	No

Table B.1: Various AE parameters versus test time: Set of additional measurements with layered snow samples: Sample dimensions are given in the form length x height x width. The codes for the morphological snow classifications are in accordance with Fierz et al. (2009): RGlr means "large rounded grains", DFdc stands for "partly decomposed precipitation particles", FCxr for "rounded faceted particles" and DHxr for "rounding depth hoar". In case there is a second grain type in brackets, the first one is the primary and the one in the brackets the secondary type. The code for the grain type is followed by the crystal's diameter. ϕ denotes the tilt angle and $\dot{\sigma}$ the normalized load rate corresponding to the sample areas , given in Pa/s. The right column indicates if the sample ruptured or not.

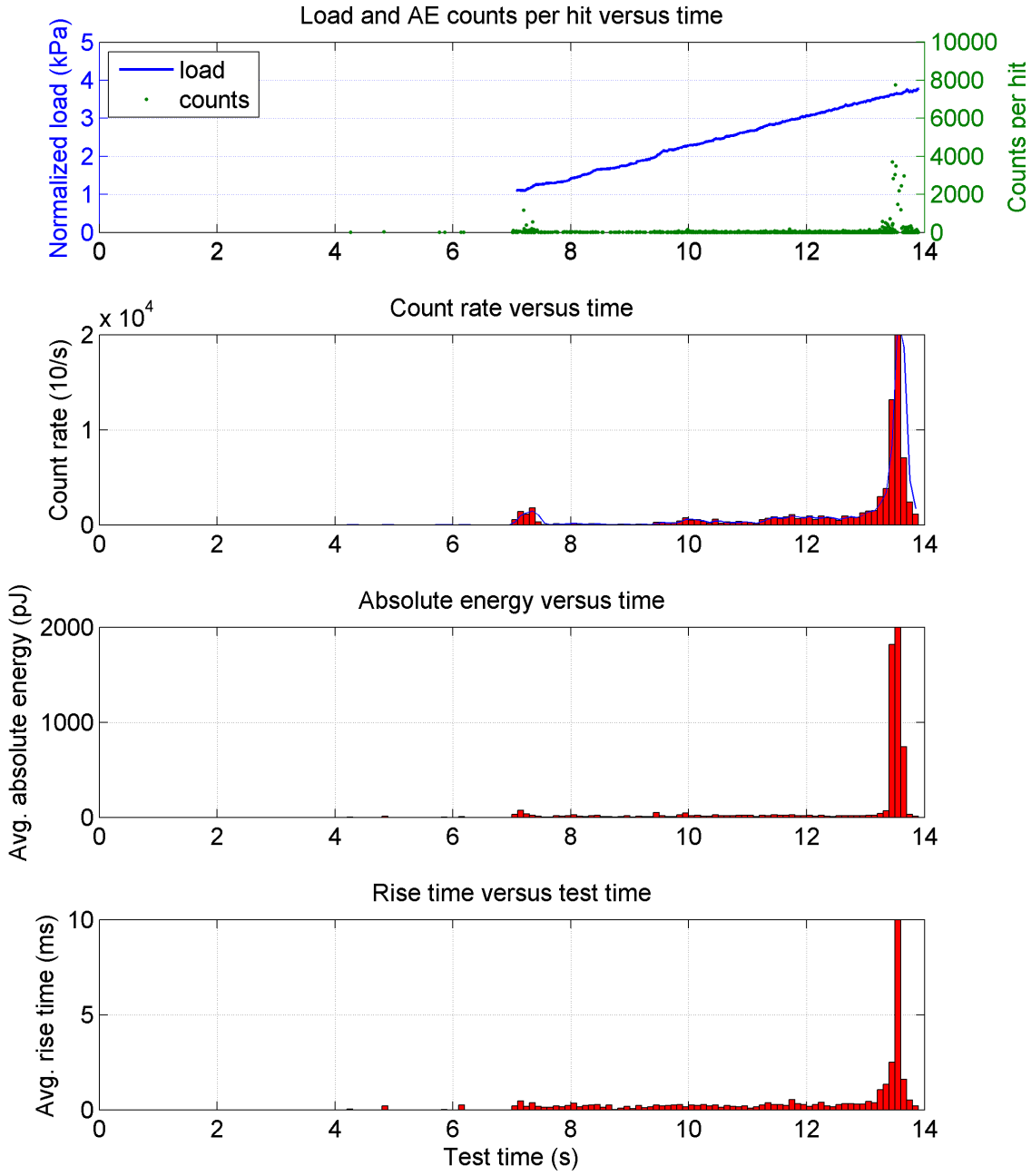

Figure B.1: Load, displacement and acoustic emissions relations for measurement DHA2.

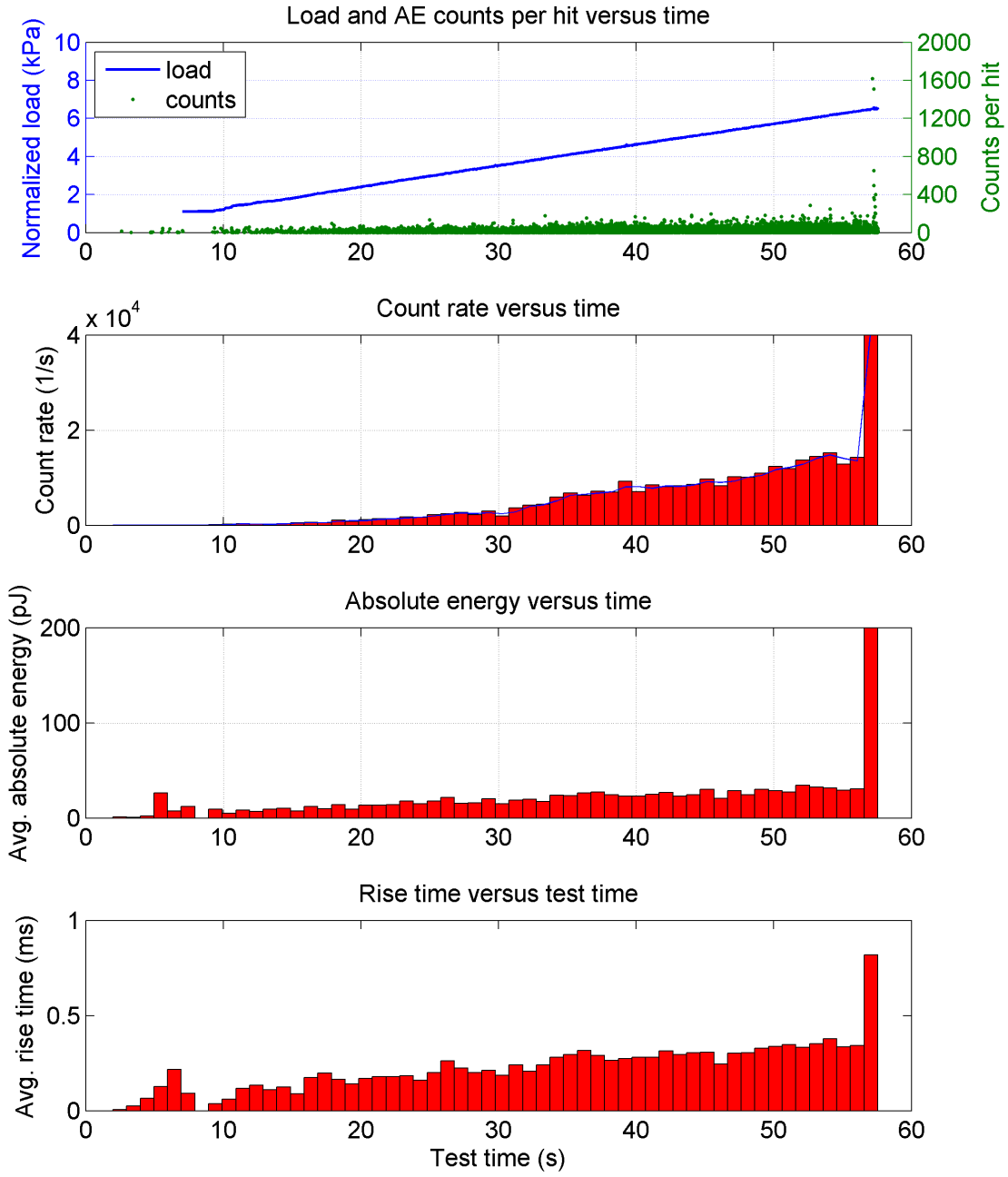

Figure B.2: Load, displacement and acoustic emissions relations for measurement DHA3.

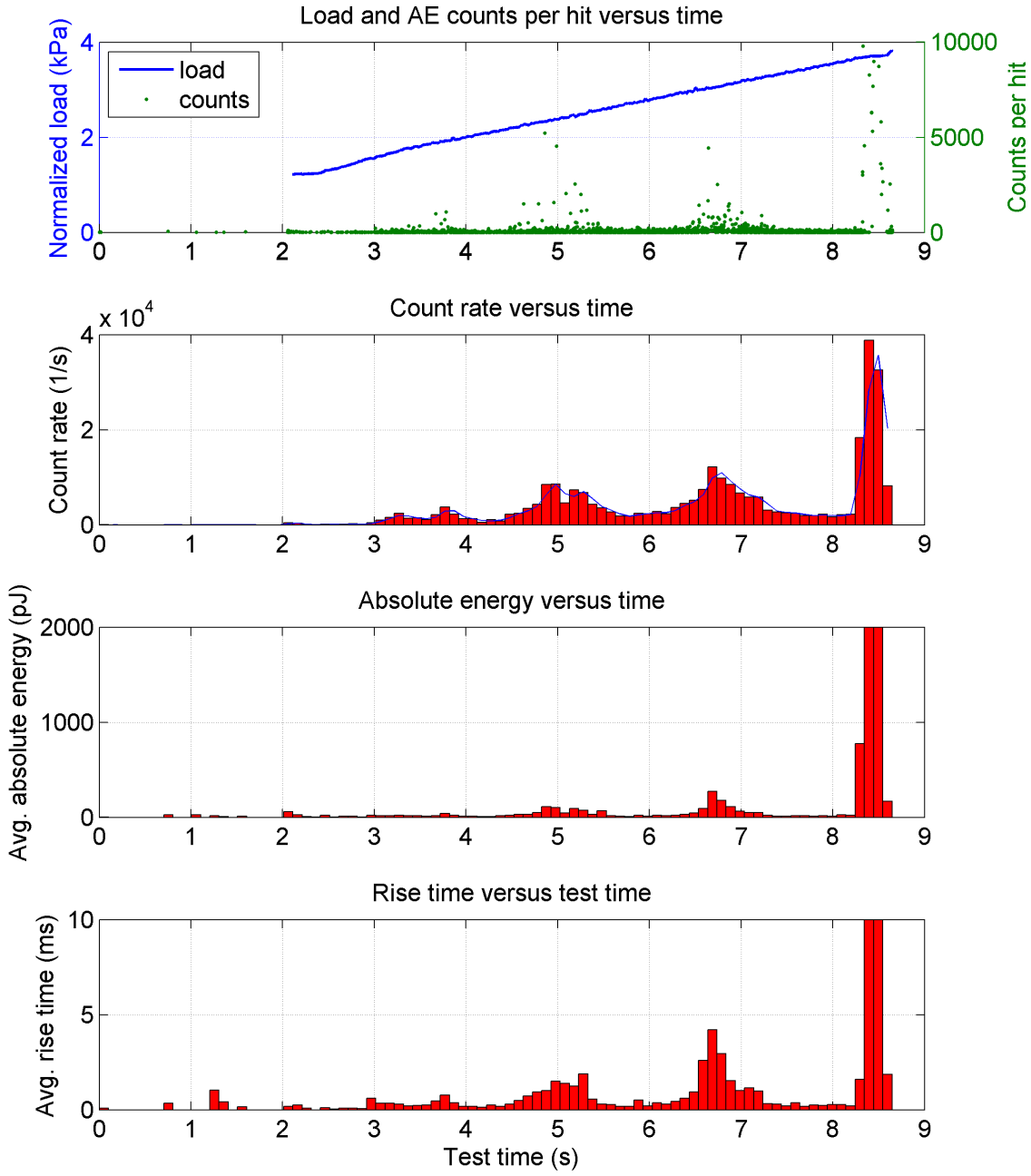

Figure B.3: Load, displacement and acoustic emissions relations for measurement DHA4.

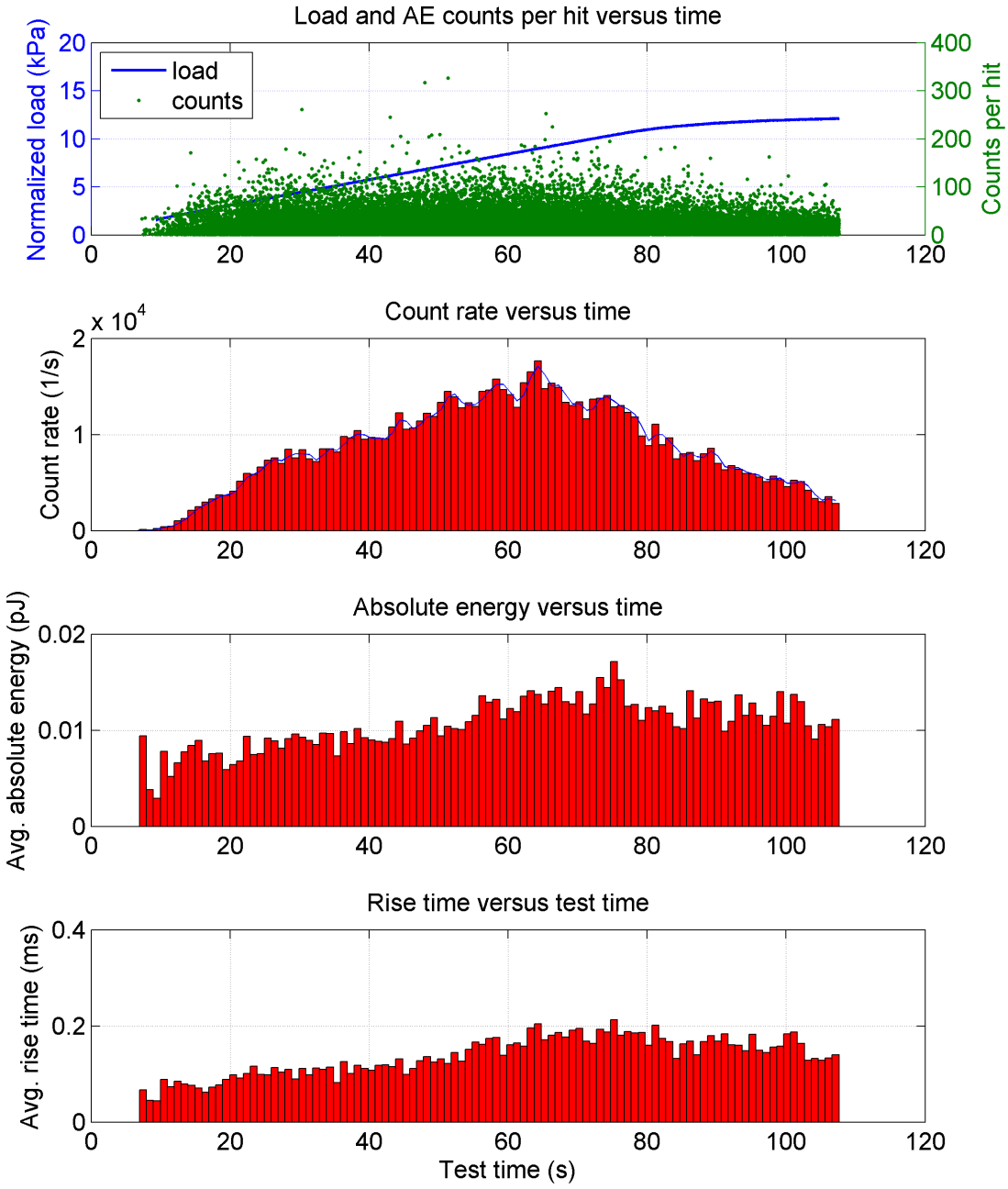

Figure B.4: Load, displacement and acoustic emissions relations for measurement DHA5.

Bibliography

Biot, M., 1962: Mechanics of deformation and acoustic propagation in porous media. *Journal of Applied Physics*, **33 (4)**, 1482–1498.

Bowles, D. and W. F. St.Lawrence, 1977: Acoustic emissions in the investigation of avalanches. *Western Snow Conference, 45th, 88-94. (Annual Meeting, 18-21 April 1977, Albuquerque, New Mexico)*.

Bradley, C. and W. St.Lawrence, 1975: Kaiser effect in snow. *IAHS-AISH P.*, **114**, 145–154.

Buser, O., 1986: A rigid frame model of porous media for the acoustic impedance of snow. *Journal of Sound and Vibration*, **111**, 71–92.

Camponovo, C. and J. Schweizer, 2001: Rheological measurements of the viscoelastic properties of snow. *Annals of Glaciology*, **32**, 44–50.

Cohen, D., M. Schwarz, G. Michlmayr, and D. Or, 2009: Precursory acoustic emissions from bench-scale landslides. *EGU General Assembly 2009*.

Dewart, G., 1968: *Seismic investigation of ice properties and bedrock topography at the confluence of two glaciers, Kaskawulsh Glacier, Yukon Territory, Canada*. Ohio State University. Institut of Polar Studies. Report No. 27.

DIN EN 1330-9, 2000: Non-destructive testing - terminology - part 9: Terms used in acoustic emission testing; trilingual version en 1330-9 : 2000. DIN EN 1330-9, DIN EN 1330-9.

Ernst, R., 2007: Konstruktion eines kraftgesteuerten Scherapparates zur Evaluation mechanischer Eigenschaften von Schneeproben. *Semesterarbeit, Swiss Federal Institut of Avalan- che Research CH-7260 Davos Dorf*.

Ernst, R., 2009: Akustische Emissionen von Schnee bei kraftgesteuerten Scherversuchen. M.S. thesis, ETH Zurich, Switzerland.

Fahy, F., 2001: *Foundations of Engineering Acoustics*. Academic Press.

Fierz, C., et al., 2009: The international classification for seasonal snow on the ground. Tech. rep., IHP-VII Technical Documents in Hydrology No.83, IACS Contribution No.1, UNESCO-IHP, Paris.

Finck, F., 2005: Untersuchung von Bruchprozessen in Beton mit Hilfe der Schallemissionsanalyse. Ph.D. thesis, Universität Stuttgart.

Fukuzawa, T. and H. Narita, 1992: An experimental study on the mechanical behavior of a depth hoar layer under shear stress. *Proceedings International Snow Science Workshop. Breckenridge, Colorado, U.S.A., 4?8 October*, 171–175.

Gallego, A., E. Suarez, J. M. Vico, C. Infantes, and R. Piotrkowski, 2010: Acoustic emission during three-point bending test of corroded galvanized steel. *European Working Group on Acoustic Emissions, Vienna*.

Gold, L., 1960: The cracking activity of ice during creep. *Canadian Journal of Physics*, **38, No. 9**, 1137 – 1148.

Graff, K. F., 1991: *Wave Motion in Elastic Solids*. Dover Publications.

Grosse, C., 1996: Quantitative zerstörungsfreie Werkstoffprüfung von Baustoffen mittels Schallemissionsanalyse und Ultraschall. Ph.D. thesis, Universität Stuttgart.

Grosse, C. and M. Ohtsu, (Eds.) , 2008: *Acoustic Emission Testing*. Springer; 1 edition.

Johnson, J., 1982: On the application ob biot's theory to acoustic wave propagation in snow. *Cold Reg. Sci. Technol.*, **6**, 49–60.

Johnson, J. and M. Schneebeli, 1999: Characterizing the microstructural and micromechanical properties of snow. *Cold Reg. Sci. Technol.*, **30**, 91–100.

Keprt, J. and P. Benes, 2008: Progress in primary calibration of acoustic emission sensors. *The Journal of the Acoustical Society of America, vol. 123*, **123, issue 5**, 3317.

Manthei, G., 2001: Moment tensor evaluation of acoustic emission in salt rock. *Construction and Building Materials*, **15**, 197–309.

Maysenhölder, W., M. Schneebeli, X. Zhou, T. Zhang, and M. Heggli, 2008: Sound absorption of snow. *IBP-Mitteilung 486: 2 S.*

McClung, D. M., 1986: Mechanics of snow slab failure from a geotechnical perspective. *Avalanche Formation, Movement and Effects (Proceedings of the Davos Symposium, September 1986). IAHS Publ. no. 162,1987.*

McClung, D. M. and P. Schaerer, 1993: *The Avalanche Handbook*. The Mountaineers, Seattle, Washington, U.S.A.

Mellor, M., 1975: A review of basic snow mechanics. *IAHS Publ.*, **114**, 251–291.

Meyers, M. A., 1994: *Dynamic behaviour of materials*. Wiley-Interscience, 1. edition.

Miller, R. K. and P. McIntire, (Eds.) , 1987: *Nondestructive Testing Handbook*, Vol. 5, Acoustic Emission Testing. American Society for Nondestructive Testing.

Munter, W., 2009: *Drei mal drei (3x3) Lawinen. Risikomanagement im Wintersport*. Pohl und Scheelhammer; Vierte, völlig neubearbeitete Auflage.

Oura, H., 1952: Sound velocity in the snow cover. *Contrib. Inst. Low Temp. Sci. Hokkaido Univ.*, 171–178.

PAC, 2007: Pci-2 based AE System User's Manual, rev.3, april 2007. *Physical Acoustics Corporation*.

Pollock, A. A., 2008: Some observations on acoustic emission/stress/time relationships. *Acoustic emission and critical phenomena*, C. Alberto and G. Lacidogna, Eds., Taylor & Francis 2008, chap. Acoustic emission and critical structural states, 29–39.

Rao, M. V. M. S. and K. J. P. Lakshmi, 2005: Analysis of b-value and improved b-value of acoustic emissions accompanying rock fracture. *Current Science*, **89, No. 9**, 1577–1582.

Reginald Hardy Jr., H., 2003: *Acoustic Emission / Microseismic Activity: Volume 1: Principles, Techniques, and Geotechnical Applications*. A.A. Balkema Publishers.

Reiweger, I., J. Schweizer, R. Ernst, and J. Dual, 2010: Load-controlled test apparatus for snow. *Cold Reg. Sci. Technol.*, **62 (2-3)**, 119–125.

Rose, J. L., 1999: *Ultrasonic Waves in Solid Media*. Cambridge University Press.

Scapozza, C., F. Bucher, P. Amann, W. J. Ammann, and P. Bartelt, 2004: The temperature- and density-dependent acoustic emission response of snow in monoaxial compression tests. *Annals of glaciology*, **38**.

Schneebeli, M., 2004: Numerical simulation of elastic stress in themicrostructure of snow. *Annals of Glaciology*, **34**, 339–342.

Schweizer, J., 1998: Laboratory experiments on shear failure of snow. *Annals of glaciology*, **26**, 97–102.

Schweizer, J., 1999: Review of dry snow slab avalanche release. *Cold regions science and technology*, **30**, 43–57.

Schweizer, J., J. Jamieson, and M. Schneebeli, 2003: Snow avalanche formation. *Reviews of Geophysics*, **41**.

Schweizer, J. and J. B. Jamieson, 2010: Snowpack tests for assessing snow-slope instability. *Annals of Glaciology*, **51 (54)**, 187–194.

Schweizer, J., A. van Herwijnen, and B. Reuter, 2010: Measurements of weak layer fracture energy. *in propgress*.

Sentler, L., 1971: *A strength theory for viscoelastic materials*. Document D9, Swedish Council for Building Research.

Shiotani, T., S. Yuyama, Z. W. Li, and M. Ohtsu, 2001: Application of the ae improved b-value to qualitative evaluation of fracture process in concrete materials. *J. Acoust. Emission*, **19**, 118–132.

Sigrist, C., 2006: Measurement of fracture mechanical properties of snow and application to dry snow slab avalanche release. Ph.D. thesis, ETH Zürich.

Smith, J. L., 1965: The elastic constants, strength and density of greenland snow as determinded from measurements of sonic wave velocity. *Tech Report. 216, U.S: Army Cold Reg. Res. and Eng. Lab., Hanover, N.H.*

Sommerfeld, R., 1982: A review of snow acoustics. *Reviews of Geophysics and Space Physics*, **20**, 62–66.

Sommerfeld, R. A., 1977: Preliminary obsevations of acoustic emissions preceding avalanches. *Journal of Glaciology*, **19**, 399–409.

Sommerfeld, R. A. and H. Gubler, 1983: Snow avalanches and acoustic emissions. *Annals of Glaciology*, **4**, 271–276.

Staack, N., 2004: Entwicklung eines akustischen Schneepenetrometers : Trainings- und Coaching Hinweise. M.S. thesis, Technische Universität Hamburg-Harburg.

St.Lawrence, W. and C. Bradley, 1977: Spontaneous fracture initiation in mountain snow-packs. *Jou*, **19**, 411–417.

St.Lawrence, W. and T. Williams, 1976: Seismic signals associated with avalanches. *Journal of Glaciology*, **17**, 521–526.

St.Lawrence, W. F., 1980: The acoustic emission response of snow. *Journal of Glaciology*, **26**, 209–216.

St.Lawrence, W. F., T. Lang, R. Brown, and C. Bradley, 1973: Acoustic emission in snow at constant rates of deformation. *Journal of Glaciology*, **12**, 144–146.

van Herwijnen, A. and J. Schweizer, 2011: Seismic sensor array for monitoring an avalanche start zone: design, deployment and preliminary results. *Journal of Glaciology*, **57(202)**, 267–276.

Yamada, T., T. Hasemi, K. Izumi, and A. Sato, 1974: On the dependencies of the velocities of p and s waves and thermal conductivity upon the texture of snow. *Contrib. Inst. Low Temp. Sci. Hokkaido Univ., Ser. A, 32*, 71–80.